RF Project 765353/718266
Report No. 386

MODELING AND ESTIMATION OF A LOW DEGREE GEOPOTENTIAL MODEL FROM TERRESTRIAL GRAVITY DATA

Nikolaos K. Pavlis
Department of Geodetic Science and Surveying

NATIONAL AERONAUTICS AND SPACE ADMINISTRATION
Orbiting Satellites Project
Space And Earth Sciences Directorate
Goddard Space Flight Center
Greenbelt, Maryland 20771

Grant No. NAG 5-781, Supp. No. 1

March 1988

The Ohio State University Research Foundation
1314 Kinnear Road
Columbus, Ohio 43212

MODELING AND ESTIMATION OF A LOW DEGREE GEOPOTENTIAL MODEL FROM TERRESTRIAL GRAVITY DATA

By
Nikolaos K. Pavlis

Report No. 386

Department of Geodetic Science and Surveying
The Ohio State University
Columbus, Ohio 43210-1247

March 1988

ABSTRACT

The development of appropriate modeling and adjustment procedures for the estimation of harmonic coefficients of the geopotential, from surface gravity data was studied, in order to provide an optimum way of utilizing the terrestrial gravity information in combination solutions currently developed at NASA/Goddard Space Flight Center, for use in the TOPEX/POSEIDON mission.

The mathematical modeling was based on the fundamental boundary condition of the linearized Molodensky boundary value problem. Atmospheric and ellipsoidal corrections were applied to the surface anomalies. The 1°x1° mean free-air anomalies of the Ohio State University's June 1986 global anomaly field were used. Low degree (<50) potential coefficient sets were estimated through a rigorous least squares adjustment. The high frequency content of the anomalies was removed prior to the adjustment using the OSU86F high degree expansion.

Terrestrial gravity solutions were found to be in good agreement with the satellite ones over areas which are well surveyed (gravimetrically), such as North America or Australia. However, systematic differences between the terrestrial only models and GEMT1, over extended regions in Africa, the Soviet Union and China, were found. In Africa, gravity anomaly differences on the order of 20 mgals and undulation differences on the order of 15 meters, over regions extending 2000 km in diameter, occur. Comparison of the GEMT1 implied undulations with 32 well distributed Doppler derived undulations gave an RMS difference of 2.6 m, while corresponding comparison with undulations implied by the terrestrial solution gave RMS difference on the order of 15 m, which implies that the terrestrial data in that region are substantially in error.

FOREWORD

This report was prepared by Mr. Nikolaos K. Pavlis, Graduate Research Associate, Department of Geodetic Science and Surveying, under the supervision of Professor Richard H. Rapp. This study was supported by NASA Grant NAG 5-781, The Ohio State University Research Foundation Project No. 718266. This grant was administrated by the NASA Goddard Space Flight Center, Greenbelt Maryland 20771. The NASA Technical Officer for this grant is Mr. James Marsh, Code 621. Substantial computer support was provided by the Instruction and Research Computer Center, The Ohio State University. For the computations made for this research substantial use was made of the CRAY X-MP/48 supercomputer at the Pittsburgh Supercomputing Center. These computer resources were made available through the Pittsburgh Supercomputing Center Grant PSCA17.

A slightly modified version of this report was submitted to the Graduate School of The Ohio State University in partial fulfillment of the requirements for the Degree Master of Science.

The reproduction and distribution of this report was carried out with funds supplied, in part, by the Department of Geodetic Science and Surveying.

ACKNOWLEDGMENTS

I express my sincere appreciation to my adviser Prof. Richard H. Rapp for his guidance, help and support throughout this research work. Working under his supervision for this research has been a most educating experience. To him and to Prof. Clyde C. Goad I am most indebted for their constructive criticism on my work and their suggestions and comments.

The technical assistance for the use of the supercomputer, provided by Mr. Aaron J. Supowit, senior computer specialist of the Instruction and Research Computer Center at the Ohio State University, Mr. Alvin E. Stutz, Associate Director at the User Services of the Ohio Supercomputing Center and Mr. Bob Whitney, Cray Analyst at the Pittsburgh Supercomputing Center, is most gratefully acknowledged.

Special thanks go to my friends from the Department of Geodetic Science and Surveying whose interaction and friendship has made my stay at the Ohio State University a most enjoyable experience so far. In particular I offer sincere thanks to Dr. George Dedes, Dr. Petros Patias and Dr. Theodossios Engelis for their friendship and willingness to share with me their knowledge and experience on a variety of topics.

Last but not least, I am indebted to Miss Tracy Runyon who typed part of the first two chapters and Mrs. Linda Lentz who typed the bulk of this manuscript. Their excellent typing and patience in making a number of modifications are responsible for the present form of this material.

TABLE OF CONTENTS

ABSTRACT..... ii

FOREWORD..... iii

ACKNOWLEDGMENTS..... iv

LIST OF TABLES..... vii

LIST OF FIGURES..... ix

CHAPTER PAGE

I. INTRODUCTION..... 1

1.1 Previous Investigations..... 3
1.2 Objective and Organization of the Present Study..... 5

II. MODELING OF THE TERRESTRIAL GRAVITY DATA..... 8

2.1 Molodensky's Boundary Value Problem..... 8
2.1.1 The Fundamental Boundary Condition..... 9
2.1.2 Definition of the Telluroid..... 18
2.2 Gravity Anomaly and Potential Coefficient Relations.. 19
2.2.1 The Boundary Condition Considering Ellipsoidal Terms to Order e^2..... 21
2.2.2 Spherical Harmonic Representation of the Gravity Anomaly..... 24
2.3 The Mathematical Model - Practical Aspects..... 26
2.3.1 The Observable..... 27
2.3.2 Atmospheric Effect..... 29
2.3.3 Ellipsoidal Effects..... 31
2.3.4 Transition from Point to Area Mean Values..... 34
2.3.5 Vertical Datum Inconsistencies..... 39
2.3.6 Computational Formulas..... 42
2.4 The Alternative Use of Terrain Corrected Anomalies... 47

III. DATA USED IN THIS STUDY..... 50

3.1 Data Requirements for Surface Gravity Analysis..... 50
3.1.1 The June 1986 Gravity Data Base..... 50
3.1.2 The Mean Elevation Data..... 63

IV. ESTIMATION OF HARMONIC COEFFICIENTS OF THE GEOPOTENTIAL.. 65

4.1 Combination Solutions..... 65
4.2 Estimation of Potential Coefficients from Surface Gravity..... 68
4.2.1 Structure and Characteristics of the Normal Equations..... 71
4.2.2 The Least Squares Adjustment as Compared to Quadrature Formulas..... 80

V. NUMERICAL RESULTS AND COMPARISONS..... 87

5.1 The Computational Task - Organization of the Numerical Analysis..... 87
5.2 Preliminary Investigations..... 92
5.2.1 Description of the Datasets Used..... 92
5.2.2 The Experiments to be Presented..... 96
5.2.3 Criteria Adopted for the Comparisons..... 98
5.2.4 Recovery of Harmonic Coefficients and Aliasing Effects..... 100
5.2.5 Removal of High Frequency Content of the Gravity Anomalies..... 104
5.2.6 Weighting of the Surface Gravity Data..... 110
5.2.7 The Use of Terrain Corrections..... 116
5.3 Validation..... 118
5.3.1 Comparisons With Existing Geopotential Models. 120
5.3.2 Systematic Inconsistencies Between Satellite Only and Terrestrial Only Solutions..... 135
5.3.3 Downweighting of Selected Terrestrial Gravity Data..... 141
5.3.4 Computation of Degree Variances..... 145

VI. SUMMARY - CONCLUSIONS - RECOMMENDATIONS..... 149

APPENDICES

A. Systematic Effects..... 153

B. Combination Solution Adjustment Models..... 161

LIST OF REFERENCES..... 167

LIST OF TABLES

TABLE PAGE

1. Some Currently Used Global Geopotential Models..... 4

2. Statistical Characteristics of the June 1986 Anomaly Field.. 52

3. Ordering Patterns for the Unknown Coefficients..... 78

4. Comparison of Input and Output Potential Coefficient Sets... 83

5. CPU Times for the CRAY X-MP/48 at PSC..... 89

6. Datasets Used in the Numerical Analysis..... 93

7. The Experiments to be Presented..... 97

8. Comparison of the Coefficients Obtained From Solutions ADJ020 and ADJ021 with the Original Coefficients (December 1981 Field)..... 101

9. Comparison of the Coefficients Obtained From Solutions SOLV18 and SOLV19 with the Original Coefficients (December 1981 Field)..... 102

10. Intercomparison of Terrestrial Only Solutions Where Different High Degree Models Were Used for the Removal of the High Frequency Content of the Gravity Anomalies..... 107

11. Comparison of Solutions ADJUST02 and ADJUST20 to the OSU86F Geopotential Model..... 111

12. Comparison of Solutions SOLV01, SOLV02, SOLV03 to the OSU86F Geopotential Model..... 114

13. Undulation Comparison at Laser Stations in the Western United States..... 119

14. Undulation Comparisons at Doppler Stations in Africa..... 138

15. 10° Equal Area Gravity Anomaly Comparisons in Africa..... 139

16. Overall Comparison Between Terrestrial-Only Solutions Without and With Downweighting of Selected Anomaly Data..... 144

LIST OF FIGURES

FIGURE		PAGE
1.	Basic Geometry Associated With Molodensky's Boundary Value Problem	10
2.	The Local Astronomic and Geodetic Frames	15
3.	The Geometry Associated With the Boundary Condition (2.44)	20
4.	The Coordinate Surface Through the Telluroid Point Q	22
5.	Geometry Associated With the Observable	27
6.	Atmospheric Correction	29
7.	Geometry of the Surface Element σ_{ij}	35
8.	Location of the 48955 1°x1° Anomalies of the June 1986 Field	53
9.	Location of the 5684 Geophysical Anomalies of the June 1986 Field	54
10.	Location of the 43271 Anomalies of the June 1986 Field that Exclude 5684 Geophysical Anomalies	55
11.	Location of the 21010 Anomalies that Have Standard Deviation $\leq$ 10 mgals	56

12. Location of the 9972 Anomalies that Have Standard Deviation ≥ 20 mgals..... 57

13. Undulation Correction $\delta N_h{}^2$ Based on a 5°x5° Grid (Contour Interval is 20 cm)..... 59

14. Location of the 5911 1°x1° Blocks Where $|\bar{H}_{ijTUG87} - \bar{H}_{ijOCT85.MELEV}| > 1000$ m..... 64

15. Structure of Correlation Matrices..... 79

16. Network Topology..... 90

17. Location of the 466 1°x1° Mean Terrain Corrections Received from DMA/AC..... 94

18. Location of the 11404 Residuals in ADJUST02 Exceeding in Absolute Value 10 mgals..... 109

19. Locations of the 9416 Residuals in ADJUST20 Exceeding in Absolute Value 10 mgals..... 109

20. Undulation Differences - ADJUST20 Minus ADJUST30 (Contour Interval is 1 m, Based on a 2°x2° Grid). Superimposed are the Locations of Selected Laser Stations..... 117

21. Locations of the 17082 1°x1° Blocks Where $|\bar{\Delta}g_{GEM} - dg_{in}| \geq 10$ mgals (Geophysical Data are Included in the Comparison)... 122

22. Locations of the 14412 1°x1° Blocks Where $|\bar{\Delta}g_{GEM} - dg_{in}| \geq$ 10 mgals (Geophysical Data are Excluded from the Comparison) 122

23. Locations of the 9745 1°x1° Blocks Where $|\bar{\Delta}g_{GEM} - \bar{\Delta}g_{A20}| \geq 10$ mgals (Locations Corresponding to Geophysical Data are Included in the Comparison)..... 123

24. Locations of the 7545 1°x1° Blocks Where $|\bar{\Delta}g_{GEM} - \bar{\Delta}g_{A40}| \geq$ 10 mgals (Locations Corresponding to Geophysical Data are Included in the Comparison)..... 123

25. Locations of the 10149 1°x1° Blocks Where Condition (5.19) is Fulfilled. (Locations Corresponding to Geophysical Data are Included in the Comparison)..... 126

26. Locations of the 6933 1°x1° Blocks Where Condition (5.20) is Fulfilled. (Locations Corresponding to Geophysical Data are Included in the Comparison)..... 126

27. The Least Squares Adjustment and the Data Sampling..... 127

28. Locations of the 6833 1°x1° Blocks Where $|dg - \bar{\Delta}g_{alt}| \geq 10$ mgals..... 129

29. Locations of the 3574 1°x1° Blocks Where $|\bar{\Delta}g_{GEM} - (\bar{\Delta}g_{alt} - hf_s)| \geq 10$ mgals..... 129

30. Gravity Anomaly Differences: GEMT1 Minus ADJUST20 Based on a 5°x5° Grid (Contour Interval is 4 mgals)..... 130

31. Undulation Differences: GEMT1 Minus ADJUST20 Based on a 5°x5° Grid (Contour Interval is 4 m)..... 131

32. Undulation Differences: GEMT1 Minus ADJUST40 Based on a 5°x5° Grid (Contour Interval is 4 m)..... 131

33. Gravity Anomaly Differences: OSU86F Minus ADJUST20 Based on a 5°x5° Grid (Contour Interval is 4 mgals)..... 132

34. Undulation Differences: OSU86F Minus ADJUST20 Based on a 5°x5° Grid (Contour Interval is 4 m)..... 133

35. Percentage Differences Between OSU86F Versus ADJUST20 and OSU86F Versus PGS3041..... 134

36. Gravity Anomaly Differences: GEMT1 Minus ADJUST20 Based on a 2°x2° Grid (Contour Interval is 2 mgals)..... 136

37. Undulation Differences: GEMT1 Minus ADJUST20 Based on a 2°x2° Grid (Contour Interval is 4 m). Superimposed are Selected Doppler Station Locations..... 137

38. Locations of the 2550 1°x1° Blocks Where $|\bar{\Delta g}_{1°x1°OSU86F2\to36} - \bar{\Delta g}_{1°x1°ADJUST20}| \geq 10$ mgals..... 142

39. Locations of the 1985 1°x1° Blocks Where $|\bar{\Delta g}_{1°x1°OSU86E2\to36} - \bar{\Delta g}_{1°x1°ADJUST40}| \geq 10$ mgals..... 143

40. Anomaly Degree Variances Implied by GEMT1 and ADJUST20..... 145

41. Anomaly Degree Variances Implied by GEMT1 and ADJUST40..... 146

42. Undulation Corrections Implied by IE_h (Contour Interval is 5 cm)..... 158

43. Undulation Corrections Implied by IE_γ (Contour Interval is 5 cm)..... 159

44. Undulation Corrections Implied by IE_r (Contour Interval is 5 mm)..... 159

CHAPTER I

INTRODUCTION

Accurate knowledge of the external gravity field of the earth is a prerequisite for various geodetic and geophysical investigations and applications. It is essential for accurate determination of the orbits of artificial satellites, since the earth's gravitational perturbations are (for common satellite altitudes) the most significant ones experienced by the satellites. Accurate gravity field models are also important for geophysical investigations of the earth's interior, and for oceanographic studies related to ocean dynamics.

The estimation of the external gravity field of the earth, on a global basis, has been investigated in the past from the theoretical as well as the computational point of view. Improvement in our knowledge of the gravity field has become a continuous effort, primarily due to the following reasons:

- the quality, quantity and distribution of the necessary data for accurate global gravity modeling, is improving with time as well as with the development and use of more accurate observational systems as the modern, highly accurate and stable laser tracking systems and the altimeter satellites.

- the availability of more accurate data requires more rigorous and complete mathematical modeling, since the effects of certain approximations made in the past become non-negligible in the presence of more accurate and complete data.

- some of the approximations which were applied in order to make the estimation of global gravity models a computationally manageable problem, become unnecessary in view of the computational resources available nowadays, especially after the development of vector processors. Estimation techniques which have found very limited or no application in the past due to their computational load, can now be implemented and their possible merits can be investigated.

Currently, the estimation of global gravity field models is based on the combination of information coming from the following main sources:

(a) Artificial satellite observations, such as laser ranging, radar and optical observations,
(b) Terrestrial gravity measurements, primarily gravity anomalies,
(c) Satellite altimeter observations.

Satellite observations provide a global sampling of the gravity field, but lack detailed information due to the attenuation of the field at satellite altitudes (LAGEOS, for example, is practically insensitive to harmonics of degree larger than eight). For this reason, satellite observations can support accurate determination of the low frequency part of the spectrum of the gravity field, but are inadequate for estimation of the medium and high frequency part of it.

The opposite is true for terrestrial measurements, which provide detailed sampling of the gravity field, but lack global coverage due to the existing data gaps.

The altimeter observations constitute a special case of satellite observations which provide a quite detailed and accurate sampling of the field over the oceanic areas but suffer from the large gaps generated by the land discontinuities. Therefore, their character and information content correspond, as far as the estimation of the gravity field is concerned, more to the terrestrial measurements than to the

satellite ones.

Consequently, global gravity models developed for "general purpose", i.e. both for terrestrial use and for satellite orbit computations, need to utilize both satellite and terrestrial data sources in a complementary way, so that an optimum determination of the gravity field over a wider band of its spectrum could be achieved. At this point "special purpose" gravity models such as PGS-S4 [Lerch et al, 1982b] "tailored" to fit the orbits of particular satellites (in the above case SEASAT) or the Rapp 1977 model [Rapp, 1977], computed from terrestrial data alone will not be considered.

1.1 Previous Investigations

The necessity to determine optimum ways of combining the satellite information with the terrestrial data, for the estimation of global gravity models, has been recognized early in the past. Investigations by Kaula (1966b) and Rapp (1967) resulted in the formulation of two main estimation techniques. The basic difference between the two methods is the way that the terrestrial gravity data are being treated. In Kaula's approach the orthogonality relations are used in order to determine potential coefficients from gravity anomalies. In Rapp's approach the problem is essentially inverted and a least squares adjustment is used to fit a truncated set of potential coefficients to the given gravity anomalies.

Rapp (1969) has compared both analytically and numerically the two estimation techniques and has investigated the conditions under which they yield similar results.

The major disadvantage of Kaula's approach as opposed to Rapp's is that the gravity anomalies need to be reduced to a spherical surface so that the orthogonality relations can be implemented. On the other hand, in Rapp's method a truncated set of coefficients is used to fit the data; consequently, aliasing effects will occur (in general) if the

data contain frequencies beyond the maximum frequency implied by the truncation [Desrochers, 1971]. Attempts to overcome this problem by extending the expansion to higher degrees result in large and computationally unmanageable normal matrices.

A detailed comparison of these two techniques will be presented in Chapter IV.

An alternative approach to the problem was proposed and tested by Colombo (1981). His method uses again the orthogonalities but now a linear estimator, optimal in the sense that it minimizes the sum of squares of the coefficient errors, is used in order to provide estimates of the potential coefficients.

These main estimation methods (with some modifications) have been implemented in the past by several investigators to provide combination solutions for potential coefficient expansions to various degrees. In Table 1 some of these solutions which are currently used in several studies are presented.

Table 1. Some Currently Used Global Geopotential Models

Name	Author	Date	N_{max}
Rapp78	Rapp	1978	180
GEM10B	Lerch et al	1981	36
GEM10C	Lerch et al	1981	180
Rapp81	Rapp	1981	180
Hajela84	Hajela	1984	250
GRIM3-L1	Reigber	1985	36
GPM2	Wenzel	1985	200
OSU86C/D	Rapp and Cruz	1986	250
OSU86E/F	Rapp and Cruz	1986	360

In view of the wide applications that such gravity models have found and the increasing demand for accurate high degree potential coefficient expansions, it has become quite critical to investigate and reconsider both the modeling and estimation part of the combination solutions.

The implementation of refined models to account for the effects of the earth's ellipticity, the atmosphere and the terrain has been investigated by Rapp (1977, 1984, 1986), and special emphasis was placed on the problem of the continuation of surface gravity data to a spherical bounding surface. Cruz (1985, 1986) has also studied the effects of the earth's ellipticity and of the downward continuation and his proposed approach has been implemented in recent high degree expansions at The Ohio State University [Rapp and Cruz, 1986a, b].

Although (as it is evident from the above) the various aspects of the determination of gravity models have been extensively studied in the past, it is not reasonable to believe that all the problems have found satisfactory answers and that there is no possibility of further improvement. Rather, the previous investigations and experiences have raised new questions that warrant careful study.

1.2 Objective and Organization of the Present Study

Currently, an effort to provide a highly accurate global gravity model, to be used for the TOPEX/POSEIDON mission [JPL, 1985], is undertaken by three main research centers:

(1) NASA/Goddard Space Flight Center (GSFC)
(2) University of Texas at Austin
(3) The Ohio State University.

The task here is to investigate optimum modeling and estimation procedures for the processing and the analysis of the terrestrial gravity information. This information, in the form of a system of normal equations referring to a low degree (<50) harmonic expansion of the geopotential, will then be combined at NASA/GSFC with the corresponding normal equations obtained from the analysis of satellite observations, in order to provide an optimum combination solution for the potential coefficients.

The potential coefficient estimates obtained from the terrestrial gravity data alone, although they do not constitute the final product of this work, are obviously of great value for comparison purposes, in order to investigate possible problems related to the surface gravity data and to indicate necessary improvements in the modeling or estimation techniques used.

The investigation which was conducted in order to accomplish the purpose of this study, can be divided into four main parts as follows:

(a) Theoretical investigation of the appropriate mathematical models that should be used in order to relate the surface mean free-air anomalies to potential coefficients. The intention here is to establish rigorous mathematical models and avoid any kind of unnecessary approximations. These aspects are presented in Chapter II in an explicit and detailed form, following a step-by-step discussion which, starting from the formulation of Molodensky's boundary value problem (which constitutes the underlying theoretical background of the problem at hand), leads to the final analytical formulation used in the estimation procedure.

(b) Description of the available data. The plan in this study is to use the most up to date gravity and elevation information that is available. In Chapter III the description of the main data sets that were examined and/or used in this study is given, focusing on some of their characteristics that should be taken into account for the appropriate

use of these data and the accurate interpretation of the results.

(c) The estimation procedure. In this study the estimation of potential coefficients from surface gravity is to be made through a least squares adjustment procedure as it was proposed by Rapp (1967). In Chapter IV the detailed formulation of this procedure is given. In addition its properties are examined and a comparison of this technique to the quadrature formulas is presented.

(d) The numerical analysis. In Chapter V the results of a number of experiments performed, are presented and discussed. These include both the results of experiments performed with simulated data, in order to examine several aspects of the procedure, and the results obtained from actual data. The latter are compared with existing geopotential models in order to validate the solutions and investigate the agreement of the gravity models implied by terrestrial data alone, with the satellite only or the combined geopotential models.

Finally, in the last chapter a summary of this work, a presentation of the conclusions drawn from it, and recommendations for further investigation are given.

CHAPTER II

MODELING OF THE TERRESTRIAL GRAVITY DATA

2.1 Molodensky's Boundary Value Problem

The determination of the geometric shape and the external gravity potential of the earth from observations carried out on its unknown surface, is a non-linear free boundary value problem (bvp), in the sense that the geometric shape of the boundary surface is also unknown. This geodetic bvp or Molodensky's problem can be formulated as follows:

Given at all points of the physical surface of the earth (S) the gravity potential W and the gravity vector $\vec{g}$, find the shape of the surface (S), as well as, the potential W outside (S), so that W consists of a regular at infinity harmonic part V, satisfying Laplace's equation $\nabla^2 V = 0$ and a known centrifugal part, and, satisfies known boundary conditions on (S).

This type of problem can be considerably simplified after application of a linearization procedure. Linearization, in the context of the modern approach of Molodensky, consists of the introduction of a known surface (Σ), the telluroid, which is "sufficiently close" to the physical surface of the earth (S), and the introduction of a normal gravity potential U as an analytical approximation of the actual gravity potential W. A point P on (S) (Figure 1) will be mapped to a point Q on (Σ) through a one-to-one correspondence. The particular rules that can be used to define this mapping will be discussed in Section 2.1.2. The important issue here is that (Σ) is defined in such a way that the value of a function on (S) can be obtained from the corresponding value of this function on (Σ) by applying a linear correction. If

$\vec{\zeta} = \overrightarrow{QP}$, then a Taylor series expansion in terms of $\vec{\zeta}$ around (Σ) can be performed, where all second and higher order terms in $\vec{\zeta}$ can be neglected without any significant loss of accuracy (see also the discussion at the end of Section 2.1.1).

After linearization the geodetic bvp becomes a linear non-free bvp for the disturbing potential T=W-U, which satisfies Laplace's equation outside (Σ) with known boundary conditions on (Σ). Once this problem is solved, the deviation $\vec{\zeta}$ of (Σ) from (S) can be determined and consequently both the external gravity potential W = U + T and the shape of the earth (S) can be defined.

The approach outlined above is in contrast to the traditional approach of Stokes where gravity observations on the earth's surface are first reduced to the geoid, which in turn is approximated by a rotational ellipsoid (spheroid) or a sphere.

2.1.1 The Fundamental Boundary Condition

Krarup (1973) has rigorously linearized the free non-linear geodetic bvp. We are presenting in the following an outline of his approach following Moritz's (1980) notations.

The basic geometry associated with our problem is described in Figure 1.

We proceed with some basic definitions:

W = gravity potential of the earth

U = normal gravity potential defined through an ellipsoid of revolution whose surface is an equipotential surface of its gravity field (Somigliana-Pizzetti normal field) [Heiskanen and Moritz, 1967, Sec. 2-7].

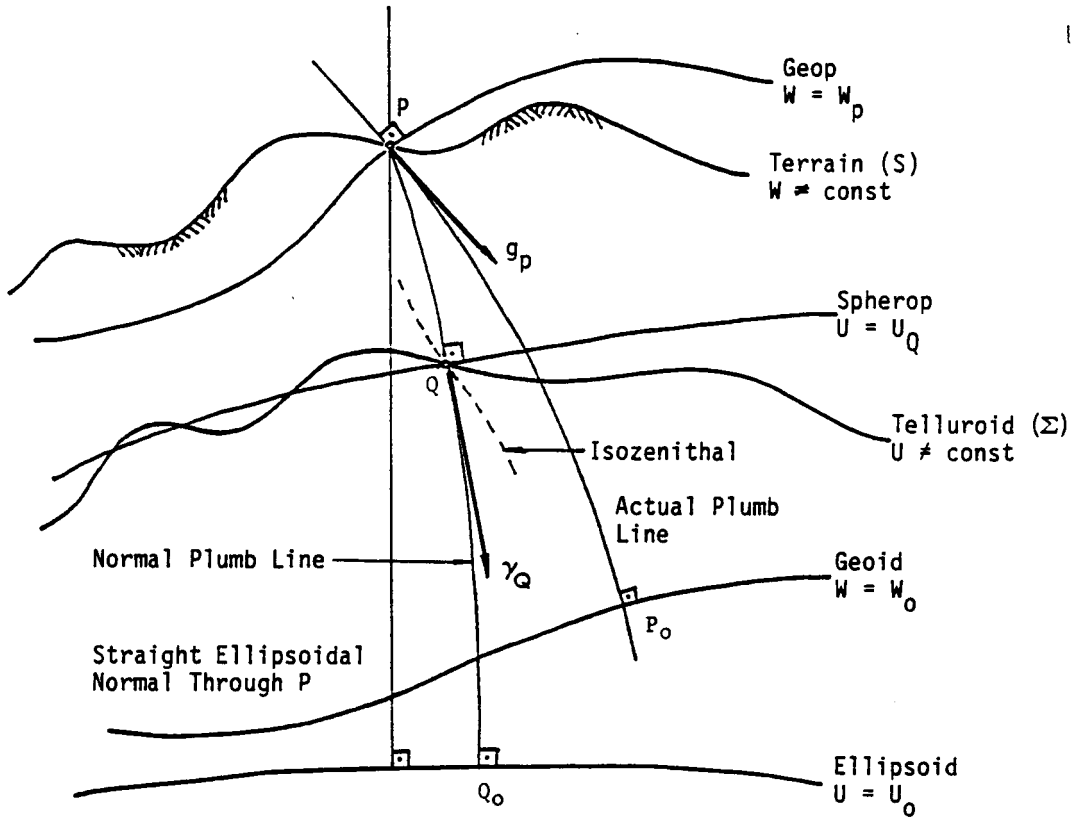

Figure 1. Basic Geometry Associated With Molodensky's Boundary Value Problem.

gravity vector: $\vec{g} = \text{grad}W$ (2.1)

normal gravity vector: $\vec{\gamma} = \text{grad}U$ (2.2)

potential anomaly: $\Delta W = W_P - U_Q$ (2.3)

gravity anomaly vector: $\vec{\Delta g} = \vec{g}_P - \vec{\gamma}_Q$ (2.4)

disturbing potential: $T_P = W_P - U_P$ (2.5)

gravity disturbance vector: $\vec{\delta} = \vec{g}_P - \vec{\gamma}_P$ (2.6)

height anomaly vector: $\vec{\zeta} = \overrightarrow{QP}$ (2.7)

We have

$$U_P = U_Q + (\text{grad}U)_Q \cdot \vec{\zeta} \tag{2.8}$$

where the dot is used to denote scalar product, and

$$\vec{\gamma}_P = \vec{\gamma}_Q + M_Q\vec{\zeta} \tag{2.9}$$

where

$$M_Q = \begin{bmatrix} \frac{\partial^2 U}{\partial x^2} & \frac{\partial^2 U}{\partial x \partial y} & \frac{\partial^2 U}{\partial x \partial z} \\ \frac{\partial^2 U}{\partial y \partial x} & \frac{\partial^2 U}{\partial y^2} & \frac{\partial^2 U}{\partial y \partial z} \\ \frac{\partial^2 U}{\partial z \partial x} & \frac{\partial^2 U}{\partial z \partial y} & \frac{\partial^2 U}{\partial z^2} \end{bmatrix}_Q \tag{2.10}$$

is the (second-order) normal gravity gradient tensor (Marussi tensor). From (2.2) and (2.8) we have

$$U_P = U_Q + \vec{\gamma}_Q \cdot \vec{\zeta} \tag{2.11}$$

Similarly,

$$T_P = T_Q + (\mathrm{grad}T)_Q \cdot \vec{\zeta} \tag{2.12}$$

However, since $\mathrm{grad}T \cdot \vec{\zeta}$ is $O(\zeta^2)$ it can be neglected in the context of linearization, so that

$$T_P = T_Q \tag{2.13}$$

Omissions as the above will be uniformly applied in the following derivations. In other words, no distinction will be made between (S) and (Σ) as far as quantities of the anomalous field such as T, $\overrightarrow{\Delta g}$, gradT, $\vec{\zeta}$ etc. are concerned [Moritz, 1980, pp. 339-341]. Hence,

$$\begin{aligned} \Delta W &= W_P - U_Q \\ &= T_P + U_P - U_Q \\ &= T_Q + U_Q + \vec{\gamma}_Q \cdot \vec{\zeta} - U_Q \quad \text{or} \end{aligned}$$

$$\Delta W = T_Q + \vec{\gamma}_Q \cdot \vec{\zeta} \tag{2.14}$$

and

$$\begin{aligned} \overrightarrow{\Delta g} &= \vec{g}_P - \vec{\gamma}_Q \\ &= \vec{g}_P - \vec{\gamma}_P + M_Q\vec{\zeta} \\ &= [\mathrm{grad}(W-U)]_P + M_Q\vec{\zeta} \quad \text{or} \end{aligned}$$

$$\vec{\Delta g} = (\text{grad}T)_P + M_Q\vec{\zeta}$$

and since $(\text{grad}T)_P \approx (\text{grad}T)_Q$ one finally has

$$\vec{\Delta g} = (\text{grad}T)_Q + M_Q\vec{\zeta} \tag{2.15}$$

Assuming that $\det(M_Q) \neq 0$, so that M_Q^{-1} exists one has from (2.15)

$$\vec{\zeta} = M_Q^{-1}[\vec{\Delta g} - (\text{grad}T)_Q] \tag{2.16}$$

so that (2.14) can be written as

$$T_Q + \vec{m}_Q\cdot(\text{grad}T)_Q = \Delta W + \vec{m}_Q\cdot\vec{\Delta g} \tag{2.17}$$

where

$$\vec{m}_Q = -M_Q^{-1}\vec{\gamma}_Q \tag{2.18}$$

defines a vector tangent to the isozenithal lines [Moritz, 1980, p. 345] of the normal gravity field. Equation (2.17) is the <u>fundamental boundary condition</u> of the linearized Molodensky bvp.

Introducing the orthogonal curvilinear coordinates ρ, ϕ, λ where ϕ is the normal latitude, λ the normal longitude (see also [Moritz, 1980, p. 338]) and ρ is measured along the isozenithal, we can define a set of generalized coordinates as

$$\begin{bmatrix}\gamma_1\\ \gamma_2\\ \gamma_3\end{bmatrix} = \begin{bmatrix} -\frac{1}{\rho^2}\cos\phi\cos\lambda \\ -\frac{1}{\rho^2}\cos\phi\sin\lambda \\ -\frac{1}{\rho^2}\sin\phi \end{bmatrix} \tag{2.19}$$

With respect to these coordinates, equation (2.17) takes the form [Moritz, 1980, pp. 342-348]

$$\Delta g' = -\left(\frac{\partial T}{\partial \tau}\right)_Q + \frac{1}{\gamma_Q}\left(\frac{\partial \gamma}{\partial \tau}\right)_Q T_Q - \frac{1}{\gamma_Q}\left(\frac{\partial \gamma}{\partial \tau}\right)_Q \Delta W \tag{2.20}$$

where

γ is the magnitude of the normal gravity vector $\vec{\gamma}$

τ is the arc length along the isozenithal line

$\Delta g'$ is the magnitude of the projection of $\overrightarrow{\Delta g}$ along the isozenithal line passing through Q.

According to the above, the procedure for the determination of (S) and W can be idealistically outlined as follows:

(a) At every point P on (S) gravimetric and astronomical observations provide the magnitude and direction of the gravity vector $\vec{g}_P$. On the other hand, leveling combined with the gravimetric observations provide the gravity potential W up to an unknown constant that can be determined indirectly by distance measurement(s) [Heiskanen and Moritz, 1967, Sec. 2-19, 2-20].

(b) At every corresponding point Q on the telluroid (Σ) the magnitude and direction of the normal gravity vector $\vec{\gamma}_Q$ can be computed since both the surface (Σ) and the normal gravity potential are known.

(c) The direction of the isozenithal line passing through Q can be determined, once the normal potential is defined. Hence the magnitude of the isozenithal projection $\Delta g'$, of $\overrightarrow{\Delta g}$, can be determined.

(d) Once the mapping P → Q, that defines the telluroid (Σ) is established, the quantity ΔW in (2.20) will be defined. Hence, (2.20) takes the form

$$C_1\left(\frac{\partial T}{\partial \tau}\right)_Q + C_2 T_Q = C_3 \qquad (2.21)$$

with known constant coefficients

$$\left.\begin{aligned} C_1 &= -1 \\ C_2 &= \frac{1}{\gamma_Q}\left(\frac{\partial\gamma}{\partial\tau}\right)_Q \\ C_3 &= \Delta g' + C_2\Delta W \end{aligned}\right\} \qquad (2.22)$$

(e) Disregarding the fact that the telluroid can be below the surface of the earth [Moritz, 1980, p. 355], and assuming that the effect of the mass of the atmosphere has been taken into account [ibid, p. 442], we can consider the disturbing potential T to be harmonic outside (Σ), i.e.

$$\nabla^2 T = 0, \quad \text{outside } (\Sigma). \qquad (2.23)$$

Consequently, the problem here is to solve (2.23) for T, subject to the boundary condition (2.21). This corresponds to a third bvp of potential theory (Robin's problem - see [Lebedev et al., 1979, p. 27]) although it is considerably more complicated because it involves oblique derivatives (the isozenithal lines are not normal to the telluroid (Σ)). In any case once this bvp is solved for T, then $\vec{\zeta}$ (and thus the geometric shape of S) can be obtained from equation (2.16).

The steps outlined above are meant to describe the principles behind the formulation of Molodensky's bvp. From the practical point of view, the prerequisites of Molodensky's problem, especially the continuous coverage of the whole earth's surface with gravity measurements raise serious questions about the relevancy of the problem itself from the geodetic point of view [Moritz, 1980].

Although equation (2.20) is theoretically rigorous, it is not convenient for practical purposes, due to the presence of the isozenithal in both the definition of the directional derivatives $\partial/\partial\tau$, and of $\Delta g'$. However, since the curvature of the normal plumb line is very small and regular [Heiskanen and Moritz, 1967, p. 196; Moritz, 1983, p. 7], the normal plumb line can be considered to coincide with the straight ellipsoidal normal, in which case the isozenithal will also coincide with the straight ellipsoidal normal [Moritz, 1980, pp. 345-346].

Accordingly, if

isozenithal ≡ normal plumb line ≡ straight ellipsoidal normal (2.24)

equation (2.20) becomes

$$\Delta g' = -\left[\frac{\partial T}{\partial h}\right]_Q + \frac{1}{\gamma_Q}\left[\frac{\partial \gamma}{\partial h}\right]_Q T_Q - \frac{1}{\gamma_Q}\left[\frac{\partial \gamma}{\partial h}\right]_Q \Delta W \qquad (2.25)$$

where $\Delta g'$ is hereon to be considered the magnitude of the ellipsoidal normal projection of $\overrightarrow{\Delta g}$ and h denotes the arc length along the ellipsoidal normal.

Consider now, $\{\vec{e}_\Lambda, \vec{e}_\phi, \vec{e}_H\}_P$ the unit vectors on the three axes of the local astronomic frame (east, north, zenith) at P, and $\{\vec{e}_\lambda, \vec{e}_\phi, \vec{e}_h\}_P$ the corresponding unit vectors for the local normal frame (Figure 2); then

$$(\vec{e}_H)_P = (\xi\ \vec{e}_\phi + \eta\ \vec{e}_\lambda + \cos\theta\ \vec{e}_h)_P \qquad (2.26)$$

where θ is the total deflection of the vertical and ξ, η are its latitudinal and longitudinal components respectively [Heiskanen and Moritz, 1967, fig. 2-13].

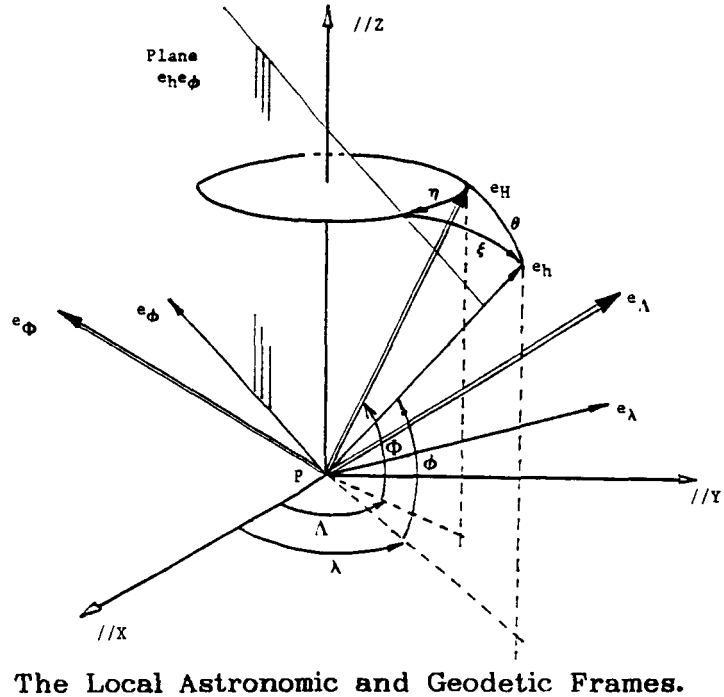

Figure 2. The Local Astronomic and Geodetic Frames.

The gradient of the gravity potential with respect to the local normal frame is

$$(\text{grad}W)_P = \left[\frac{\partial W}{M\partial\phi}\,\vec{e}_\phi + \frac{\partial W}{N\cos\phi\,\partial\lambda}\,\vec{e}_\lambda + \frac{\partial W}{\partial h}\,\vec{e}_h\right]_P \tag{2.27}$$

where M and N are the meridional and prime vertical radii of curvature respectively. Accordingly,

$$\Delta g' = -(\vec{g}_P - \vec{\gamma}_Q)\cdot\vec{e}_{h_Q} \qquad \text{or}$$

$$\Delta g' = -(\text{grad}W)_P\cdot\vec{e}_{h_Q} - |\vec{\gamma}_Q| \tag{2.28}$$

If we assume that point Q lies on the straight ellipsoidal normal through P then

$$\vec{e}_{h_Q} = \vec{e}_{h_P} \tag{2.29}$$

and (2.28) yields

$$-|\vec{\gamma}_Q| = \Delta g' + \left[\frac{\partial W}{\partial h}\right]_P \tag{2.30}$$

But

$$|\vec{g}_P| = -(\text{grad}W)_P\cdot\vec{e}_{H_P}$$

$$= -\left[\frac{\partial W}{M\partial\phi}\,\vec{e}_\phi + \frac{\partial W}{N\cos\phi\,\partial\lambda}\,\vec{e}_\lambda + \frac{\partial W}{\partial h}\,\vec{e}_h\right]_P\cdot(\xi\,\vec{e}_\phi + \eta\,\vec{e}_\lambda + \cos\theta\,\vec{e}_h)_P$$

or

$$|\vec{g}_P| = \left[-\xi\,\frac{\partial W}{M\partial\phi} - \eta\,\frac{\partial W}{N\cos\phi\,\partial\lambda} - \cos\theta\,\frac{\partial W}{\partial h}\right]_P \tag{2.31}$$

Adding (2.30) and (2.31) by parts one finally gets

$$|\vec{g}_P| - |\vec{\gamma}_Q| = \Delta g' + \left[(1-\cos\theta)\,\frac{\partial W}{\partial h} - \xi\,\frac{\partial W}{M\partial\phi} - \eta\,\frac{\partial W}{N\cos\phi\,\partial\lambda}\right]_P \tag{2.32}$$

or

$$\Delta g = \Delta g' + \varepsilon_P \tag{2.33}$$

with

$$\varepsilon_P = \left[(1-\cos\theta)\,\frac{\partial W}{\partial h} - \xi\,\frac{\partial W}{M\partial\phi} - \eta\,\frac{\partial W}{N\cos\phi\,\partial\lambda}\right]_P \tag{2.34}$$

and $\Delta g = |\vec{g}_P| - |\vec{\gamma}_Q|$ being the usual gravity anomaly as obtained from surface observations of the magnitude of the gravity acceleration.

According to the above, equation (2.25) becomes

$$\Delta g = -\left(\frac{\partial T}{\partial h}\right)_Q + \frac{1}{\gamma_Q}\left(\frac{\partial \gamma}{\partial h}\right)_Q T_Q - \frac{1}{\gamma_Q}\left(\frac{\partial \gamma}{\partial h}\right)_Q \Delta W + \varepsilon_P \qquad (2.35)$$

which is the form of the boundary condition of the linearized version of the geodetic bvp, that will be used in the sequel. Jekeli (1981), using the same assumptions as above, arrived at the form (2.35) of the fundamental boundary condition using a Taylor series expansion in ζ and neglecting second and higher order terms.

It should be noted here that ε_P depends on the mapping used to define the telluroid, since to derive (2.34) one had to assume (2.29) which restricted Q to lie on the straight ellipsoidal normal through P and thus has removed two of the three degrees of freedom for the determination of the location of Q.

Concluding this section some remarks should be made about the validity of the linearized version of the geodetic bvp. As it is shown by Jekeli [1981, eq. 4.6, 4.7] linearization causes an error on the order of

$$\frac{1}{\gamma_Q}\left(\frac{\partial \gamma}{\partial h}\right)_Q \zeta^2 \qquad (2.36)$$

for the height anomaly, and on the order of

$$\left(\frac{\partial^2 \gamma}{\partial h^2}\right)_Q \zeta^2 \qquad (2.37)$$

for the gravity anomaly. Using nominal values one has an error on the order of 3 mm in the height anomaly and 1.5 μgals in the gravity anomaly. Hence, in view of the present accuracies, linearization is completely justifiable.

2.1.2 Definition of the Telluroid

In the previous discussion the mapping that defines the telluroid was left unspecified. The general requirement was that this surface should be sufficiently close to the earth's surface, so that linearization could be performed. However, as was mentioned, the form (2.35) of the boundary condition that will be used, implicitly restricts part of the definition of the telluroid point Q.

The introduction of different mappings to define the telluroid stems from the fact that for certain mappings the form of the boundary condition becomes simpler. For the Marussi mapping [Moritz, 1980, p. 338] defined by

$$U_Q = W_P \text{ and } \frac{\vec{g}_P}{|\vec{g}_P|} = \frac{\vec{\gamma}_Q}{|\vec{\gamma}_Q|} \tag{2.38}$$

and the gravimetric mapping [ibid, p. 339] defined by

$$\vec{g}_P = \vec{\gamma}_Q \tag{2.39}$$

the potential anomaly ΔW and the gravity anomaly vector $\overrightarrow{\Delta g}$ become respectively zero, making the right side of the boundary condition (2.17) simpler. The mapping that will be adopted here is defined as follows:
If

$$C_P = W_0 - W_P \tag{2.40}$$

is the geopotential number at P [Heiskanen and Moritz, 1967, p. 56], then the telluroid point Q that corresponds to P lies on the ellipsoidal normal through P and is such that

$$U_Q = U_0 - C_P \tag{2.41}$$

where U_0 is the potential on the surface of the equipotential reference ellipsoid.

According to this definition the potential anomaly becomes

$$\Delta W = W_P - U_Q$$
$$= W_o - C_P - U_o + C_P \quad \text{or}$$
$$\Delta W = W_o - U_o = \text{const.} \tag{2.42}$$

i.e. represents the constant difference between the potential on the geoid minus the potential on the surface of the reference ellipsoid. Even if one assumes that $W_o = U_o$, this mapping is different from the Marussi mapping because here

$$\frac{\vec{g}_P}{|\vec{g}_P|} \neq \frac{\vec{\gamma}_Q}{|\vec{\gamma}_Q|} .$$

Rather, one can say (neglecting the curvature of the normal plumb lines) that in this mapping

$$\frac{\vec{\gamma}_P}{|\vec{\gamma}_P|} \approx \frac{\vec{\gamma}_Q}{|\vec{\gamma}_Q|} . \tag{2.43}$$

The form (2.35) of the boundary condition which has been adopted is in agreement with the above definition of the telluroid.

Dermanis (1984) has rigorously derived the fundamental boundary condition on the telluroid for the Marussi mapping in terms of curvature parameters [Dermanis, 1984, eq. 53]. He has also given the corresponding form of the boundary condition on the reference ellipsoid in terms of ellipsoidal, geodetic and spherical coordinates [ibid, eq. 82, 85, 86].

2.2 Gravity Anomaly and Potential Coefficient Relations

The linearization procedure as presented before has lead to the boundary condition

$$\Delta g = -\left(\frac{\partial T}{\partial h}\right)_Q + \frac{1}{\gamma_Q}\left(\frac{\partial \gamma}{\partial h}\right)_Q T_Q - \frac{1}{\gamma_Q}\left(\frac{\partial \gamma}{\partial h}\right)_Q \Delta W + \varepsilon_P \tag{2.44}$$

with

$$\left.\begin{aligned} \Delta g &= |\vec{g}_P| - |\vec{\gamma}_Q| \\ \Delta W &= W_o - U_o \\ \varepsilon_P &= \left[(1-\cos\theta)\,\frac{\partial W}{\partial h} - \xi\,\frac{\partial W}{M\partial\phi} - \eta\,\frac{\partial W}{N\cos\phi\,\partial\lambda}\right]_P \end{aligned}\right\} \qquad (2.45)$$

valid under the approximation (2.24) on the telluroid (Σ) as defined by (2.29), (2.40), and (2.41). The geometry of the original problem (Figure 1) has now been simplified, due to the approximations (2.24) and (2.29), and is now described in Figure 3.

However, since both the geometrical shape and the gravity field of the reference ellipsoid differ from the corresponding features of a homogeneous rotating ball by quantities on the order of the flattening (~ 1/300), one can expand geometrical and dynamcial quantities refering to the ellipsoid around their "spherical" values in a Taylor series in terms of any parameter characterizing the departures from the "spherical case" (e.g. f, e^2, e'^2, etc.). Truncation of such series to

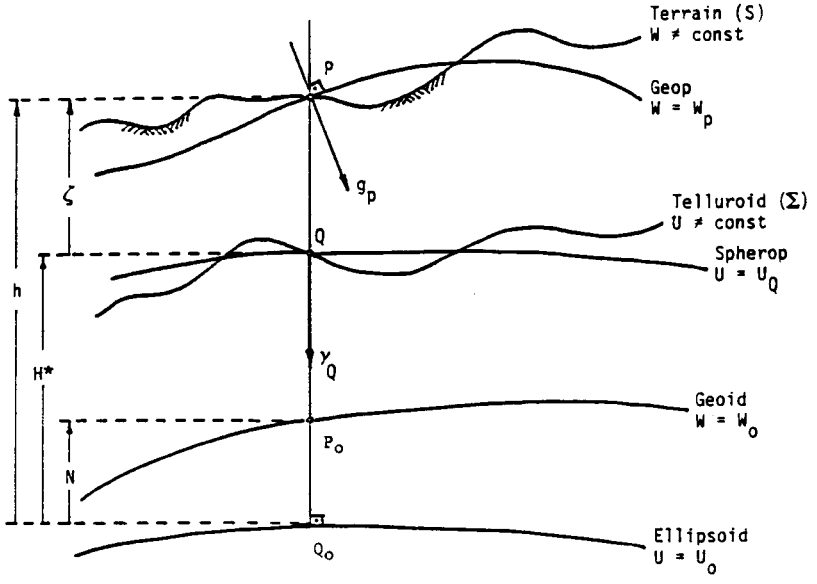

Figure 3. The Geometry Associated with the Boundary Condition (2.44).

different orders, results in different approximations. For example, omission of all but the zeroth term results in the well known "spherical approximation" [Moritz, 1980, Sec. 4.2]. It should be carefully kept in mind that such series expansions are not meant to change either the reference surface, which always remains the telluroid, or the computation of normal gravity at the telluroid points. Such computations should be carried out to a high degree of accuracy.

The importance of these series expansions rests on the fact that their zeroth order (spherical) terms provide, through the boundary condition, a simple way of relating gravity anomalies to potential coefficients through a spherical harmonic representation. The remaining ellipsoidal terms due to their small magnitude can be treated otherwise.

In the following, the form of the boundary condition when ellipsoidal terms to $O(e^2)$ are modeled is presented, following Jekeli's (1981) formulation.

2.2.1 The Boundary Condition Considering Ellipsoidal Terms to Order e^2

Consider through the telluroid point Q a coordinate surface [Heiskanen and Moritz, 1967, Sec. 1-19], $u = b_Q$ (Figure 4). For each telluroid point Q_i, the corresponding coordinate surface will have constant linear eccentricity (by definition), but a different semi-minor axis $u_i = b_{Q_i}$. Accordingly, since

$$E = b_{Q_i}(1-e_i^2)^{-\frac{1}{2}}e_i \qquad (2.46)$$

each coordinate surface will be characterized by a different eccentricity e_i. However, to the accuracies involved here and for points close to the earth's surface, the eccentricity of all coordinate surfaces can be considered constant, equal to the eccentricity of the reference ellipsoid [Jekeli, 1981, p. 122]. Consider a local spherical

coordinate system at Q (Figure 4) with unit vectors $\vec{e}_{r_Q}$ in the direction of the geocentric radius and positive outwards, $\vec{e}_{\theta_Q}$ along the

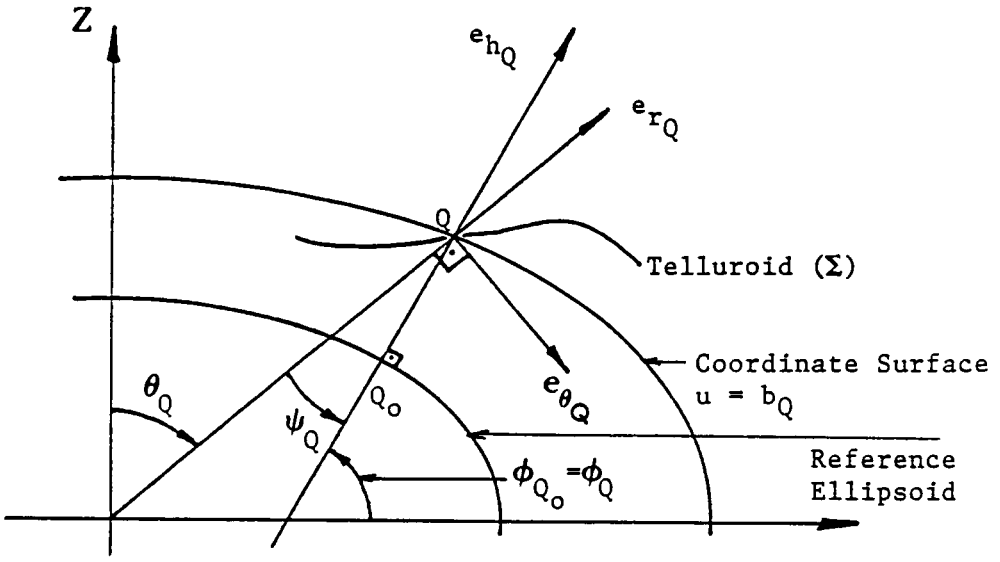

Figure 4. The Coordinate Surface Through the Telluroid Point Q.

increasing geocentric co-latitude and $\vec{e}_{\lambda_Q}$ along the increasing longitude. Then

$$\vec{e}_{h_Q} = \cos\psi_Q \vec{e}_{r_Q} - \sin\psi_Q \vec{e}_{\theta_Q} \tag{2.47}$$

and the gradient vector with respect to this system becomes

$$(\text{grad } \cdot)_Q = \left(\frac{\partial \cdot}{\partial r}\right)_Q \vec{e}_{r_Q} + \left(\frac{\partial \cdot}{r\partial\theta}\right)_Q \vec{e}_{\theta_Q} + \left(\frac{\partial \cdot}{r\sin\theta\partial\lambda}\right)_Q \vec{e}_{\lambda_Q} \tag{2.48}$$

Since,

$$\left(\frac{\partial \cdot}{\partial h}\right)_Q = (\text{grad } \cdot)_Q \cdot \vec{e}_{h_Q} \tag{2.49}$$

we have

$$\left(\frac{\partial \cdot}{\partial h}\right)_Q = \cos\psi_Q \left(\frac{\partial \cdot}{\partial r}\right)_Q - \sin\psi_Q \left(\frac{\partial \cdot}{r\partial\theta}\right)_Q \tag{2.50}$$

It can also be shown easily that to the order of e^2,

$$\left.\begin{aligned} \sin\psi_Q &\approx e^2\sin\theta_Q\cos\theta_Q \\ \cos\psi_Q &\approx 1 \end{aligned}\right\} \qquad (2.51)$$

Accordingly,

$$\left(\frac{\partial \bullet}{\partial h}\right)_Q = \left(\frac{\partial \bullet}{\partial r}\right)_Q - e^2\sin\theta_Q\cos\theta_Q \left(\frac{\partial \bullet}{r\partial\theta}\right)_Q + O(e^4) \qquad (2.52)$$

On the other hand, the normal gravity potential U is given by [Heiskanen and Moritz, 1967, Sec. 2-9]

$$U(r, \theta) = \frac{GM'}{r}\left[1 - \sum_{n=1}^{\infty} J_{2n}\left(\frac{a}{r}\right)^{2n} P_{2n}(\cos\theta)\right] + \frac{1}{2}\omega^2 r^2\sin^2\theta \qquad (2.53)$$

where G is the Universal gravitational constant
M′ is the mass of the reference ellipsoid (r.e.)
a is the semi-major axis of the r.e.
ω is the rotational rate of the r.e.
J_{2n} are the even degree zonal harmonic coefficients of the normal gravity field
$P_{2n}(\cos\theta)$ are the even degree Legendre polynomials.

However, since $J_{2n} = O(e^{2n})$, equation (2.53) truncated to the $O(e^2)$ becomes

$$U(r, \theta) \approx \frac{GM'}{r}\left[1 - J_2\left(\frac{a}{r}\right)^2 P_2(\cos\theta)\right] + \frac{1}{2}\omega^2 r^2\sin^2\theta \qquad (2.54)$$

Hence,

$$\gamma = -\frac{\partial U}{\partial h} = -\frac{\partial U}{\partial r} + e^2\sin\theta\cos\theta\,\frac{\partial U}{r\partial\theta} \qquad \text{yields for point Q}$$

$$\gamma_Q \approx \frac{GM'}{r_Q^2}\left[1 - 3J_2\left(\frac{a}{r_Q}\right)^2 P_2(\cos\theta_Q)\right] - \omega^2 r_Q\sin^2\theta_Q\,(1 - e^2\cos^2\theta_Q) \qquad (2.55)$$

and

$$\frac{\partial\gamma}{\partial h} = \frac{\partial\gamma}{\partial r} - e^2\sin\theta\cos\theta\,\frac{\partial\gamma}{r\partial\theta} \qquad \text{yields for Q}$$

$$\left(\frac{\partial\gamma}{\partial h}\right)_Q \approx -\frac{2GM'}{r_Q^3}\left[1 - 6J_2\left(\frac{a}{r_Q}\right)^2 P_2(\cos\theta_Q)\right] - \omega^2\sin^2\theta_Q(1 - 3e^2\cos^2\theta_Q) \qquad (2.56)$$

Inserting (2.55) and (2.56) to (2.44) and carrying out the algebra consistently omitting terms smaller than $O(e^2)$, one finally gets

$$\begin{aligned}\Delta g = &- \left[\frac{\partial T}{\partial r}\right]_Q - \frac{2}{r_Q} T_Q \\ &+ e^2 \sin\theta_Q \cos\theta_Q \left[\frac{\partial T}{r\partial\theta}\right]_Q + \left[6J_2 \frac{a^2}{r_Q^3} P_2(\cos\theta_Q) - \frac{3\omega^2 r_Q^2}{GM'} \sin^2\theta_Q\right] T_Q \\ &+ \frac{2}{r_Q} \Delta W - \left[6J_2 \frac{a^2}{r_Q^3} P_2(\cos\theta_Q) - \frac{3\omega^2 r_Q^2}{GM'} \sin^2\theta_Q\right] \Delta W + \varepsilon_p \end{aligned} \qquad (2.57)$$

which is the form of the fundamental boundary condition when ellipsoidal terms are considered only up to $O(e^2)$. The following abbreviations will be used:

$$\left.\begin{aligned} \varepsilon_h &= e^2 \sin\theta\cos\theta \left[\frac{\partial T}{r\partial\theta}\right] \qquad (a) \\ \varepsilon_\gamma &= \left[6J_2 \frac{a^2}{r^3} P_2(\cos\theta) - \frac{3\omega^2 r^2}{GM'} \sin^2\theta\right] T \qquad (b) \end{aligned}\right\} \qquad (2.58)$$

2.2.2 Spherical Harmonic Representation of the Gravity Anomaly

For the moment let us assume that there are no masses outside of the telluroid. Then, if V and V′ are the gravitational potentials of the earth and the reference ellipsoid respectively, then they are both harmonic in the space outside of the telluroid. Hence they can both be expanded into series of <u>solid spherical harmonics</u> [Heiskanen and Moritz, 1967, Sec. 1-9] as

$$V(r,\theta,\lambda) = \frac{GM}{r}\left[1 + \sum_{n=1}^{\infty} \left(\frac{a}{r}\right)^n \sum_{m=0}^{n} (\bar{C}_{nm}\cos m\lambda + \bar{S}_{nm}\sin m\lambda)\bar{P}_{nm}(\cos\theta)\right] \qquad (2.59)$$

and

$$V'(r,\ \theta) = \frac{GM'}{r}\left[1 + \sum_{n=1}^{\infty} \left(\frac{a}{r}\right)^{2n} \bar{C}'_{2n}\bar{P}_{2n}(\cos\theta)\right] \qquad (2.60)$$

where

M is the mass of the earth (in contrast to M′ which denotes the mass of the ref. ellipsoid)

$\bar{P}_{nm}$ are the fully normalized associate Legendre functions of the first kind

$\left\{ \begin{matrix} \bar{C}_{nm} \\ S_{nm} \end{matrix} \right\}$ are the fully normalized potential coefficients (referring to the earth's gravitational field)

$\bar{C}'_{2n}$ are the corresponding coefficients of the ellipsoidal field

(r,θ,λ) always denote geocentric radius, co-latitude and longitude respectively.

The difference

$$\delta M = M - M' \tag{2.61}$$

is assumed to be sufficiently small that for the first and higher order terms M′ can be replaced by M in (2.60).

If the rotational rate of the reference ellipsoid is assumed to be the same as the actual rotational rate of the earth then

$$T = W - U = V - V' \tag{2.62}$$

As the difference of two harmonic functions is harmonic in the space outside (Σ) so that

$$T(r,\theta,\lambda) = \frac{G\delta M}{r} + \frac{GM}{r} \sum_{n=1}^{\infty} \left(\frac{a}{r}\right)^n \sum_{m=0}^{n} (\bar{C}^{*}_{nm}\cos m\lambda + \bar{S}_{nm}\sin m\lambda)\bar{P}_{nm}(\cos\theta) \tag{2.63}$$

with

$$\bar{C}^{*}_{nm} = \begin{cases} \bar{C}_{nm} - \bar{C}'_{nm} & \text{if } m = 0,\ n = 2k,\ k \in N \\ \bar{C}_{nm} & \text{otherwise} \end{cases} \tag{2.64}$$

Inserting (2.63) into (2.57) one gets

$$\Delta g = -\frac{G\delta M}{r_Q^{\,2}} + \frac{GM}{r_Q^{\,2}} \sum_{n=2}^{\infty} (n-1)\left(\frac{a}{r_Q}\right)^n \sum_{m=0}^{n} (\bar{C}^{*}_{nm}\cos m\lambda_Q + \bar{S}_{nm}\sin m\lambda_Q)\bar{P}_{nm}(\cos\theta_Q)$$
$$+ (\varepsilon_h)_Q + (\varepsilon_\gamma)_Q + \frac{2}{r_Q}\Delta W - \left[6J_2 \frac{a^2}{r_Q^{\,3}} P_2(\cos\theta_Q) - \frac{3\omega^2 r_Q^{\,2}}{GM} \sin^2\theta_Q\right]\Delta W$$
$$+ \varepsilon_p \tag{2.65}$$

where M′ has been replaced by M in the sixth term following similar reasoning as before (equation (2.60)).

2.3 The Mathematical Model - Practical Aspects

Equation (2.65) constitutes the fundamental mathematical model which establishes the functional relationship between the gravity anomaly Δg and the potential coefficients $\{\bar{C}^{*}_{nm}, \bar{S}_{nm}\}$. Therefore, it provides the basis for the formulation of observation equations to be used in a least squares adjustment for the estimation of $\{\bar{C}^{*}_{nm}, \bar{S}_{nm}\}$ from Δg. The variables appearing in (2.65) are classified as follows:

(a) Observed quantities are considered the gravity anomalies Δg, while unknown parameters are the potential coefficients $\{\bar{C}^{*}_{nm}, \bar{S}_{nm}\}$, as well as the quantities $G\delta M = GM - GM'$ and $\Delta W = W_o - U_o$.

(b) The quantities $\{a, GM, J_2, \omega\}$ are constants and refer to the adopted mean earth ellipsoid, while $\{r, \theta, \lambda\}_Q$ are considered known for each telluroid point Q.

Prior to the formation of the observation equation it is necessary to examine how the available data comply with the requirements and assumptions of the mathematical model and to determine the reductions that need to be applied to the data and the modifications that should be made to the model so that any incompatibilities between the model and the data are removed.

Also, the varying magnitude and information content of the components of the mathematical model justify special treatment of certain terms (such as ε_h and ε_γ), so that a more computationally convenient formulation can be achieved.

These aspects will be discussed in detail in the following sections. As a result of this discussion the final formulation that was used in the computations will be presented.

2.3.1 The Observable

The primary observable from terrestrial measurements is the magnitude of the gravity acceleration $g_P = |\vec{g}_P|$ at the surface point P (see Figure 5).

To evaluate the surface free-air gravity anomaly Δg [Heiskanen and Moritz, 1967, p. 293], which appears in equation (2.65), it is needed to evaluate the magnitude of the normal gravity acceleration $\gamma_Q = |\vec{\gamma}_Q|$ at the corresponding telluroid point Q.

If γ_{Q_o} denotes the normal gravity at the footpoint Q_o on the surface of the reference ellipsoid (Figure 5), then

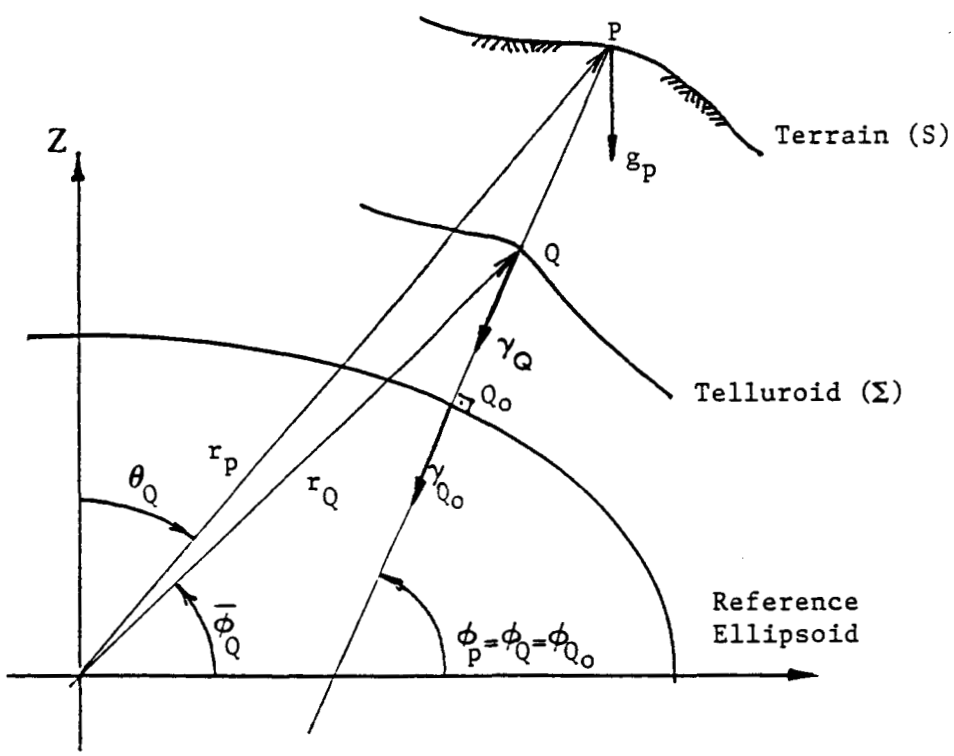

Figure 5. Geometry Associated With the Observable.

$$\gamma_Q \approx \gamma_{Q_o} + \left(\frac{\partial\gamma}{\partial h}\right)_{Q_o} H^* + \frac{1}{2!}\left(\frac{\partial^2\gamma}{\partial h^2}\right)_{Q_o} H^{*2} + \cdots \tag{2.66}$$

since the distance $|\overrightarrow{Q_oQ}|$ is, according to the definition used here for the telluroid, the normal height H^* [ibid, p. 292] of the surface point P. However, it is known [ibid, p. 328], that H^* (which is usually unknown) differs from the orthometric height H at P (which is more readily available) by about one meter in the worst cases (mountainous areas). Accordingly, without significant loss of accuracy one has

$$\gamma_Q = \gamma_{Q_o} + \left(\frac{\partial\gamma}{\partial h}\right)_{Q_o} H + \frac{1}{2!}\left(\frac{\partial^2\gamma}{\partial h^2}\right)_{Q_o} H^2 + \ldots \tag{2.67}$$

and the surface free-air anomaly becomes

$$\Delta g = g_p - \left[\gamma_{Q_o} + \left(\frac{\partial\gamma}{\partial h}\right)_{Q_o} H\right] - \frac{1}{2!}\left(\frac{\partial^2\gamma}{\partial h^2}\right)_{Q_o} H^2 - \ldots \tag{2.68}$$

or [ibid, p. 293, eq. 8-9]

$$\Delta g = g_p - \gamma_{Q_o}\left[1 - 2(1 + f + m - 2f\sin^2\phi_{Q_o})\frac{H}{a}\right] - 3\gamma_{Q_o}\left(\frac{H}{a}\right)^2 \tag{2.69}$$

where

$$f = \frac{a-b}{a} \tag{2.70}$$

$$m = \frac{\omega^2 a^2 b}{GM'} \tag{2.71}$$

and γ_{Q_o} can be evaluated using Somigliana's closed formula

$$\gamma_{Q_o} = \frac{a\gamma_e\cos^2\phi_Q + b\gamma_p\sin^2\phi_Q}{(a^2\cos^2\phi_Q + b^2\sin^2\phi_Q)^{1/2}} \tag{2.72}$$

with the equatorial and polar normal gravity γ_e and γ_p given by

$$\gamma_e = \frac{GM}{ab}\left(1 - m - \frac{m}{6}\frac{e'q'_o}{q_o}\right) \tag{2.73}$$

$$\gamma_p = \frac{GM}{a^2}\left(1 + \frac{m}{3}\frac{e'q'_o}{q_o}\right) \tag{2.74}$$

with [Moritz, 1984, pp. 388-398]

$$q_o = \frac{1}{2}\left[\left(1 + \frac{3}{e'^2}\right)\arctan e' - \frac{3}{e'}\right] \qquad (2.75)$$

$$q_o' = 3\left(1 + \frac{1}{e'^2}\right)\left(1 - \frac{1}{e'}\arctan e'\right) - 1. \qquad (2.76)$$

Apart from the approximation of H^* by H, evaluation of the surface free-air gravity anomaly by equation (2.69) would be in agreement with the requirement of the mathematical model (2.65).

Additional discussion related to the surface free-air anomaly will be made in Chapter III where the description of the actual data used in this study is given.

2.3.2 Atmospheric Effect

In deriving equation (2.65) it was assumed that there are no masses outside the telluroid. However, even if we neglect the fact that the telluroid can be below the surface of the earth, there still exists the effect of the atmosphere that needs to be taken into account.

To illustrate the effect we will use a simplified atmospheric model which assumes spherical stratification [Moritz, 1980, pp. 422-425].

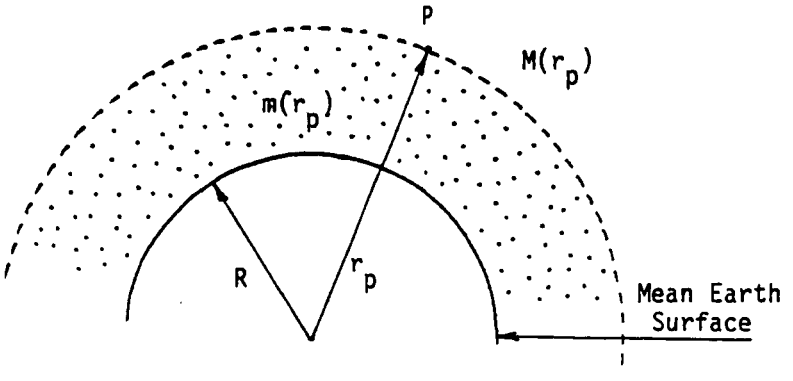

Figure 6. Atmospheric Correction.

The magnitude of the atmospheric attraction at the surface point P is in general (Figure 6)

$$F_{atm} = G \frac{m(r_p)}{r_p^2} \tag{2.77}$$

where $m(r_p)$ is the atmospheric mass below the sphere passing through P (radius r_p).

If M_A denotes the total mass of the atmosphere then

$$F_{atm} = G \frac{M_A}{r_p^2} - G \frac{M(r_p)}{r_p^2} \tag{2.78}$$

where $M(r_p)$ is the atmospheric mass above the sphere of radius r_p. F_{atm} needs to be subtracted from the observed gravity g_p for the effect of the atmosphere to be removed. However, if in the definition of the normal potential, the mass of the reference ellipsoid includes the mass of the atmosphere (as in GRS67 and GRS80) then, to remove the atmospheric effect from the gravity anomaly Δg it is required that the term

$$\delta g_A = G \frac{M(r_p)}{r_p^2} \tag{2.79}$$

be added to the gravity anomaly as obtained from (2.69).

Tabular values of δg_A are given, as a function of the elevation above sea level [IAG, 1971, p. 72]. These values have been computed based on a nearly-ellipsoidal stratification model and the use of two standard atmospheres, the CIRA 1961 and the U.S. Standard Atmosphere. The tabulated values represent rounded averages from these two atmospheric models. For computer implementation a convenient way to interpolate is to use a polynomial of the elevation that fits the tabulated values. Wichiencharoen (1982) performed such a polynomial fit; the following quadratic is the result;

$$\delta g_{A(mgals)} = 0.8658 - 9.727 \times 10^{-5} H_{(m)} + 3.482 \times 10^{-9} H^2_{(m)}. \tag{2.80}$$

This quadratic has been used in this study for the calculation of the atmospheric corrections δg_A. As it is obvious from (2.80) δg_A amounts

to about 0.9 mgals at sea level (where the correction is maximum). The indirect effect (shifting of the level surfaces due to the condensation of the atmospheric mass on the earth's surface) will not be considered due to its small magnitude (-0.7 cm at sea level) [Moritz, 1980 p. 425].

2.3.3 Ellipsoidal Effects

As it can be seen from equations (2.58a, b) the unknown potential coefficients $\{\bar{C}^{*}_{nm}, \bar{S}_{nm}\}$ appear on the right side of equation (2.65) not only in the harmonic sum but also in the terms ε_h and ε_γ. However, the magnitude and information content (see also Appendix A) of these terms suggest that it is neither reasonable from the estimability point of view, nor computationally convenient, for such terms to be incorporated into the design matrix of the adjustment. Rather, it is preferable to evaluate ε_h and ε_γ beforehand, based on some prior information for the unknown coefficients and apply these terms as corrections to the observations.

It will be assumed here that a set of potential coefficients complete to maximum degree and order N_{max} is known (e.g. Rapp81 or OSU86F). Assuming, for the present purpose that these coefficients refer to a mean earth ellipsoid with mass equal to the mass of the earth and center coinciding with the center of mass of the earth one has (see also equation (2.63)).

$$\hat{T}(r,\theta,\lambda) = \frac{GM}{r}\sum_{n=2}^{N_{max}}\left(\frac{a}{r}\right)^n\sum_{m=0}^{n}(\hat{\bar{C}}^{*}_{nm}\cos m\lambda + \hat{\bar{S}}_{nm}\sin m\lambda)\bar{P}_{nm}(\cos\theta) \qquad (2.81)$$

where ($\hat{}$) is used to denote that the truncated series with the a priori coefficients provides only an approximation to the true value of the disturbing potential. Using the well known relations

$$\left.\begin{aligned} P_{20}(\cos\theta) &= \frac{3}{2}\cos^2\theta - \frac{1}{2} && \text{(a)}\\ \sin^2\theta &= 1 - \cos^2\theta && \text{(b)}\end{aligned}\right\} \qquad (2.82)$$

and the abbreviations

$$\left.\begin{aligned} c_1 &= \frac{e^2GM}{r^2} && \text{(a)} \\ c_2 &= 3J_2\,\frac{a^2GM}{r^4} + \omega^2 r && \text{(b)} \\ c_3 &= J_2\,\frac{a^2GM}{r^4} + \omega^2 r && \text{(c)} \end{aligned}\right\} \qquad (2.83)$$

one has from (2.58a) and (2.58b)

$$\hat{\varepsilon}_h = c_1 \sum_{n=2}^{Nmax} \left(\frac{a}{r}\right)^n \sum_{m=0}^{n} (\hat{\bar{C}}^*_{nm}\cos m\lambda + \hat{\bar{S}}_{nm}\sin m\lambda)\sin\theta\cos\theta\,\frac{d\bar{P}_{nm}(\cos\theta)}{d\theta} \qquad (2.84)$$

and

$$\begin{aligned} \hat{\varepsilon}_\gamma = 3\Big[& c_2 \sum_{n=2}^{Nmax} \left(\frac{a}{r}\right)^n \sum_{m=0}^{n} (\hat{\bar{C}}^*_{nm}\cos m\lambda + \hat{\bar{S}}_{nm}\sin m\lambda)\cos^2\theta\bar{P}_{nm}(\cos\theta) \\ & - c_3 \sum_{n=2}^{Nmax} \left(\frac{a}{r}\right)^n \sum_{m=0}^{n} (\hat{\bar{C}}^*_{nm}\cos m\lambda + \hat{\bar{S}}_{nm}\sin m\lambda)\bar{P}_{nm}(\cos\theta)\Big] \end{aligned} \qquad (2.85)$$

Using the normalization factors

$$u_{nm} = \sqrt{\frac{(2n+1)(n-m-1)(n-m)}{(2n-3)(n+m-1)(n+m)}} \qquad n \geq 2,\ m \leq n \qquad (2.86)$$

$$v_{nm} = \sqrt{\frac{(2n+1)(n+m+1)(n+m+2)}{(2n+5)(n-m+1)(n-m+2)}} \qquad n \geq 0,\ m \leq n \qquad (2.87)$$

and the recursive relations for $\sin\theta\cos\theta\,\frac{dP_{nm}}{d\theta}$ [Moritz, 1980, p. 321, eq. 39-46] and for $\cos^2\theta P_{nm}$ [ibid, p. 326, eq. 39-76] one finally has

$$\sin\theta\cos\theta\,\frac{d\bar{P}_{nm}}{d\theta} = a_{nm}v_{nm}\bar{P}_{n+2,m} + b_{nm}\bar{P}_{nm} + c_{nm}u_{nm}\bar{P}_{n-2,m} \qquad (2.88)$$

with [ibid, p. 321, eq. 39-47]

$$\left.\begin{aligned} a_{nm} &= -\frac{n(n-m+1)(n-m+2)}{(2n+1)(2n+3)} \\ b_{nm} &= \frac{n^2-3m^2+n}{(2n+3)(2n-1)} \\ c_{nm} &= \frac{(n+1)(n+m)(n+m-1)}{(2n+1)(2n-1)} \end{aligned}\right\} \qquad (2.89)$$

and

$$\cos^2\theta\bar{P}_{nm} = \alpha_{nm}v_{nm}\bar{P}_{n+2,m} + \beta_{nm}\bar{P}_{nm} + \gamma_{nm}u_{nm}\bar{P}_{n-2,m} \tag{2.90}$$

with [ibid, p. 326, eq. 39-77]

$$\left.\begin{aligned} \alpha_{nm} &= \frac{(n-m+1)(n-m+2)}{(2n+1)(2n+3)} \\ \beta_{nm} &= \frac{2n^2-2m^2+2n-1}{(2n+3)(2n-1)} \\ \gamma_{nm} &= \frac{(n+m)(n+m-1)}{(2n+1)(2n-1)} \end{aligned}\right\}. \tag{2.91}$$

Using the abbreviation

$$\hat{D}_{nm}(\lambda) = \hat{\bar{C}}^{*}_{nm}\cos m\lambda + \hat{\bar{S}}_{nm}\sin m\lambda \tag{2.92}$$

from (2.84) and (2.88) one gets

$$\begin{aligned} \hat{\varepsilon}_h = c_1\Bigg[& \sum_{n=2}^{Nmax}\left(\frac{a}{r}\right)^n \sum_{m=0}^{n}\hat{D}_{nm}(\lambda)a_{nm}v_{nm}\bar{P}_{n+2,m} \\ & + \sum_{n=2}^{Nmax}\left(\frac{a}{r}\right)^n \sum_{m=0}^{n}\hat{D}_{nm}(\lambda)b_{nm}\bar{P}_{nm} \\ & + \sum_{m=2}^{Nmax}\left(\frac{a}{r}\right)^n \sum_{m=0}^{n-2}\hat{D}_{nm}(\lambda)c_{nm}u_{nm}\bar{P}_{n-2,m}\Bigg] \end{aligned} \tag{2.93}$$

while from (2.85) and (2.90) one gets

$$\begin{aligned} \hat{\varepsilon}_\gamma = 3\Big\{ c_2\Bigg[& \sum_{n=2}^{Nmax}\left(\frac{a}{r}\right)^n \sum_{m=0}^{n}\hat{D}_{nm}(\lambda)\alpha_{nm}v_{nm}\bar{P}_{n+2,m} \\ & + \sum_{n=2}^{Nmax}\left(\frac{a}{r}\right)^n \sum_{m=0}^{n}\hat{D}_{nm}(\lambda)\beta_{nm}\bar{P}_{nm} \\ & + \sum_{n=2}^{Nmax}\left(\frac{a}{r}\right)^n \sum_{m=0}^{n-2}\hat{D}_{nm}(\lambda)\gamma_{nm}u_{nm}\bar{P}_{n-2,m}\Bigg] \\ & - c_3\sum_{n=2}^{Nmax}\left(\frac{a}{r}\right)^n \sum_{m=0}^{n}\hat{D}_{nm}(\lambda)\bar{P}_{nm}\Big\} \end{aligned} \tag{2.94}$$

Using equations (2.93) and (2.94), the ellipsoidal terms $\hat{\varepsilon}_h$ and $\hat{\varepsilon}_\gamma$ can be computed from a set of potential coefficients complete to maximum

degree and order N_{max}.

As it will be seen in the next section, the actual evaluation of the ellipsoidal terms $\hat{\varepsilon}_h$ and $\hat{\varepsilon}_\gamma$ in this study was made in terms of area mean values (see equations (2.111) and (2.112)), so that these corrections are compatible with the data used here.

From the previous discussion it becomes clear that the approach adopted here for the computation of the ellipsoidal corrections is the reverse of the one proposed by Cruz (1986) and implemented in the development of the OSU86 series of high degree geopotential models [Rapp and Cruz, 1986a,b]. In this formulation the corrections are applied to the gravity data and not to the potential coefficients obtained from them. The reason, being rather obvious, is that the combination solutions for the TOPEX gravity models are to be performed at NASA/(Goddard Space Flight Center) and not at the Ohio State University. Hence, operationally corrections to the coefficients obtained from these solutions cannot be applied. The normal equations formed from surface gravity should include any systematic reductions necessary to make them compatible with the satellite data derived normals.

In Appendix A numerical values related to the magnitude of these corrections and Figures illustrating their geographical distribution are given. These, compared to the corresponding Figures given in [Cruz, 1986] verify the equivalence between the two methods.

2.3.4 Transition from Point to Area Mean Values

To this point the discussion on the modeling of surface gravity data was restricted to point value considerations. The gravity anomaly Δg in equation (2.65) represents a point value referring to the telluroid point Q or equivalently (see discussion after equation (2.13)) to a surface point P. However, for global gravity modeling one is

restricted, in practice, to use area-mean values of Δg, due to the lack of point data and economy considerations.

Area-mean values of Δg, hereon to be denoted by $\bar{\Delta}g$, are usually defined over either equi-angular or equal-area blocks. In view of the data to be used in this study (see also Chapter III), it will be considered in the following that $\bar{\Delta}g$ refers to equi-angular blocks, i.e. blocks bounded by meridional and parallel arcs of equal angular extent.

Consider an equi-angular grid on the ellipsoid and let $\Delta\lambda$ be the angular distance between two successive meridians. Such a grid forms $N = \pi/\Delta\lambda$ latitudinal bands and $2N$ longitudinal sectors on the ellipsoid, creating in total $2N^2$ equi-angular blocks. Each block will be hereon identified by two subscripts i and j, implicitly defining the latitude and longitude bounds of the block, so that $\phi_0 = \pi/2$, $\phi_N = -\pi/2$ and $\lambda_0 = 0$, $\lambda_{2N} = 2\pi$.

Let $\bar{H}_{ij}$ denote the mean orthometric height of the ij^{th} block. Then $\bar{\Delta}g_{ij}$ is interpreted to represent the average behavior (value) of the spatial function $\Delta g(r,\theta,\lambda)$ over the surface σ_{ij} located at constant distance $\bar{H}_{ij}$ from the surface of the reference ellipsoid (Figure 7).

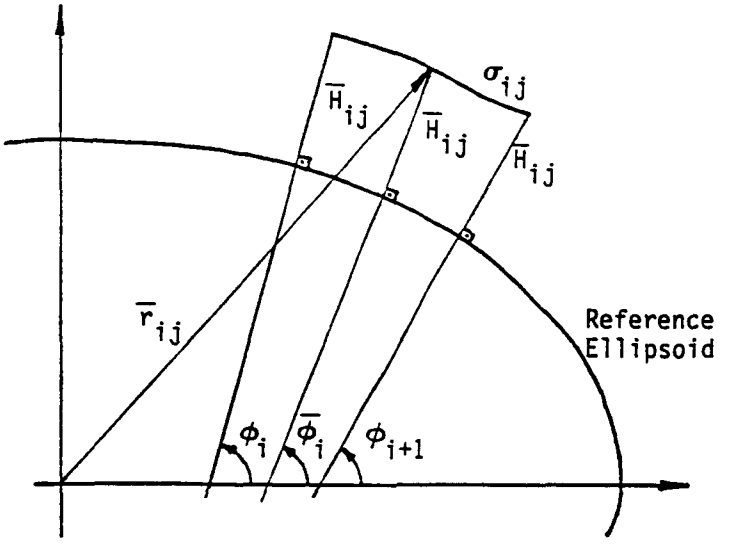

Figure 7 Geometry of the Surface Element σ_{ij}.

It is obvious that although $\bar{H}_{ij}$ is considered constant over the block, the geocentric distance r varies (in the latitudinal direction) over the surface element σ_{ij}. Let

$$\left.\begin{aligned} \bar{\phi}_i &= \frac{1}{2}(\phi_i + \phi_{i+1}) \quad (a) \\ \bar{\lambda}_j &= \frac{1}{2}(\lambda_j + \lambda_{j+1}) \quad (b) \end{aligned}\right\} \tag{2.95}$$

be the geodetic coordinates of the center of the ij^{th} block. Then

$$\bar{r}_{ij} = (\bar{X}_{ij}^2 + \bar{Y}_{ij}^2 + \bar{Z}_{ij}^2)^{1/2} \tag{2.96}$$

where

$$\left.\begin{aligned} \bar{X}_{ij} &= (\bar{N}_i + \bar{H}_{ij})\cos\bar{\phi}_i\cos\bar{\lambda}_j \\ \bar{Y}_{ij} &= (\bar{N}_i + \bar{H}_{ij})\cos\bar{\phi}_i\sin\bar{\lambda}_j \\ \bar{Z}_{ij} &= [\bar{N}_i(1-e^2) + \bar{H}_{ij}]\sin\bar{\phi}_i \end{aligned}\right\} \tag{2.97}$$

For an arbitrary point on σ_{ij} with geodetic latitude ϕ we have

$$r(\phi) = \bar{r}_{ij} + \frac{\partial r}{\partial \phi}\Big|_{\phi=\bar{\phi}_i} (\phi - \bar{\phi}_i) + \ldots \tag{2.98}$$

One can easily find [see also Rapp, 1983b, p. 67, eq. 48], that

$$r(\phi) = \bar{r}_{ij} - \frac{1}{2}\frac{e^2\sin 2\bar{\phi}_i}{\bar{r}_{ij}}\bar{N}_i(\bar{M}_i + \bar{H}_{ij})(\phi - \bar{\phi}_i) + \ldots \tag{2.99}$$

with

$$\bar{N}_i = \frac{a}{(1-e^2\sin^2\bar{\phi}_i)^{1/2}} \tag{2.100}$$

$$\bar{M}_i = \frac{a(1-e^2)}{(1-e^2\sin^2\bar{\phi}_i)^{3/2}} \tag{2.101}$$

The term $\partial r/\partial\phi$ as it can be seen from (2.99) becomes maximum (in the absolute sense) around ϕ=45°, where its value is about -370 m/deg. Here the variation of r over the surface σ_{ij} will be disregarded and it will be assumed that $r = \bar{r}_{ij}$ = const. over σ_{ij}. Additional discussion on this approximation is given in Appendix A.

Now consider equation (2.65) and apply on both sides the integral operator

$$\text{Int}\{\bullet\} = \iint_{\sigma_{ij}} \bullet \sin\theta d\theta d\lambda \tag{2.102}$$

which represents the surface integral over the surface element σ_{ij} (where $r = \bar{r}_{ij} = \text{const.}$). If (2.65) is divided by the spherical area of σ_{ij} (given by Int{1}), then the left side becomes

$$\frac{\text{Int}\{\Delta g(r=\bar{r}_{ij},\ \theta,\ \lambda)\}}{\text{Int}\{1\}} \tag{2.103}$$

which represents the area-mean value $\bar{\Delta g}_{ij}$ of $\Delta g(r,\theta,\lambda)$ over the surface element σ_{ij}. Accordingly, from (2.65) one gets

$$\bar{\Delta g}_{ij} = \frac{1}{\Delta\sigma_i}\frac{GM}{\bar{r}_{ij}^2}\sum_{n=2}^{\infty}(n-1)\left(\frac{a}{\bar{r}_{ij}}\right)^n\sum_{m=0}^{n}(\bar{C}^*_{nm}IC_m^j + \bar{S}_{nm}IS_m^j)I\bar{P}_{nm}^i + I\hat{E}_n^{ij} + I\hat{E}_\gamma^{ij} + a_1 G\delta M + a_2\Delta W + IE_p^{ij} \tag{2.104}$$

where

$$\Delta\sigma_i = \text{Int}\{1\} = \iint_{\sigma_i}\sin\theta d\theta d\lambda = \int_{\theta_i}^{\theta_{i+1}}\sin\theta d\theta\int_{\lambda_j}^{\lambda_{j+1}}d\lambda \tag{2.105}$$

$$\begin{Bmatrix} IC_m \\ IS_m \end{Bmatrix}^j = \int_{\lambda_j}^{\lambda_{j+1}}\begin{Bmatrix}\cos \\ \sin\end{Bmatrix} m\lambda d\lambda \tag{2.106}$$

$$I\bar{P}_{nm}^i = \int_{\theta_i}^{\theta_{i+1}}\bar{P}_{nm}(\cos\theta)\sin\theta d\theta \tag{2.107}$$

$$IE_p^{ij} = \frac{1}{\Delta\sigma_i}\text{Int}\{\varepsilon_p\} \tag{2.108}$$

$$a_1 = -\frac{1}{\bar{r}_{ij}^2} \tag{2.109}$$

$$a_2 = \frac{2}{\bar{r}_{ij}} - \left[3J_2 \frac{a^2}{\bar{r}_{ij}^3} + \frac{\omega^2 \bar{r}_{ij}^2}{GM}\right](\cos^2\theta_i + \cos\theta_i\cos\theta_{i+1} + \cos^2\theta_{i+1})$$

$$+ 3\left[J_2 \frac{a^2}{\bar{r}_{ij}^3} + \frac{\omega^2 \bar{r}_{ij}^2}{GM}\right] \qquad (2.110)$$

The terms $I\hat{E}_h^{ij}$ and $I\hat{E}_\gamma^{ij}$ are computed from equations (2.93) and (2.94) respectively, after averaging over the surface element σ_{ij}. However, it can be verified numerically that without significant loss of accuracy these terms may be evaluated on the surface of the ellipsoid rather than on the ground level. Hence

$$I\hat{E}_h^{ij} = \frac{1}{\Delta\sigma_i} c_1' \left[\sum_{n=2}^{Nmax}\left(\frac{a}{\bar{r}_{E_i}}\right)^n \sum_{m=0}^{n} I\hat{D}_{nm}^j a_{nm} v_{nm} I\bar{P}_{n+2,m}^i \right.$$

$$+ \sum_{n=2}^{Nmax}\left(\frac{a}{\bar{r}_{E_i}}\right)^n \sum_{m=0}^{n} I\hat{D}_{nm}^j b_{nm} I\bar{P}_{nm}^i$$

$$\left. + \sum_{n=2}^{Nmax}\left(\frac{a}{\bar{r}_{E_i}}\right)^n \sum_{m=0}^{n-2} I\hat{D}_{nm}^j c_{nm} u_{nm} I\bar{P}_{n-2,m}^i\right] \qquad (2.111)$$

$$I\hat{E}_\gamma^{ij} = \frac{1}{\Delta\sigma_i} 3\left\{c_2'\left[\sum_{n=2}^{Nmax}\left(\frac{a}{\bar{r}_{E_i}}\right)^n \sum_{m=0}^{n} I\hat{D}_{nm}^j \alpha_{nm} v_{nm} I\bar{P}_{n+2,m}^i \right.\right.$$

$$+ \sum_{n=2}^{Nmax}\left(\frac{a}{\bar{r}_{E_i}}\right)^n \sum_{m=0}^{n} I\hat{D}_{nm}^j \beta_{nm} I\bar{P}_{nm}^i$$

$$\left.\left. + \sum_{n=2}^{Nmax}\left(\frac{a}{\bar{r}_{E_i}}\right)^n \sum_{m=0}^{n-2} I\hat{D}_{nm}^j \gamma_{nm} u_{nm} I\bar{P}_{n-2,m}^i\right]\right.$$

$$\left. - c_3' \sum_{n=2}^{Nmax}\left(\frac{a}{\bar{r}_{E_i}}\right)^n \sum_{m=0}^{n} I\hat{D}_{nm}^j I\bar{P}_{nm}^i\right\} \qquad (2.112)$$

where

$$I\hat{D}_{nm}^j = \hat{\bar{C}}_{nm}^* IC_m^j + \hat{\bar{S}}_{nm} IS_m^j \qquad (2.113)$$

and $\bar{r}_{Ei}$ is obtained from (2.96) and (2.97) for $\bar{H}_{ij} = 0$. The terms c_1', c_2', c_3' are computed from (2.83) by replacing r with $\bar{r}_{Ei}$. The geocentric co-latitude θ appearing in the above equations is computed from the geodetic latitude by

$$\theta = \frac{\pi}{2} - \arctan[(1-e^2)\tan\phi] \qquad (2.114)$$

In addition, since we have assumed constant orthometric height $\bar{H}_{ij}$ over the ij^{th} block, the atmospheric correction δg_A^{ij} to be applied to $\bar{\Delta g}_{ij}$ will be given by equation (2.80) for $H = \bar{H}_{ij}$. Hence, the mathematical model relating area-mean values of surface free-air anomalies to potential coefficients becomes

$$\bar{\Delta g}_{ij} + \delta g_A^{ij} = \frac{1}{\Delta\sigma_i}\frac{GM}{\bar{r}_{ij}^2}\sum_{n=2}^{\infty}(n-1)\left(\frac{a}{\bar{r}_{ij}}\right)^n\sum_{m=0}^{n}(\bar{C}^*_{nm}IC_m^j + \bar{S}_{nm}IS_m^j)I\bar{P}_{nm}^i$$

$$+ I\hat{E}_h^{ij} + I\hat{E}_\gamma^{ij} + a_1 G\delta M + a_2\Delta W + IE_p^{ij} \qquad (2.115)$$

2.3.5 Vertical Datum Inconsistencies

Modeling of a global set of gravity anomalies based on equation (2.115) assumes that all gravity anomalies $\bar{\Delta g}_{ij}$ refer to a unique global vertical datum. In the absence of such a datum it is possible that subsets of a global gravity data base contain anomalies referring to different (regional) vertical datums. Such inconsistencies between the data have to be considered in the mathematical modeling [Rapp, 1984].

Let H^* be the normal height [Heiskanen and Moritz, 1967, p. 292] of a point P with respect to a unique (but unknown) fundamental level surface, and H_k^* the normal height of the same point referring to the k^{th} regional level surface. Then the normal gravity γ_Q for the corresponding telluroid point Q is (see equation (2.66))

$$\gamma_Q = \gamma_{Q_o} + \left(\frac{\partial\gamma}{\partial h}\right)_{Q_o} H^* + \frac{1}{2!}\left(\frac{\partial^2\gamma}{\partial h^2}\right)_{Q_o} H^{*2}$$

$$= \gamma_{Q_o} + \left(\frac{\partial\gamma}{\partial h}\right)_{Q_o} H_k^* + \frac{1}{2}\left(\frac{\partial^2\gamma}{\partial h^2}\right)_{Q_o} H_k^{*2}$$

$$+ \left[\left(\frac{\partial\gamma}{\partial h}\right)_{Q_o} + \frac{1}{2}\left(\frac{\partial^2\gamma}{\partial h^2}\right)_{Q_o}(H^* + H_k^*)\right](H^* - H_k^*)$$

or

$$\gamma_Q = \gamma_Q^k + \left[\left(\frac{\partial\gamma}{\partial h}\right)_{Q_o} + \left(\frac{\partial^2\gamma}{\partial h^2}\right)_{Q_o}\frac{H^*+H_k^*}{2}\right](H^* - H_k^*) \qquad (2.116)$$

where γ_Q^k is the normal gravity computed from elevation information referring to the regional level surface. Hence,

$$\Delta g \approx \Delta g^k - \left[\left(\frac{\partial\gamma}{\partial h}\right)_{Q_o} + \left(\frac{\partial^2\gamma}{\partial h^2}\right)_{Q_o} H_k^*\right](H^* - H_k^*) \qquad (2.117)$$

where Δg^k denotes the gravity anomaly that refers to the k^{th} regional reference level surface. Parametrization in terms of potential differences is also possible since [Heiskanen and Moritz, 1967, eq. 4-44]

$$H^* = \frac{C_p}{\gamma_{Q_o}}\left[1 + (1 + f + m - 2f\sin^2\phi)\frac{C_p}{a\gamma_{Q_o}} + \left(\frac{C_p}{a\gamma_{Q_o}}\right)^2\right] \qquad (2.118)$$

and

$$C_p = W_o - W_p \qquad (2.119)$$

$$C_p^k = W_o^k - W_p \qquad (2.120)$$

so that

$$\Delta C_p^k = C_p - C_p^k = W_o - W_o^k = \Delta W_o^k \qquad (2.121)$$

Accordingly, equation (2.117) becomes

$$\Delta g \approx \Delta g^k - \frac{1}{\gamma_{Q_o}}\left[\left(\frac{\partial\gamma}{\partial h}\right)_{Q_o} + \left(\frac{\partial^2\gamma}{\partial h^2}\right)_{Q_o} H_k^*\right]\Delta W_o^k \qquad (2.122)$$

In terms of area-mean values equation (2.122) takes the form

$$\bar{\Delta}g_{ij} = \bar{\Delta}g^{k}_{ij} + \left[\frac{2}{\bar{r}_{E_i}} - \left(3J_2\frac{a^2}{\bar{r}_{E_i}^3} + \frac{\omega^2\bar{r}_{E_i}^2}{GM}\right)(\cos^2\theta_i+\cos\theta_i\cos\theta_{i+1}+\cos^2\theta_{i+1})\right.$$

$$\left. + 3\left(J_2\frac{a^2}{\bar{r}_{E_i}^3} + \frac{\omega^2\bar{r}_{E_i}^2}{GM}\right) - 6\frac{H^*_k}{a^2}\right]\Delta W^k_o \qquad (2.123)$$

According to (2.123) equation (2.115) becomes

$$\bar{\Delta}g^{k}_{ij} + \delta g^{ij}_A = \frac{1}{\Delta\sigma_i}\frac{GM}{\bar{r}_{ij}^2}\sum_{n=2}^{\infty}(n-1)\left(\frac{a}{\bar{r}_{ij}}\right)^n\sum_{m=o}^{n}(\bar{C}^*_{nm}IC^j_m + \bar{S}_{nm}IS^j_m)I\bar{P}^i_{nm}$$

$$+ I\hat{E}^{ij}_h + I\hat{E}^{ij}_\gamma + a_1G\delta M + a_2\Delta W + a_3\Delta W^k_o + IE^{ij}_p \qquad (2.124)$$

with

$$a_3 = -\frac{2}{\bar{r}_{E_i}} + \left(3J_2\frac{a^2}{\bar{r}_{E_i}^3} + \frac{\omega^2\bar{r}_{E_i}^2}{GM}\right)(\cos^2\theta_i + \cos\theta_i\cos\theta_{i+1} + \cos^2\theta_{i+1})$$

$$- 3\left(J_2\frac{a^2}{\bar{r}_{E_i}^3} + \frac{\omega^2\bar{r}_{E_i}^2}{GM}\right) + 6\frac{H^*_k}{a^2} \qquad (2.125)$$

As it can be seen from equations (2.110) and (2.125)

$$a_2 \approx -a_3 \qquad (2.126)$$

a relationship which expresses none other than the fact that ΔW and ΔW^k_o cannot be recovered simultaneously from gravity anomaly observations alone. Rather their linear combination

$$\Delta W - \Delta W^k_o = W^k_o - U_o \qquad (2.127)$$

is the only parameter that one might attempt to recover from such data.

2.3.6 Computational Formulas

Equation (2.124) represents the mathematical relationship between surface mean free-air gravity anomalies and potential coefficients, when atmospheric effects, ellipsoidal effects to $O(e^2)$ and vertical datum inconsistencies are taken into account. It is valid with respect to an arbitrary reference ellipsoid since the terms $G\delta M$ and ΔW are accounted for. Before presenting the final formulation used in this study two specific terms in (2.124) must be considered.

The term $a_1 G\delta M + a_2 \Delta W$ will give rise to a nearly constant term in the gravity anomaly if evaluation of (2.124) is made on the surface of a sphere (radius R). It can be easily seen that in such case

$$a_1 G\delta M + a_2 \Delta W = \frac{G\delta M}{R^2} + \frac{2}{R}\Delta W - \left[6J_2 \frac{a^2}{R^3} IP_{20} - \frac{\omega^2 R^2}{GM} IP_{22}\right]\Delta W. \qquad (2.128)$$

The values of $G\delta M$ and ΔW are anticipated to be in the order of the uncertainties of the currently used best estimates of these parameters (see also Rapp, 1983a). Consequently, the very long wavelength latitudinal variation caused by the last term can be neglected in view also of the magnitude of its coefficient. Note that the average gravity anomaly over the sphere R is independent of this term, since its effect will be eliminated if $a_1 G\delta M + a_2 \Delta W$ is averaged over the whole sphere.

If the latitude dependence of $a_1 G\delta M + a_2 \Delta W$ is neglected, one has

$$a_1 G\delta M + a_2 \Delta W \approx -\frac{G\delta M}{\bar{r}_{ij}^{\,2}} + \frac{2}{\bar{r}_{ij}}\Delta W$$

or

$$a_1 G\delta M + a_2 \Delta W \approx -\frac{GM}{\bar{r}_{ij}^{\,2}}\left(\frac{G\delta M}{GM}\right) + \frac{GM}{\bar{r}_{ij} R}\left(\frac{2R\Delta W}{GM}\right) \qquad (2.129)$$

In the analysis of gravity anomalies located on the surface of the earth, the difference between $\bar{r}_{ij}$ and R is disregarded and (2.129) is written as

$$a_1 G\delta M + a_2 \Delta W \approx - \frac{GM}{\bar{r}_{ij}^2} \left(\frac{G\delta M}{GM} - \frac{2R\Delta W}{GM} \right) \qquad (2.130)$$

with R being a mean earth radius. This term can now be incorporated in the harmonic summation in equation (2.124) so that

$$\bar{\Delta g}_{ij}^{k} + \delta g_A^{ij} = \frac{1}{\Delta\sigma_i} \frac{GM}{\bar{r}_{ij}^2} \sum_{\substack{n=0 \\ n\neq 1}}^{\infty} (n-1) \left(\frac{a}{\bar{r}_{ij}} \right)^n \sum_{m=0}^{n} (\bar{C}^{*}_{nm} IC_m^j + \bar{S}_{nm} IS_m^j) I\bar{P}_{nm}^i$$

$$+ I\hat{E}_h^{ij} + I\hat{E}_\gamma^{ij} + a_3 \Delta W_o^k + IE_p^{ij} \qquad (2.131)$$

where

$$\bar{C}^{*}_{oo} = \frac{G\delta M}{GM} - \frac{2R\Delta W}{GM} \; . \qquad (2.132)$$

If $\Delta W=0$, then equation (2.131) is rigorously equivalent to (2.124). However, if $\Delta W\neq 0$, then (2.131) and (2.132) provide only an approximation to (2.124). As it is explained later, in the analysis of an incomplete set of gravity anomalies on the surface of the earth it is crucial to incorporate the $\bar{C}^{*}_{oo}$ term in the modeling, even if $G\delta M=\Delta W=0$, due to the correlations between the unknowns arising from the incomplete coverage. The recovered $\bar{C}^{*}_{oo}$ from such analysis may then be interpreted according to (2.132), mainly to check the consistency of the solution, since physical constants such as GM and W_o (which is related to the semi-major axis a) are more accurately determined from satellite techniques [Rapp, 1983a].

On the other hand, the term ε_p is primarily a function of the deflection of the vertical as it can be seen from equation (2.34). From [Jekeli, 1981, eq. 4.22, with the sign of the fourth term corrected] one has

$$\varepsilon_p = \left[(1-\cos\theta) \frac{\partial W}{\partial h} - \xi \frac{\partial T}{M\partial\phi} - \eta \frac{\partial T}{N\cos\phi\partial\lambda} - \xi \frac{\partial U}{M\partial\phi} \right]_p \qquad (2.133)$$

since $W=U+T$ and U is longitude independent. To examine the magnitude and information content of ε_p, it is helpful to consider the

following approximations

$$\left.\begin{aligned} &\frac{\partial W}{\partial h} \approx -g && \text{(a)}\\ &\frac{\partial T}{M\partial\phi} \approx -\gamma\xi \approx -\frac{\partial T}{r\partial\theta} && \text{(b)}\\ &\frac{\partial T}{N\cos\phi\partial\lambda} \approx -\gamma\eta && \text{(c)}\\ &\frac{\partial U}{M\partial\phi} = -\frac{\partial U}{M\partial\theta} \approx -\frac{\partial U}{r\partial\theta} && \text{(d)}\\ &1-\cos\theta \approx \frac{1}{2}\theta^2 && \text{(e)} \end{aligned}\right\}. \qquad (2.134)$$

According to the above, equation (2.133) becomes

$$\varepsilon_p \approx \left[-\frac{1}{2}\theta^2 g + (\xi^2+\eta^2)\gamma\right]_p + \left[\frac{1}{\gamma}\frac{\partial U}{r\partial\theta}\frac{\partial T}{r\partial\theta}\right]_p. \qquad (2.135)$$

The first term is (2.135) is approximately equal to $\theta^2 g/2$ (since $\theta^2=\xi^2+\eta^2$, and $g_p\approx\gamma_p$). With $g_p\approx\gamma_p\approx 9.8$ m/sec^2 and $\xi=\eta=10''$, the magnitude of this term is found to be about 2 μgals, so that such a term can be safely neglected.

On the other hand, from equation (2.54) one has

$$\frac{\partial U}{\partial\theta} \approx \left[\frac{3GM'}{r} J_2 \left(\frac{a}{r}\right)^2 + \omega^2 r^2\right]\sin\theta\cos\theta \qquad (2.136)$$

and using (2.55) one gets

$$\frac{1}{\gamma}\frac{\partial U}{\partial\theta} \approx \left[3J_2\frac{a^2}{r} + \frac{\omega^2 r^4}{GM'}\right]\sin\theta\cos\theta. \qquad (2.137)$$

Accordingly, equation (2.135) becomes

$$\varepsilon_p \approx \left\{\left[3J_2\left(\frac{a}{r}\right)^2 + \frac{\omega^2 r^3}{GM'}\right]\sin\theta\cos\theta\,\frac{\partial T}{r\partial\theta}\right\}_p. \qquad (2.138)$$

Using a nominal value of 6371 km for r one can verify numerically that

$$3J_2\left(\frac{a}{r}\right)^2 + \frac{\omega^2 r^3}{GM'} \approx e^2 \tag{2.139}$$

Comparing now (2.58a) to (2.138) (in view also of (2.139)), one concludes that the effects of ε_h and ε_p are almost identical both in terms of frequency content and magnitude. Area-mean values of ε_p can thus be computed by rescaling the area-mean values of ε_h, i.e.

$$I\hat{E}_p^{ij} = \frac{c_i''}{c_i'} I\hat{E}_h^{ij} \tag{2.140}$$

where

$$c_i'' = 3J_2 \frac{a^2 GM}{\bar{r}_{E_i}^4} + \omega^2 \bar{r}_{E_i} \tag{2.141}$$

and c_i' is given by (2.83a) with $r = \bar{r}_{E_i}$.

Summarizing, the mathematical model relating area-mean values of surface free-air anomalies to potential coefficients, considered in this study is

$$\bar{\Delta g}_{ij}^k + \delta g_{ij}^s = \frac{1}{\Delta\sigma_i} \frac{GM}{\bar{r}_{ij}^2} \sum_{\substack{n=0 \\ n\neq 1}}^{\infty} (n-1)\left(\frac{a}{\bar{r}_{ij}}\right)^n \sum_{m=0}^{n} (\bar{C}_{nm}^* IC_m^j + \bar{S}_{nm} IS_m^j) I\bar{P}_{nm}^i$$

$$+ a_3 \Delta W_o^k \tag{2.142}$$

where δg_{ij}^s represents the systematic reductions necessary to be applied to the surface mean free-air anomalies and is given by

$$\delta g_{ij}^s = \delta g_A^{ij} - (I\hat{E}_h + I\hat{E}_\gamma + I\hat{E}_p)^{ij} \quad \text{or}$$

$$\delta g_{ij}^s = \delta g_A^{ij} - \left[\left(1 + \frac{c_i''}{c_i'}\right) I\hat{E}_h + I\hat{E}_\gamma\right]^{ij} \tag{2.143}$$

A step-by-step procedure for the numerical evaluation of the terms in (2.142) and (2.143) can be outlined as follows; (the assumption is made in the following that an approximate set of coefficients complete to degree and order N_{max}, and a set of area-mean values of orthometric heights are available).

(i) Evaluate IC_m^j and IS_m^j by

$$IC_m^j = \begin{cases} \frac{2}{m} \sin \frac{m\Delta\lambda}{2} \cos m\bar{\lambda}_j & \text{if } m \neq 0 \\ \Delta\lambda & \text{if } m = 0 \end{cases} \qquad (2.144)$$

and

$$IS_m^j = \begin{cases} \frac{2}{m} \sin \frac{m\Delta\lambda}{2} \sin m\bar{\lambda}_j & \text{if } m \neq 0 \\ 0 & \text{if } m = 0 \end{cases} \qquad (2.145)$$

(ii) Evaluate $I\bar{P}^i_{nm}$. This can be done efficiently using the recurrence relations of Paul (1978). Note that $I\bar{P}^i_{oo}$ yields the spherical area $\Delta\sigma_i$ of the ij^{th} block.

(iii) Evaluate $\bar{r}_{ij}$ from equations (2.95) through (2.97). From the same equations, with $\bar{H}_{ij} = 0$, evaluate $\bar{r}_{Ei}$.

(iv) Evaluate δg^j_λ from (2.80) and $I\hat{E}^j_h$, $I\hat{E}^j_\gamma$ from equations (2.111) and (2.112). Consequently, the systematic reduction δg^s_{ij} to the mean anomaly can be evaluated by (2.143).

(v) If vertical datum inconsistencies are to be parameterized then a_3 in (2.142) can be evaluated from equation (2.125).

A setup as the one described above will enable one to numerically evaluate all coefficients necessary for the formation of observation equations based on the model (2.142).

Concluding this section an important remark should be made about equation (2.142). Theoretically, the convergence of the infinite series in (2.142) is guaranteed only in the region outside the smallest sphere enclosing all the generating masses of the potential (Brillouin sphere). However, to now no successful theoretical argument has been given proving or disproving the convergence of the series on the earth's surface [Jekeli, 1981, p.4]. The intention in this study is to use a truncated version of (2.142) (to $N_{max} \approx 50$), for evaluation on the earth's surface. To this extent the problem of convergence will not be addressed here in view also of the numerical results reported by Jekeli (1981).

2.4 The Alternative Use of Terrain Corrected Anomalies

It was proposed by Moritz (1966, p. 104) that linear solutions to the bvp of Molodensky can be obtained using anomalies reduced to the surface of the reference ellipsoid through the free-air gradient, as follows

$$\Delta g^* = \Delta g - \frac{\partial \Delta g}{\partial h} h \qquad (2.146)$$

where Δg is the surface free-air anomaly and Δg^* the downward continued anomaly.

Moritz [ibid, p. 105, equation 280] has proved that

$$\Delta g^* = \Delta g + G_1 + \frac{1}{R} \sum_{n=0}^{\infty} n(h\Delta g)_n \qquad (2.147)$$

where G_1 is the Molodensky correction term [Heiskanen and Moritz, 1967, p. 307].

For <u>lower degree harmonics</u> one can neglect the term

$$\frac{1}{R} \sum_{n=0}^{\infty} n(h\Delta g)_n \qquad (2.148)$$

as being of the order of h/R. Hence, from (2.147) one obtains

$$\Delta g^* = \Delta g + G_1 \qquad (2.149)$$

On the other hand, it is shown by Moritz (1966, p. 105, equation 285b) that

$$G_1 = G' - \frac{1}{2R} \sum_{n=0}^{\infty} n(\Delta h \Delta g)_n \qquad (2.150)$$

where

$$\Delta h = h - h_m \qquad (2.151)$$

and h_m is a mean elevation of the area in question. G' is a correction term associated with the "Pellinen type solutions" to the bvp of Molodensky [ibid, p. 92]. Neglecting the term

$$-\frac{1}{2R} \sum_{n=0}^{\infty} n(\Delta h \Delta g)_n \qquad (2.152)$$

with the same reasoning as in (2.148), for lower degree harmonics, one has

$$\Delta g^* = \Delta g + G' \qquad (2.153)$$

or in view of (2.146)

$$-\frac{\partial \Delta g}{\partial h} h = G'. \qquad (2.154)$$

In addition, if the assumption is made that the surface free-air anomalies are linearly correlated with elevation, i.e.

$$\Delta g = a + bh \tag{2.155}$$

with a,b being approximately constant, then it is proven in [ibid, equation 262] that G´ becomes identical to the conventional terrain correction tc [Heiskanen and Moritz, 1967, p. 131]. Hence for lower degree harmonics and under the assumption (2.155) one has

$$\Delta g^* = \Delta g + tc. \tag{2.156}$$

Accordingly, if terrain corrections $\bar{tc}_{ij}$ are available in terms of area mean values of the same blocksize as the anomaly data, one can use the values

$$\bar{\Delta g}^*_{ij} = \bar{\Delta g}_{ij} + \bar{tc}_{ij} \tag{2.157}$$

as "observations" in the adjustment, considering these values to refer to the surface of the ellipsoid. Of course the systematic reductions $\delta g^{\bar{s}}_{ij}$ have to be applied in this case as well.

CHAPTER III

DATA USED IN THIS STUDY

3.1 Data Requirements for Surface Gravity Analysis

Estimation of harmonic coefficients of the earth's gravitational potential based on the mathematical formulation presented in Chapter II, requires two types of surface observations; area-mean values of free-air gravity anomalies and area-mean values of orthometric heights. As it was mentioned in the introduction, this study aims to provide optimum estimates of the geopotential based on terrestrial measurements alone. Accordingly, altimetric observations as well as any other type of observations obtained from satellite techniques will not be considered here.

A brief description of the fundamental data bases that were used in this study is given in the following sections, mainly focusing on some of their characteristics that are important to consider for the appropriate use of these data and for accurate interpretation and evaluation of the results.

3.1.1 The June 1986 Gravity Data Base

The surface free-air anomalies used in this study are taken from the "June 1986" data base [Despotakis, 1986], which is the most recent update of the OSU gravity data bank. The June 86 anomaly field contains 48955 1°x1° surface mean free-air anomalies based on the

GRS '67 normal gravity formula [IAG, 1971].

The compilation and updating of global anomaly fields, as the above, is based on the collection and processing of gravity information referring to smaller (regional) areas. Such data subsets ("data sources") contain gravity material in various forms, both in terms of data type (point or area-mean values at various subdivisions, of free-air or Bouger anomalies), as well as in terms of format (maps, tabulated data, magnetic tapes). To obtain from these sources a uniform global set of mean free-air anomaly estimates, some kind of prediction technique (the term prediction is used here in a broad sense) has to be applied to the data of each source. Depending on the nature of the source, the estimation technique varies accordingly, ranging from visual estimation performed on maps, to least squares collocation performed usually to point data or mean data of smaller subdivisions. The task of obtaining a reliable global anomaly field becomes more complicated by the fact that valuable information related to the original observations from which a data source has been compiled (such as the vertical datum to which the gravity anomalies refer or the exact way of computation of normal gravity), is usually not provided. The validity and reliability of the gravity anomaly estimates is deduced from comparisons with previous estimates (wherever possible) or "independent" data sources, such as satellite altimetry derived anomalies (in oceanic areas), or even from the experience and intuition of the person performing the compilation.

Of equal importance with the anomaly estimate itself, is the estimate of its accuracy, which is deduced in most cases in a more or less empirical fashion. Although it is not reasonable to claim that the anomaly estimates in global anomaly fields are uncorrelated, no global field exists at present for which an error covariance function is defined. For regional and more homogeneous data sources, error covariance functions have been developed and tested [Weber and Wenzel, 1982]. However, the inhomogeneity of the data from which global anomaly fields are compiled, as well as the size of these data

bases introduce serious problems on the estimation of global error covariance functions. In this study the error covariance matrix associated with the June 86 anomaly field will be assumed diagonal.

Of particular interest is a subset of 5684 values (about 12%) of the June 86 field, that consists of 1°x1° anomaly estimates which have been derived by means of geophysical correlation (Figure 9). Detailed discussion on that estimation technique is given by Wilcox (1966, 1974, 1978). These anomaly estimates are of inferior quality as compared to observed gravity (Figure 12). The poor quality of these data, in conjunction with their geographical distribution (they cover mostly the extended areas of USSR and China), creates a quite unfavorable environment for the estimation of long wavelength features of the gravity field.

In Table 2 certain statistical quantities referring to the June 86 field are given, while Figures 8 through 12 illustrate some aspects of the geographical distribution and quality of these data.

Table 2. Statistical Characteristics of the June 1986 Anomaly Field

	Northern Hemisphere	Southern Hemisphere	Globally
No. of anom.	28005	20950	48955
Mean value	-0.2	-0.6	-0.4
RMS value	28.1	26.6	27.5
Min value	-270	-222	-270
Max value	340	192	340
Wtd. mean	-0.9	0.4	-0.3
Wtd. RMS	28.5	26.1	27.5
Min. std. dev.	1.0	1.0	1.0
Max. std. dev.	62	47	62
RMS std. dev.	14.0	14.6	14.2

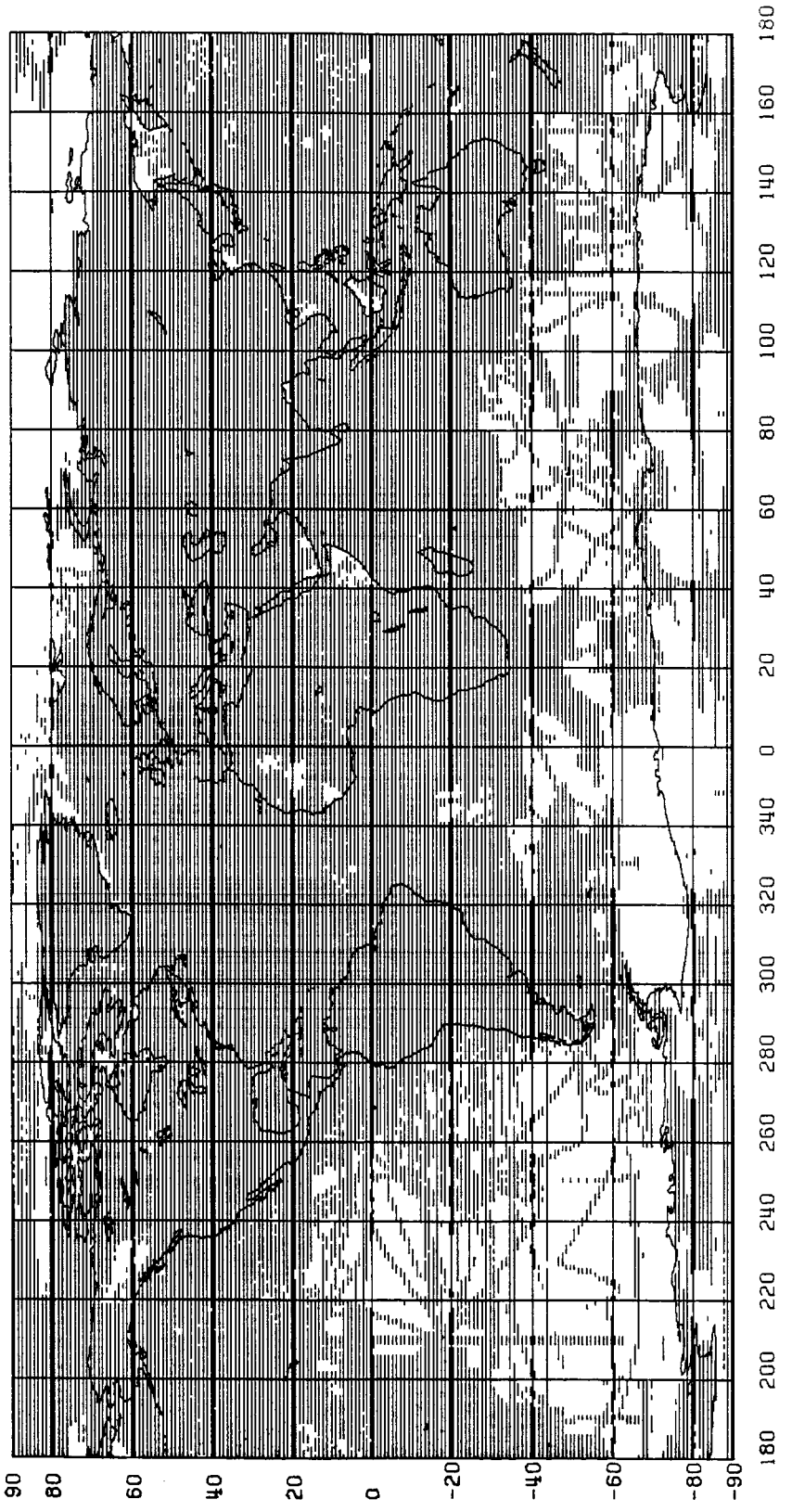

Figure 8. Location of the 48955 1°x1° Anomalies of the June 1986 Field.

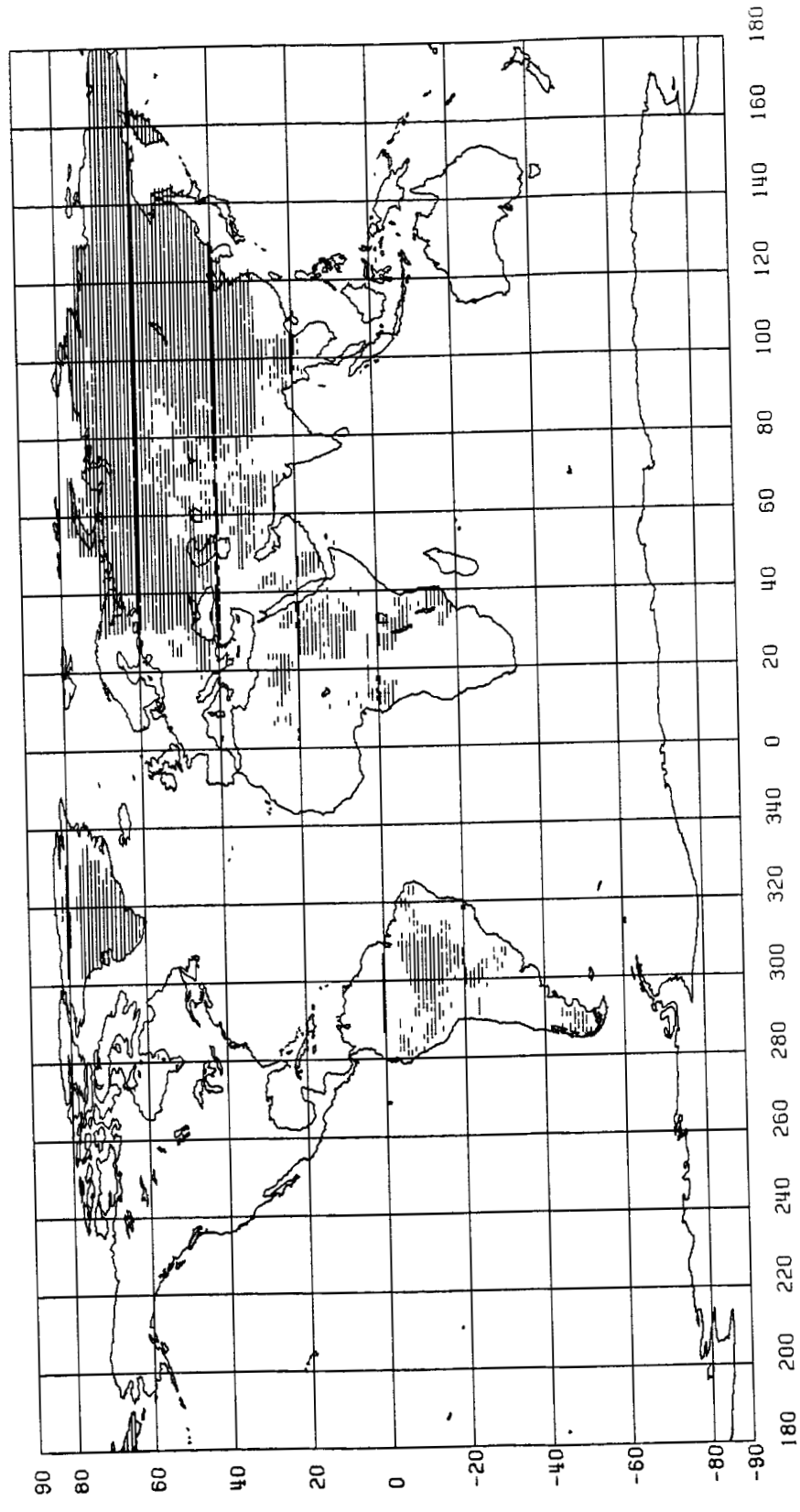

Figure 9. Location of the 5684 Geophysical Anomalies of the June 1986 Field.

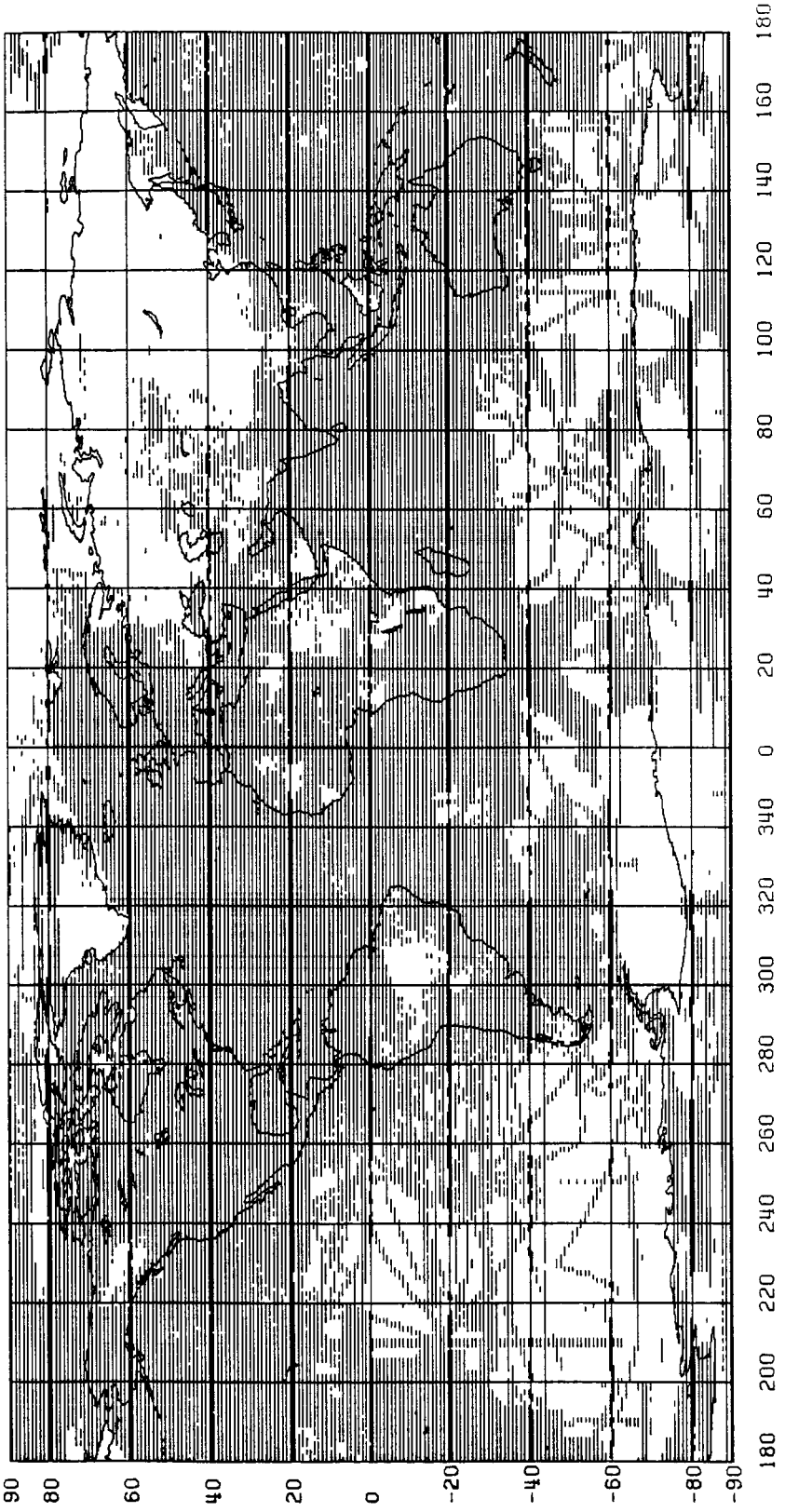

Figure 10. Location of the 43271 Anomalies of the June 1986 Field that Exclude 5684 Geophysical Anomalies

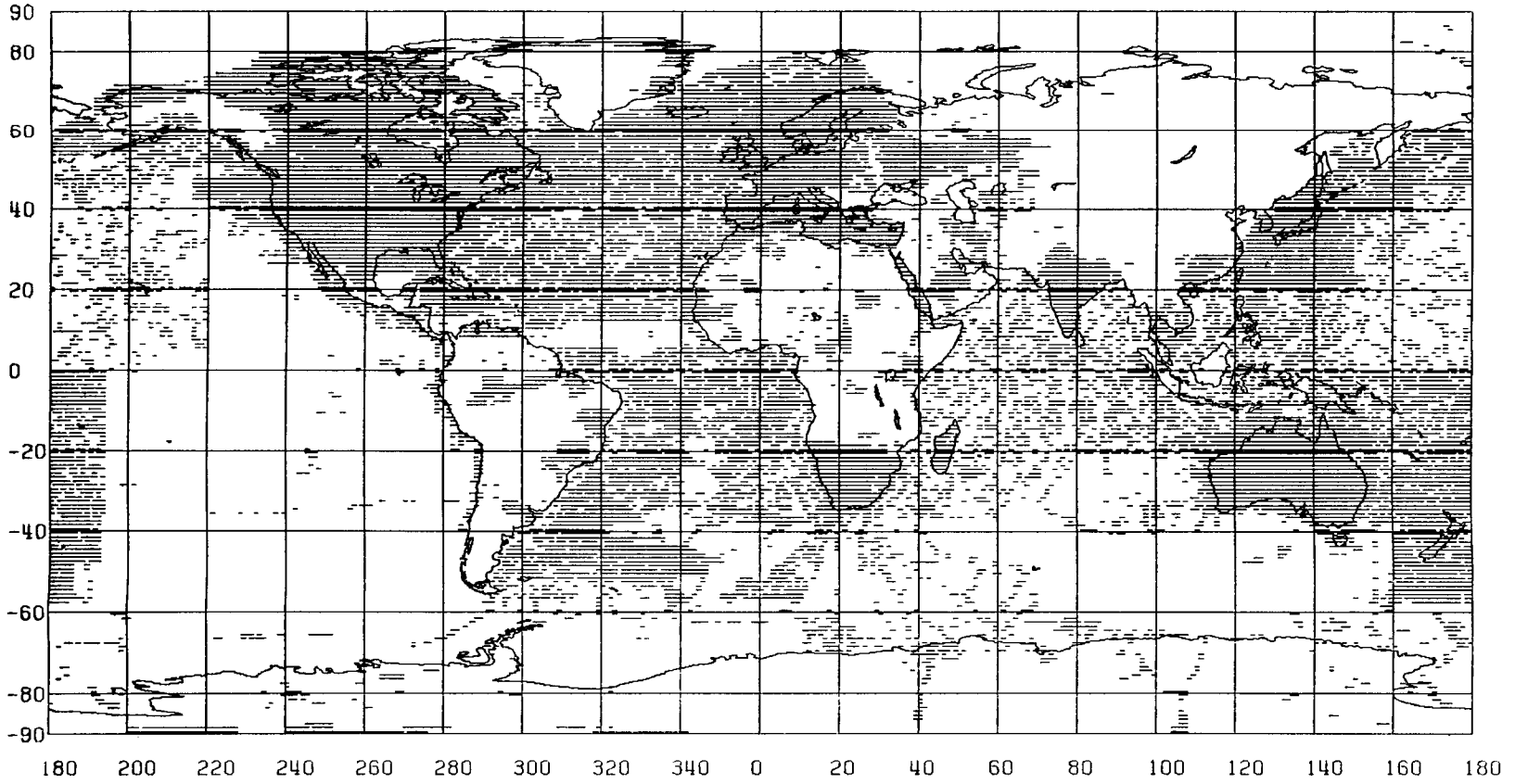

Figure 11. Location of the 21010 Anomalies That Have Standard Deviation ≤ 10 mgals.

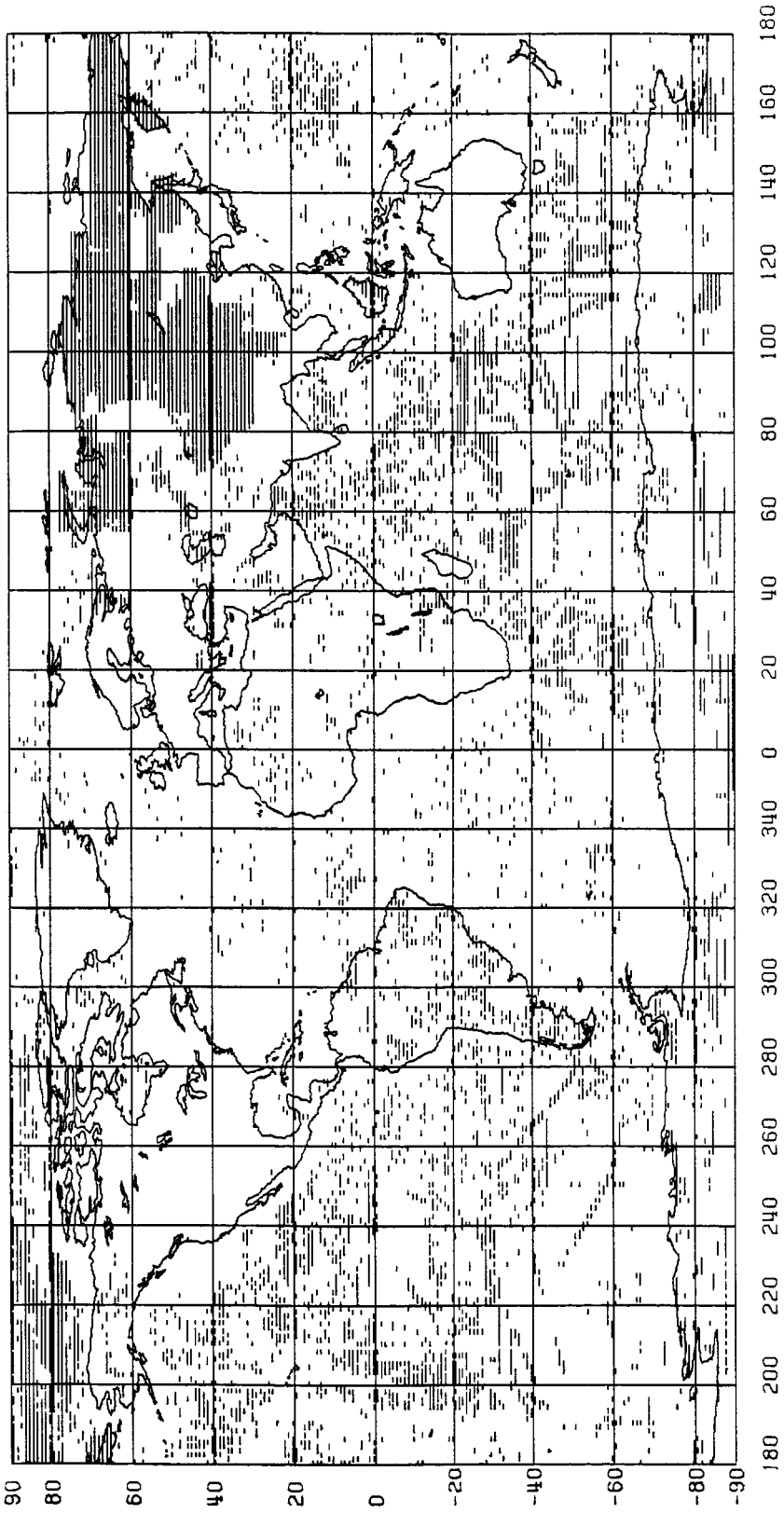

Figure 12. Location of the 9972 Anomalies That Have Standard Deviations ≥ 20 mgals.

In the course of this study three particular issues related to the gravity data have been reconsidered and examined due to their influence on the results; namely

(i) The exact means of computation of the normal gravity γ_Q (see equations (2.67) and (2.69)), which is necessary to define the surface free-air anomaly.

(ii) The conversion of the anomaly data from one reference system (e.g. GRS '67) to another (e.g. the system defined by the constants used in the development of the GEMT1 satellite-only field [Marsh et al, 1987]).

(iii) The frequency content of the 1°x1° mean anomalies of the June 86 field.

(i)

In section 2.3.1 the definition of the surface free-air anomaly and the computational formulas required for rigorous mathematical modeling were given in equations (2.67) through (2.76). Before using the June 86 anomalies it is necessary to examine whether these data comply with these requirements. Although for most of the gravity sources the relevant information is not provided, judging from the most reliable and accurately documented ones (e.g. Source 91 - see Despotakis, 1986), one has to conclude that the second order vertical gradient of the normal gravity is neglected in the definiton of the free-air anomaly. Consequently, in this study it will be assumed that the June 86 field contains area averages of anomalies defined by

$$\Delta g = g_p - \left[\gamma_{Q_o} + \left(\frac{\partial \gamma}{\partial h}\right)_{Q_o} H\right] \qquad (3.1)$$

Probably the terms γ_{Q_o} and $\left(\frac{\partial \gamma}{\partial h}\right)_{Q_o}$ have not been evaluated as prescribed in equations (2.69) through (2.76) (for example the term $\left(\frac{\partial \gamma}{\partial h}\right)_{Q_o}$ is most probably assumed constant, equal to 0.3086 mgal/m); however these approximations will be neglected. The neglect of

the term $\frac{1}{2}\left(\frac{\partial^2\gamma}{\partial h^2}\right)_{Q_o} H^2$ though, cannot be ignored. This term can reach a value of about 4 mgals in regions such as the Himalayas (H ≈ 7000m), and its effect is certainly non-neglible in view also of other more refined corrections (e.g. ε_h). To examine its effect the following computations were performed:

(a) Evaluate a global set (64800 values) of the quantity

$$\delta g_{h^2} = -3\gamma_{Q_o}\left(\frac{\bar{H}_{ij}}{a}\right)^2 \qquad (3.2)$$

The evaluation of γ_{Q_o} is performed on the mid latitude of each block.

(b) Perform a harmonic analysis of the above global set, to define a corresponding set of harmonic coefficients.

(c) From these harmonic coefficients the implied undulation corrections δN_{h^2} can be evaluated in terms of either point or area-mean values. Figure 13 illustrates the corrections δN_{h^2} evaluated on a 5°x5° grid from a harmonic set corresponding to δg_{h^2} which is complete up to N_{max} = 36 (These corrections are to be added to the undulation obtained by omitting δg_{h^2}).

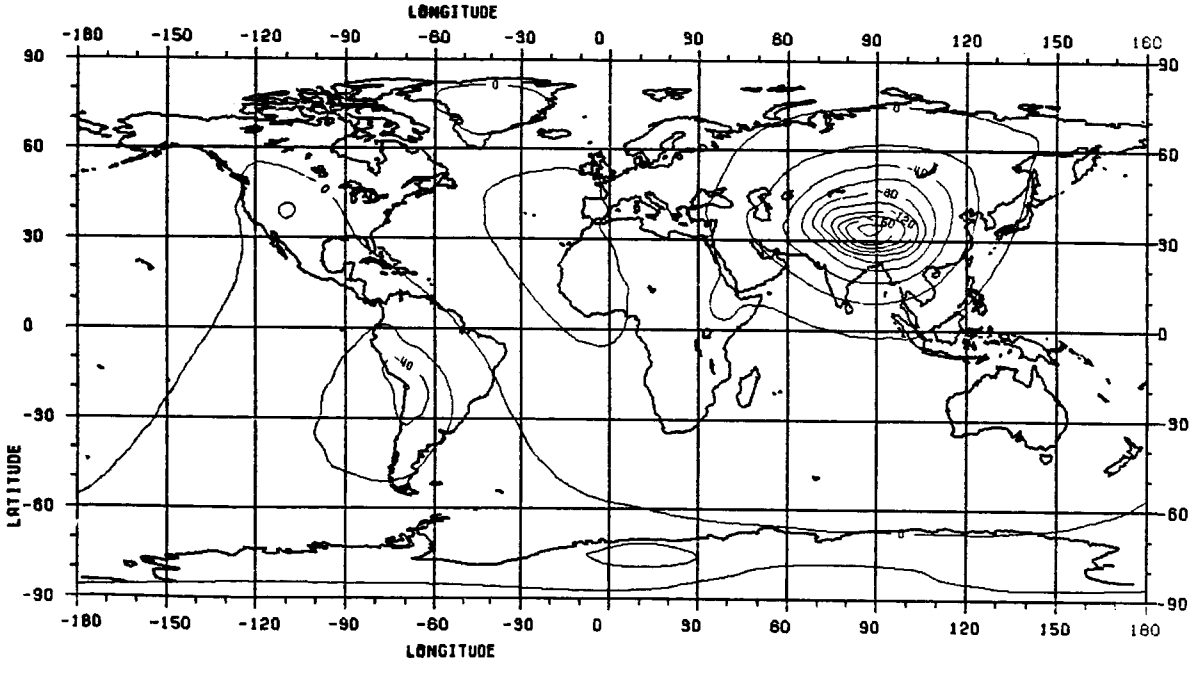

Figure 13. Undulation Correction δN_{h^2} Based on a 5°x5° Grid (Contour Interval is 20 cm).

As it can be seen, the effect reaches a maximum (absolute) of about -1.80 m in the Himalayas. The RMS magnitude of δg_{h^2} (up to N_{max} = 36) is 0.12 mgals, while the RMS δN_{h^2} is 0.22 m. In view of its systematic character and its magnitude (compare with ε_h), it is clear that such a term has to be included in the modeling.

(ii)

The normal equations obtained from the analysis of the surface gravity data are to be combined with the corresponding normal equations from the analysis of the satellite data. For that reason, a common reference system has to be adopted in the analysis of both data sources. In this study such a system will be defined by the "TOPEX constants" [Marsh et al, 1987 Section 4.1.4], i.e.

$$\left.\begin{array}{lll} a & = 6378137. & m \\ 1/f & = 298.257 & \\ GM & = 3986004.36\times10^{8} & m^3/sec^2 \\ \omega & = 7.292115\times10^{-5} & rad/sec \end{array}\right\}. \qquad (3.3)$$

To convert the 1°x1° anomalies of the June 86 field, from the GRS '67 to the TOPEX system, the following formulas are used

$$\bar{\Delta}g_{ij(TOPEX)} = \bar{\Delta}g_{ij(GRS\ 67)} + \delta g^{r}_{ij} \qquad (3.4)$$

where

$$\delta g^{r}_{ij} = d_0 + d_2\sin^2\bar{\phi}_i + d_4\sin^4\bar{\phi}_i \qquad (3.5)$$

and the coefficients d_0, d_2, d_4 are given by [Moritz, 1984]

$$\left.\begin{array}{l} d_0 = \gamma_{e_{GRS67}} - \gamma_{e_{TOPEX}} \\ d_2 = a_{2_{GRS67}} - a_{2_{TOPEX}} \\ d_4 = a_{4_{GRS67}} - a_{4_{TOPEX}} \end{array}\right\} \qquad (3.6)$$

and

$$\left.\begin{aligned} a_2 &= \frac{1}{2}\, e^2 + k \\ a_4 &= \frac{3}{8}\, e^4 + \frac{1}{2}\, e^2 k \end{aligned}\right\} \qquad (3.7)$$

with

$$k = \frac{b\gamma_p}{a\gamma_e} - 1. \qquad (3.8)$$

In terms of numerical values one has

$$\left.\begin{aligned} \gamma_{e_{TOPEX}} &= 9.7803252176 \ \text{m/sec}^2 \\ d_0 &= -0.6762 \quad \text{mgals} \\ d_2 &= -0.0761 \quad \text{mgals/rad}^2 \\ d_4 &= \ \ 0.0007 \quad \text{mgals/rad}^4 \end{aligned}\right\}. \qquad (3.9)$$

Directly related to the reference system used, is the definition of the even degree zonals $\bar{C}^*_{2\ell,0}$ of the disturbing potential. The following are defined for this study:

$$\left.\begin{aligned} \bar{C}^*_{2\ell,0} &= \bar{C}_{2\ell,0} + J_{2\ell}(4\ell+1)^{-\frac{1}{2}} \qquad \ell = 1,2,3 \\ \bar{C}^*_{2\ell,0} &= \bar{C}_{2\ell,0} \qquad\qquad\qquad\qquad \ell > 4 \end{aligned}\right\} \qquad (3.10)$$

with [Moritz, 1984]

$$J_{2\ell} = (-1)^{\ell+1}\, \frac{3e^{2\ell}}{(2\ell+1)(2\ell+3)} \left[1 - \ell + 5\ell\, \frac{J_2}{e^2}\right] \qquad (3.11)$$

and

$$J_2 = \frac{e^2}{3} \left[1 - \frac{2}{15}\, \frac{me'}{q_0}\right]. \qquad (3.12)$$

The numerical values implied for J_2, J_4, J_6 using the TOPEX constants are

$$\left.\begin{aligned} J_2 &= \ \ 0.1082631478 \times 10^{-2} \\ J_4 &= -0.2370919611 \times 10^{-5} \\ J_6 &= \ \ 0.608351 \times 10^{-8} \end{aligned}\right\} \qquad (3.13)$$

The significant digits given here for the zonal coefficients of the normal potential do not imply any truncation of these values. Here the constants given in (3.3), exact to the given digits were used to define the reference system, along with the above equations. The derived values of J_2, J_4, J_6 were transmitted to NASA/GSFC along with the normal equation sets. There, prior to the combination solutions the right side vectors of all normal equation subsets were translated in order to refer to a unique reference system.

It should be mentioned here, that in the course of this study various other sets of constants (such as the OSU 1986 [Rapp and Cruz, 1986a, p. 4] or the GRS '80 [Moritz, 1984]) have been used for the purpose of various experiments (simulated data tests etc). Although these tests could have been performed equally well using the TOPEX constants and their results are hardly affected by the change of the reference values, to avoid confusion the reference values used for each experiment discussed in the sequel are explicitly stated.

(iii)

As it will be discussed in more detail in the next chapter, in the harmonic analysis of an incomplete set of data on the surface of the earth, it is of critical importance that the frequency content of the signal to be analysed be known, at least to an approximate degree. The frequency content of each 1°x1° mean anomaly estimate is primarily a function of the number and distribution of the more detailed data inside the block, from which the 1°x1° mean value has been estimated, as well as, of the estimation method (viewed as a low-pass filter) used to define the 1°x1° mean value. To illustrate the problem, consider the signal being continuously known over the surface of the earth, which for the purpose of this discussion can be viewed as a sphere. Then it would be possible to design an averaging operator (low pass filter) with such response (transfer function), so that any desired band of frequencies would be eliminated from the mean values. However, in fact the type and distribution of detailed data inside each 1°x1° block varies, and so does the prediction techniques used between different

data sources. Hence the frequency content of each area-mean value in a global anomaly field should not be expected to be the same.

The consequences of that problem have been experienced in the current study as will be seen in Section 5.2.5.

3.1.2 The Mean Elevation Data

In the course of this investigation three elevation data bases have been examined:

(i) OCT85.MELEV

(ii) TUG86, and

(iii) TUG87

(i) OCT85.MELEV

This digital terrain model (DTM) is a global complete set (64800 values) of 1°x1° mean elevations and has been compiled based on the DMA 79 model, after gross error corrections have been applied by R.H. Rapp. This set accompanies the June 86 gravity data [Despotakis, 1986], since at that time it was considered the most up to date elevation data base.

This set was not used in any of the computations involved in this study.

(ii) TUG86

This set was compiled by H. Sünkel at the Technical University of Graz and became available at OSU on July 11, 1986. It is also a complete set of 1°x1° mean elevations. It has been compiled based on the OCT85.MELEV for the continental areas and the 5′x5′ SYNBAPS bathymetric data for the oceans. This set was used in almost all of the preliminary investigations in this study.

(iii) TUG87

This set has the same origin and author as the previous one and became available at OSU on July 8, 1987. It has been compiled based

on two DTMs provided by the National Geophysical Data Center in Boulder, the ETOPO5 and the DBDB5 (formerly called SYNBAPS). Details on the set up and characteristics of the TUG87 are given by Wieser (1987). At present TUG87 (which became available in the form of 5′x5′, 30′x30′ and 1°x1° mean values), is considered the most reliable source of elevation information. As soon as it became available, it has replaced TUG86 in the computations made for this study.

In Figure 14 the locations of the 5911 1°x1° blocks where the absolute difference between the TUG87 and the OCT85.MELEV elevation exceeds 1000 m are shown.

It should be mentioned here that the gravity anomaly and elevation data used, should be consistent (see equation (2.69)). However, in the absence of elevation information related to the gravity data sources, one can only use the most reliable elevation data available with reservations concerning their compatibility with the gravity data.

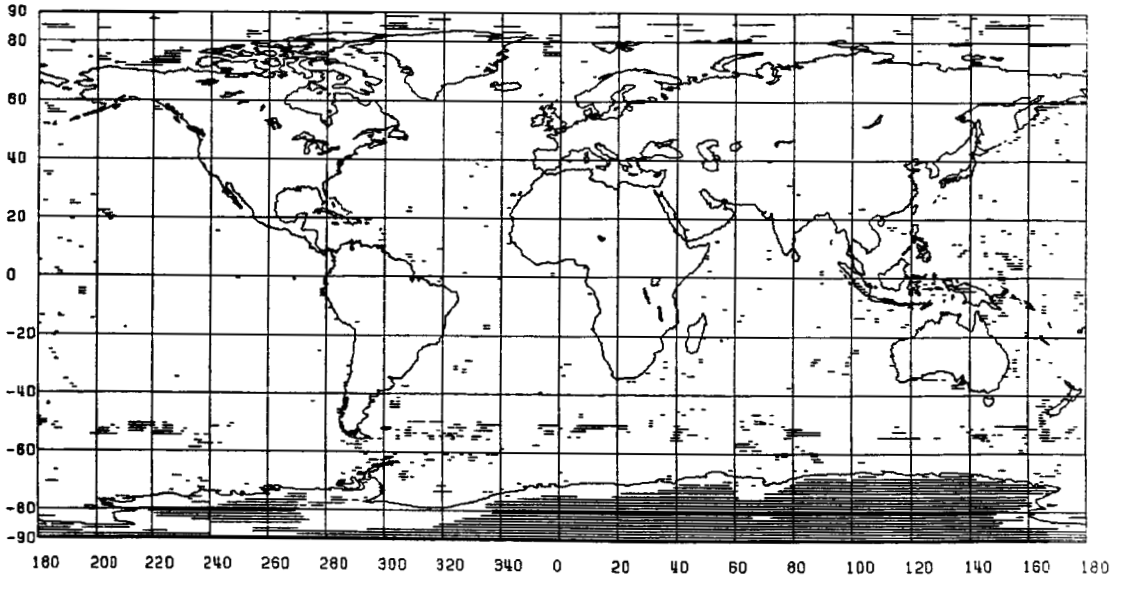

Figure 14. Locations of the 5911 1°x1° Blocks Where $|\bar{H}_{ijTUG87} - \bar{H}_{ijOCT85.MELEV}| > 1000$ m.

CHAPTER IV

ESTIMATION OF HARMONIC COEFFICIENTS OF THE GEOPOTENTIAL

4.1 Combination Solutions

The complementary spectral sensitivity of satellite versus terrestrial observables with respect to the gravity field, necessitates the combination of both data sources in order to obtain optimum estimates for those harmonic coefficients that correspond to frequencies recoverable by both techniques. The fact that satellite observations, such as ranges, range rates etc., can be safely assumed uncorrelated with terrestrial measurements, such as gravity anomalies, permits the combination solutions to be performed in a sequential mode. First two independent estimates of a potential coefficient set are obtained, one from the analysis of satellite data and one from surface gravity data. Then, based on these estimates and their associated covariance matrices an adjustment can be performed in order to yield a unique (with respect to the optimization principle adopted) set of coefficient estimates.

Estimates of harmonic coefficients from orbital analyses are obtained from general dynamical solutions. In these solutions several subsets of observations (different satellites and data types) are used, and the potential coefficients constitute only a subset of the total set of parameters being estimated. This set also includes station coordinates, earth orientation, tidal and orbital parameters.

The modeling and estimation techniques used is such solutions will not be discussed here, since these topics are beyond the scope of the

present study. Elaborate discussions on related topics can be found in Kaula (1966a), Cappellari et al. (1976), Martin et al. (1980) or Marsh et al. (1987). For the purposes of this discussion it suffices to consider a simplified, schematic description of the adjustment process used in satellite solutions.

Let X^a denote the set of potential coefficient parameters, while Y^a the set of all other parameters (orbit, earth orientation, tides). Then, linearization of the functional relations of the satellite observables with respect to X^a and Y^a leads to observation equations of the form (see also Appendix B for the notation)

$$v_s = B\hat{Y} + A_s\hat{X}_s + L_s \qquad (4.1)$$

where

$$L_s = L_s^o - L_s^b \qquad (4.2)$$

and L_s^o denotes the approximate values of the observables computed from the approximate values X^o and Y^o of the parameters. Matrices A_s and B contain the partial derivatives of the observables with respect to X^a and Y^a (evaluated at X^o and Y^o). In principle, the spectrum of the gravitational field extends to infinity so that matrix A_s should have an infinite number of columns. However, at satellite altitudes, only the lower degree harmonics perturb the orbits to the extent that these perturbations can be observed and separated from measurement noise. Therefore, for satellite applications, it is justifiable to truncate the spectrum of the gravitational field to a finite degree.

If P_s denotes the weight matrix associated with L_s^b then minimization of the weighted norm of the residuals $v_s^T P_s v_s$ under the condition (4.1) leads to the normal equation system

$$\begin{bmatrix} B^T P_s B & B^T P_s A_s \\ A_s^T P_s B & A_s^T P_s A_s \end{bmatrix} \begin{bmatrix} \hat{Y} \\ \hat{X}_s \end{bmatrix} = -\begin{bmatrix} B^T P_s L_s \\ A_s^T P_s L_s \end{bmatrix} \tag{4.3}$$

Elimination of the $\hat{Y}$ unknowns from the system (4.3) will result in a system

$$N_s \hat{X}_s = U_s \tag{4.4}$$

where

$$N_s = [A_s^T P_s A_s - (A_s^T P_s B)(B^T P_s B)^{-1}(B^T P_s A_s)] \tag{4.5}$$

$$U_s = [(A_s^T P_s B)(B^T P_s B)^{-1}(B^T P_s L_s) - A_s^T P_s L_s] \tag{4.6}$$

A modification of the above procedure was used in some GEM models [Lerch et al., 1979]. The modification consists of the use of a-priori information for the geopotential coefficients in the form of an a-priori weight matrix P_x which is diagonal with elements equal to the reciprocal degree variances per coefficient as implied by a specified degree variance model (Kaula's rule of $10^{-5}/n^2$). This scheme corresponds to the case of "weighted parameters" [Uotila, 1986, Section 5.5] where the target function to be minimized is not $v_s^T P_s v_s$ but

$$v_s^T P_s v_s + v_x^T P_x v_x = \min \tag{4.7}$$

with v_x denoting the residual associated with the "observed" parameters L_x (see also Appendix B). The effect of this modification in the formulation given above is that the submatrix $A_s^T P_s A_s$ of the normals has to be replaced by $(A_s^T P_s A_s + P_x)$. The advantage of this procedure is that $(A_s^T P_s A_s + P_x)$ is better conditioned than $A_s^T P_s A_s$, a fact which improves the estimability of certain (higher degree) coefficients which are highly correlated [Lerch et al, 1979]. In this particular application of this procedure the observed values of the parameters, L_x, are assumed equal to zero, so that v_x becomes identical to $\hat{X}_s$ [Marsh et al., 1987,

Section 8.1].

In any case, relevant to the following discussion is that a set of normal equations as (4.4) can be obtained from the orbital analysis.

If a corresponding set

$$N_T \hat{X}_T = U_T \tag{4.8}$$

is formed based on terrestrial gravity information, then, in principle, the combination solution can be obtained by

$$\hat{X}_c = (N_s + N_T)^{-1}(U_s + U_T) \tag{4.9}$$

Of course, for (4.9) to be valid the same approximate values have to be used in both the satellite and terrestrial adjustments. Also, questions of relative weighting between N_s and N_T may have to be considered. However, these issues do not change the general principle and strategy of the combination solution as presented above. In the remaining part of this chapter various aspects related to the formation and structure of the normal system (4.8) are examined.

4.2 Estimation of Potential Coefficients from Surface Gravity

The problem of estimating a set of harmonic coefficients of the geopotential from surface gravity data is formulated as follows:

Given:

(a) A set of equi-angular area-mean values of surface free-air anomalies (June 1986 field), which constitutes a subset of the Nx2N ($N = \pi/\Delta\lambda$) set that covers the entire area of the ellipsoid.

(b) A diagonal Σ_{Lb} matrix containing estimates of the error variances of the above data.

(c) A complete (Nx2N) set of mean orthometric heights.

From these data, and based on the mathematical model (2.142) and the systematic reductions δg_{h^2} and δg^r as defined in equations (3.2) and (3.5), one seeks to estimate a set of harmonic coefficients of the geopotential, complete to degree and order N_{max}, where $N_{max} < N$. For reasons that will be explained in the next section, it is assumed that one can evaluate the contribution to each data value of all harmonics of degree $n > N_{max}$. Hence, define

$$(\bar{\delta g}_{hf})_{ij} = \frac{1}{\Delta\sigma_i}\frac{GM}{\bar{r}_{ij}^2}\sum_{n=Nmax+1}^{\infty}(n-1)\left(\frac{a}{\bar{r}_{ij}}\right)^n\sum_{m=0}^{n}(\bar{C}^*_{nm}IC^j_m + \bar{S}_{nm}IS^j_m)I\bar{P}^i_{nm} \tag{4.10}$$

so that one can write (see also equation (2.142))

$$dg_{ij} = \frac{1}{\Delta\sigma_i}\frac{GM}{\bar{r}_{ij}^2}\sum_{\substack{n=0\\ n\neq 1}}^{Nmax}(n-1)\left(\frac{a}{\bar{r}_{ij}}\right)^n\sum_{m=0}^{n}(\bar{C}^*_{nm}IC^j_m + \bar{S}_{nm}IS^j_m)I\bar{P}^i_{nm} \tag{4.11}$$

where

$$dg_{ij} = \bar{\Delta}g_{ij(June86)} + \delta g^s_{ij} + (\delta g_{h^2})_{ij} + \delta g^r_{ij} - (\bar{\delta g}_{hf})_{ij} \tag{4.12}$$

Since the vertical datum inconsistencies have not been modeled in the solutions made for this study, the term ΔW_0^k and the superscript k in the above equations have been omitted.

Equation (4.11) is identified as being of the general form

$$L^a = F(X^a) \tag{4.13}$$

where

$$X^a = [\ldots\ C^{\alpha}_{nm}\ \ldots]^T \quad \begin{cases} n < N_{max},\ m < n \\ \alpha = 0,1 \end{cases} \tag{4.14}$$

with

$$C_{nm} = \begin{cases} \bar{C}^{*}_{nm} & \text{if } \alpha = 0 \\ \bar{S}_{nm} & \text{if } \alpha = 1 \end{cases} \tag{4.15}$$

while the observations L^b are considered to be

$$L^b = [\ldots\ dg_{ij}\ \ldots]^T. \tag{4.16}$$

The function F, as it can be readily seen from (4.11) is linear with respect to the parameters X^a. Hence following the linear observation equations adjustment model [Uotila, 1986, Section 3.2.1], and assuming approximate values equal to zero, one has a set of observation equations

$$v = A\hat{X}^a - L^b \tag{4.17}$$

Hence, with

$$P = \sigma_0^2\ \Sigma_{L^b}^{-1} \tag{4.18}$$

minimization of the weighted norm of the residuals under condition (4.17) yields the normal equation system

$$(A^TPA)\hat{X}^a = A^TPL^b \tag{4.19}$$

and thus the least squares estimate of X^a is given by

$$\hat{X}^a = (A^TPA)^{-1}A^TPL^b \tag{4.20}$$

while the covariance matrix of $\hat{X}^a$ is given by

$$\Sigma_{\hat{X}} = \sigma_0^2(A^TPA)^{-1} \tag{4.21}$$

In terms of a geometric interpretation, it is well known that, if an inner product is defined over the column space of the design matrix A (A must have full column rank) by

$$\langle x,y\rangle_p = x^T P y \tag{4.22}$$

then, the estimate $\hat{X}^a$ above, represents the projection of L^b onto the column space of A.

The estimator $E_{\ell_s} = (A^T P A)^{-1} A^T P$ becomes also the best linear unbiased estimator if the noise n of the observations has zero mean ($E\{n\}=0$) and Σ_{Lb} is defined by

$$\Sigma_{Lb} = E\{nn^T\} \tag{4.23}$$

In addition if the probability distribution of n is Gaussian, then E_{ℓ_s} represents the maximum likelihood estimator as well [Colombo, 1981].

4.2.1 Structure and Characteristics of the Normal Equations

Although the presentation given in the previous section completely defines the adjustment procedure used in this study, it is useful to re-examine some of the equations given before when these are written in explicit analytical form rather than in compact matrix notation. Such considerations are not only useful because they provide insight on the structure and characteristics of the normal system (4.19), but, become necessary also since the large size of certain matrices involved in the adjustment process prohibits the direct use of matrix operations.

Analytical expressions for the elements of the matrices of the normal system can be derived in a compact form useful for further interpretation, only if the effect of data gaps (locations where no observation is available) is considered in an indirect manner. In the

following derivations an empty block is considered to contain an undefined data value with weight equal to zero. Such treatment of data gaps enables a compact and patterned formulation, efficient for numerical implementation, and yields identical results with the straight forward approach. It should be emphasized that this is to be interpreted only as a tool to simplify derivations and computational algorithms. It has no impact on the positive definiteness of the weight matrix of the observations or the degrees of freedom of the adjustment.

From (4.11) it can be seen that the elements of the design matrix A are given by

$$[A]^{ij}_{C^{\alpha}_{nm}} = \frac{1}{\Delta\sigma_i}\frac{GM}{\bar{r}_{ij}^{\,2}}(n-1)\left(\frac{a}{\bar{r}_{ij}}\right)^{n}\bar{Y}^{\alpha ij}_{nm} \tag{4.24}$$

where

$$\bar{Y}^{\alpha ij}_{nm} = \begin{cases} \bar{IP}^{i}_{nm}IC^{j}_{m} & \text{if } \alpha = 0 \\ \bar{IP}^{i}_{nm}IS^{j}_{m} & \text{if } \alpha = 1. \end{cases} \tag{4.25}$$

For an arbitrary element of the normal matrix $N = A^{T}PA$ corresponding to the unknowns C^{α}_{nm} and C^{β}_{rs} one has (since P is assumed diagonal)

$$[N]_{C^{\alpha}_{nm}C^{\beta}_{rs}} = \sum_{i=0}^{N-1}\sum_{j=0}^{2N-1}[A]^{ij}_{C^{\alpha}_{nm}}[A]^{ij}_{C^{\beta}_{rs}}P_{ij} \tag{4.26}$$

or

$$[N]_{C^{\alpha}_{nm}C^{\beta}_{rs}} = GM^{2}(n-1)(r-1)\sum_{i=0}^{N-1}\frac{\bar{IP}^{i}_{nm}\bar{IP}^{i}_{rs}}{\Delta\sigma_i^{\,2}}\sum_{j=0}^{2N-1}\frac{1}{\bar{r}_{ij}^{\,4}}\left(\frac{a}{\bar{r}_{ij}}\right)^{n+r}\begin{Bmatrix} IC^{j}_{m} \\ IS^{j}_{m}\end{Bmatrix}\begin{Bmatrix} IC^{j}_{s} \\ IS^{j}_{s}\end{Bmatrix}P_{ij} \tag{4.27}$$

For a diagonal element corresponding to C^{α}_{nm} one has

$$[N]_{C_{nm}^{\alpha}} = GM^2(n-1)^2 \sum_{i=o}^{N-1} \left(\frac{\bar{IP}_{nm}^{i}}{\Delta\sigma_i}\right)^2 \sum_{j=o}^{2N-1} \frac{1}{\bar{r}_{ij}^{4}} \left(\frac{a}{\bar{r}_{ij}}\right)^{2n} \begin{Bmatrix} IC_m^j \\ IS_m^j \end{Bmatrix}^2 p_{ij} \qquad (4.28)$$

while the corresponding element of $U = A^T P L^b$ is given by

$$[U]_{C_{nm}^{\alpha}} = GM(n-1) \sum_{i=o}^{N-1} \frac{\bar{IP}_{nm}^{i}}{\Delta\sigma_i} \sum_{j=o}^{2N-1} \frac{1}{\bar{r}_{ij}^{2}} \left(\frac{a}{\bar{r}_{ij}}\right)^{n} \begin{Bmatrix} IC_m^j \\ IS_m^j \end{Bmatrix} p_{ij} dg_{ij}. \qquad (4.29)$$

Consider now an idealized case where the observations are given on the surface of a sphere of radius r = a, the Nx2N data grid is full (i.e. no data gaps exist), and all observations have the same standard deviation σ, so that $P = \sigma^{-2}I$. Without loss of generality further assume $\sigma = 1$ to simplify the following expressions. In all subsequent discussion it is assumed that the coefficients being estimated, form a <u>complete</u> set up to degree and order N_{max} where N_{max} is always smaller than $N = \pi/\Delta\lambda$, the Nyquist frequency implied by the data sampling. In such case the previous equations become

$$[A]_{C_{nm}^{\alpha}}^{ij} = \frac{\gamma(n-1)}{\Delta\sigma_i} \bar{Y}_{nm}^{\alpha ij} \qquad (4.30)$$

$$[N]_{C_{nm}^{\alpha} C_{rs}^{\beta}} = \gamma^2(n-1)(r-1) \sum_{i=o}^{N-1} \frac{\bar{IP}_{nm}^{i} \bar{IP}_{rs}^{i}}{\Delta\sigma_i^{2}} \sum_{j=o}^{2N-1} \begin{Bmatrix} IC_m^j \\ IS_m^j \end{Bmatrix} \begin{Bmatrix} IC_s^j \\ IS_s^j \end{Bmatrix} \qquad (4.31)$$

$$[N]_{C_{nm}^{\alpha}} = \gamma^2(n-1)^2 \sum_{i=o}^{N-1} \left(\frac{\bar{IP}_{nm}^{i}}{\Delta\sigma_i}\right)^2 \sum_{j=o}^{2N-1} \begin{Bmatrix} IC_m^j \\ IS_m^j \end{Bmatrix}^2 \qquad (4.32)$$

and

$$[U]_{C_{nm}^{\alpha}} = \gamma(n-1) \sum_{i=o}^{N-1} \frac{\bar{IP}_{nm}^{i}}{\Delta\sigma_i} \sum_{j=o}^{2N-1} \begin{Bmatrix} IC_m^j \\ IS_m^j \end{Bmatrix} dg_{ij} \qquad (4.33)$$

where

$$\gamma = \frac{GM}{a^2} \ . \tag{4.34}$$

However, it is true that the orthogonality of the sine and cosine functions is maintained in the interval $[0,2\pi)$ when discrete mean values of these functions are regularly sampled, provided that the Nyquist frequency is not exceeded. Hence,

$$\left.\begin{aligned} \sum_{j=0}^{2N-1} IC_m^j IC_s^j &= 0 \qquad \text{if } m \neq s < N \\ \sum_{j=0}^{2N-1} IS_m^j IS_s^j &= 0 \qquad \text{if } m \neq s < N \\ \sum_{j=0}^{2N-1} IC_m^j IS_s^j &= 0 \qquad \text{for all } m \text{ and all } s \end{aligned}\right\} \tag{4.35}$$

Equations (4.35) can be proven easily if one recognizes that [Colombo, 1981, p. 4, equation 1.7]

$$\begin{Bmatrix} IC_m \\ IS_m \end{Bmatrix}^j = \begin{Bmatrix} A(m) \\ -B(m) \end{Bmatrix} \cos m j\Delta\lambda + \begin{Bmatrix} B(m) \\ A(m) \end{Bmatrix} \sin m j\Delta\lambda \tag{4.36}$$

where

$$\left.\begin{aligned} A(m) &= \begin{cases} \dfrac{\sin m\Delta\lambda}{m} & \text{if } m \neq 0 \\ \Delta\lambda & \text{if } m = 0 \end{cases} \\ B(m) &= \begin{cases} \dfrac{\cos m\Delta\lambda - 1}{m} & \text{if } m \neq 0 \\ 0 & \text{if } m = 0 \end{cases} \end{aligned}\right\} \tag{4.37}$$

and makes use of the relationships [ibid, p. 10, equation 1.20-a]

$$\left.\begin{array}{ll} \sum_{j=0}^{2N-1} \cos mj\Delta\lambda \cos pj\Delta\lambda = 0 & \text{if } m \neq p < N \\ \sum_{j=0}^{2N-1} \sin mj\Delta\lambda \sin pj\Delta\lambda = 0 & \text{if } m \neq p < N \\ \sum_{j=0}^{2N-1} \cos mj\Delta\lambda \sin pj\Delta\lambda = 0 & \text{for all } m \text{ and all } p \end{array}\right\}. \qquad (4.38)$$

In addition the equatorial symmetry of the grid ($\Delta\sigma_i = \Delta\sigma_{N-i-1}$) in conjunction with the parity properties of the integrated values of the associated Legendre functions, namely

$$I\bar{P}^{i}_{nm} = (-1)^{n-m} I\bar{P}^{N-i-1}_{nm} \qquad (4.39)$$

yield

$$\sum_{i=0}^{N-1} \frac{I\bar{P}^{i}_{nm} I\bar{P}^{i}_{rs}}{\Delta\sigma_i^2} = 0 \qquad \text{if } n-r \text{ is odd.} \qquad (4.40)$$

Hence, from (4.31), (4.35) and (4.40) follows that (see also [Colombo, 1981, equation 2.85])

$$[N]_{C^{\alpha}_{nm} C^{\beta}_{rs}} = 0 \qquad \text{if} \begin{cases} \alpha \neq \beta \text{ , } m \neq s \\ \quad \text{or} \\ n - r \text{ is odd} \end{cases} \qquad (4.41)$$

while if neither of the conditions in (4.41) apply then $[N]C^{\alpha}_{nm}C^{\beta}_{rs}$ may or may not be zero.

Since an element of the normal matrix N also represents the inner product of the corresponding columns of the design matrix A and since these columns consist of successions of the area averages of the surface spherical harmonics (see equation (4.30)), the relation (4.41) implies that:

(a) The area averages of the surface spherical harmonics do not constitute an orthogonal set of base functions on the sphere, even if the sampling is regular and the Nyquist frequency is not

exceeded. The non-orthogonality (or skewness) of this set of base functions implies that if a function (such as the gravity anomaly) defined by discrete, regular, area-mean samples of it (such as the dg_{ij}), is spectrally decomposed with respect to the above set of base functions, using quadrature formulas (see Section 4.2.2), then, synthesis of these spectral components will fail to recover the sampled values. The discrepancies between the original and the synthesized samples is due to the omission of the existing correlations between the base functions when quadrature formulas are used (see equation (4.47)). These correlations arise from the use of a finite sampling interval and occur not only in the case of area-mean samples (as stressed by Mainville (1986, p. 105)) but also in the case of regular, point value samples as it is formally shown by Colombo (1981, p. 53).

(b) Since the normal matrix N is not diagonal, the estimated coefficients from a least squares adjustment are correlated (even if the sampling is regular and the Nyquist frequency is not exceeded). Hence, if a complete set of coefficients up to N_{max} is estimated from a noiseless signal (simulated data) containing frequencies beyond N_{max}, then the estimated coefficients will be distorted with respect to the "true" ones. This effect is called aliasing. However, it should be emphasized here that the cause of it is the finite block size which destroys the orthogonality of the surface harmonics and <u>not</u> the exceeding of the Nyquist frequency by the set of coefficients being estimated. In Section 5.2.4 the results from a number of experiments performed in order to illustrate these aspects are presented.

We should note also that the conclusions drawn above are valid not only for the sphere, but in general for any surface of revolution symmetrical about the "equator" (e.g. an ellipsoid of revolution), provided that the data grid is symmetrical with respect to the equator and $\Delta\lambda$ is constant. Also the use of a unit weight matrix is not necessary. The same conclusions could have been drawn using weights for the anomaly data that are longitude independent and symmetric with

respect to the equator, i.e. $p_i = p_{N-i-1}$.

Proceeding from the idealized situation examined above to the "real world" case corresponding to the problem at hand, it is realized that the patterned structure of the normals will be destroyed once data gaps, unequal weights and data referring to the earth's surface are introduced. The dominant factor affecting the structure of the normals is the data gaps. Their arbitrary locations make it practically impossible to predict their effect on the elements of the normal system. If a rigorous adjustment procedure is to be used then the entire normal matrix (upper triangular part) has to be formed. Otherwise, if an approximate solution is sought, considering only a limited bandwidth of the normal matrix, a particular ordering of the unknowns has to be used so that the largest (in absolute sense) off-diagonal elements can be brought closest to the diagonal. Such ordering may approximately be determined by examining the pattern of the off-diagonal elements from test solutions [Wenzel, 1985]. To illustrate the effect of the ordering of the coefficients in conjunction with the data gaps, on the structure of the normal matrix, the following examples were performed. We considered six different ordering patterns of the unknown coefficients, as schematically shown on Table 3. For each particular ordering pattern two sets of normal equations were formed, both referring to an expansion up to $N_{max} = 12$. In both cases the data were assumed to refer to the surface of the reference ellipsoid and to have the same accuracy (P=I). However, the first set of normals is formed from data that are assumed to occupy the 48955 locations of Figure 8, while the second from data assumed to occupy the 43271 locations of Figure 10. From these normal matrices the corresponding correlation matrices were formed.

In Figure 15 the structure of these correlation matrices for two particular ordering patterns is illustrated, for each case of data coverage. Each "x" denotes a correlation coefficient that is larger than or equal (in absolute value) to 10%. The number of such values in cases (a) and (c) is 1569 while in cases (b) and (d) is 3724. The

Table 3. Ordering Patterns for the Unknown Coefficients

ORDERING PATTERN					
I	II	III	IV	V	VI
C00	C00	C00	C00	C00	C00
C20	C20	C20	C20	C20	C20
C21	C21	C21	C30	C30	C30
C22	C22	S21	C21	C21	C21
C30	S21	C22	C31	C31	S21
C31	S22	S22	C22	S21	C31
C32	C30	C30	C32	S31	S31
C33	C31	C31	C33	C22	C22
S21	C32	S31	S21	C32	S22
S22	C33	C32	S31	S22	C32
S31	S31	S32	S22	S32	S32
S32	S32	C33	S32	C33	C33
S33	S33	S33	S33	S33	S33

advantage of ordering V over ordering I in case of a solution considering only a limited bandwidth of the normals is rather profound. Pattern V differs from the pattern discussed by Colombo (1981, p. 53) only by the fact that the parity of n-m is not taken into account in the ordering of C^{α}_{nm}.

In our case the particular ordering used is really irrelevant since a rigorous solution considering the whole normal matrix will be pursued. For consistency purposes pattern I is used in all solutions here, which is the same with the ordering used in the formation of normals from satellite observations.

Comparing the correlation matrices of Figure 15 by columns one recognizes that the number and locations of the existing data (48955) is more or less sufficient to assure diagonal dominance of the normals. However, the exclusion of the geophysically predicted data results in practically full normal matrices. This fact has an important consequence on the computation of anomaly degree variances from the coefficients obtained from solutions where the geophysically predicted data are excluded, as will be seen in Section 5.3.4. It must be emphasized that

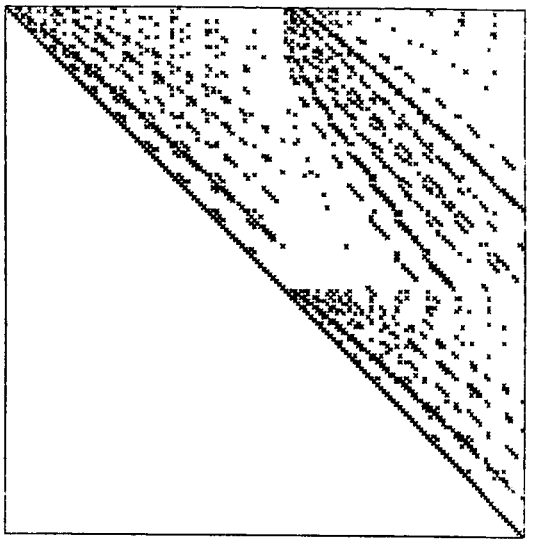

(a) Ordering I
48955 Observations

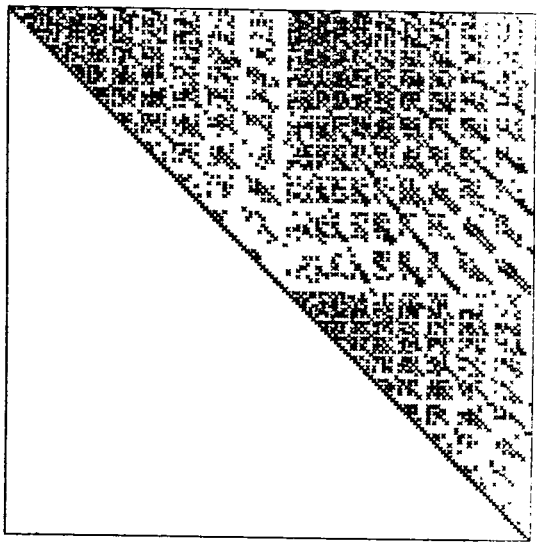

(b) Ordering I
43271 Observations

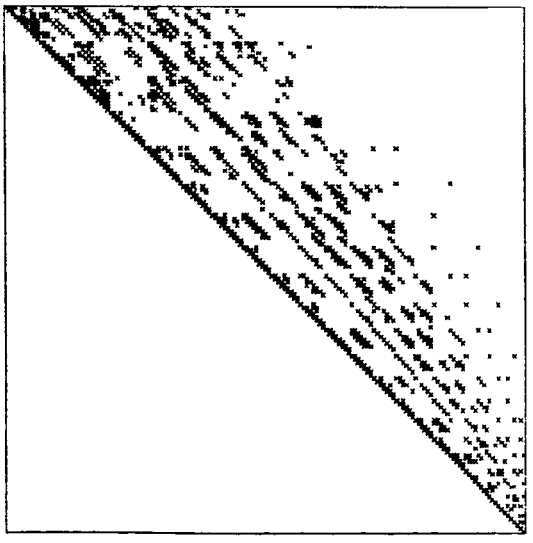

(c) Ordering V
48955 Observations

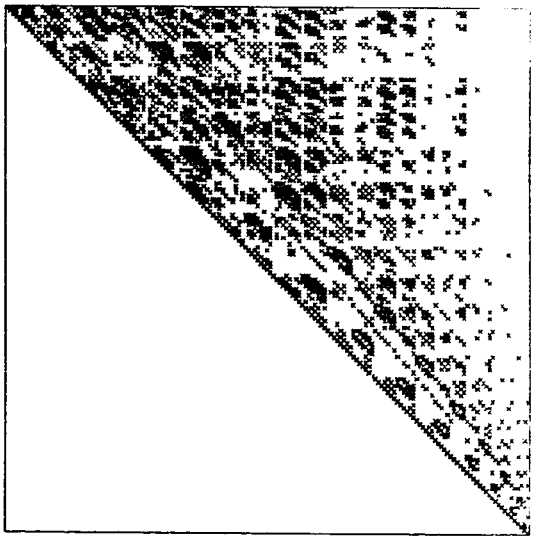

(d) Ordering V
43271 Observations

Figure 15. Structure of Correlation Matrices.

the structure of the normals is affected not only by the number of data points excluded; the location of the resulting empty blocks is also important.

Finally, it should be mentioned that the above results pertain to the case of data of the same accuracy, and thus reflect the influence of the geometry in the structure of the normals. However, in the more realistic case where the accuracy of the data varies, the structure of the normals will be also influenced by the variation of the weight from one measurement to another.

4.2.2 The Least Squares Adjustment as Compared to Quadrature Formulas

Numerical quadrature formulas (i.e. discretized couterparts of the orthogonality relations) have been proposed by Kaula (1966b) and extensively studied and used by Rapp (1969, 1977, 1981, 1984, 1986, 1986a,b) for the estimation of potential coefficients from discrete mean values of gravity anomalies. A comparison of this technique to the least squares adjustment procedure was already made at the "early days" of global gravity modeling [Rapp, 1969]. It is considered appropriate here to briefly present some important aspects of such a comparison in a slightly different way.

Consider that a complete (Nx2N) set of anomaly data dg_{ij} is defined on the surface of a sphere of radius r = a. A set of coefficients C^{α}_{nm} which would minimize the quantity

$$\Phi(C^{\alpha}_{nm}) = \sum_{i=0}^{N-1} \sum_{j=0}^{2N-1} \left[dg_{ij} - \frac{\gamma}{\Delta\sigma_i} \sum_{\substack{n=0 \\ n\neq 1}}^{Nmax} (n-1) \sum_{m=0}^{n} \sum_{\alpha=0}^{1} C^{\alpha}_{nm} \bar{Y}^{\alpha ij}_{nm} \right]^2 \Delta\sigma_i \quad (4.42)$$

is sought.

For an arbitrary coefficient C^{α}_{rs} the condition

$$\frac{\partial \Phi}{\partial C^{\alpha}_{rs}} = 0 \quad (4.43)$$

yields

$$\sum_{i=o}^{N-1}\sum_{j=o}^{2N-1} dg_{ij}\bar{Y}_{rs}^{\alpha ij} = \gamma \sum_{\substack{n=o \\ n\neq i}}^{Nmax}(n-1)\sum_{m=o}^{n}\sum_{\beta=o}^{1} C_{nm}^{\beta}\sum_{i=o}^{N-1}\sum_{j=o}^{2N-1}\frac{\bar{Y}_{nm}^{\beta ij}\bar{Y}_{rs}^{\alpha ij}}{\Delta\sigma_i} \qquad (4.44)$$

The condition

$$\sum_{i=o}^{N-1}\sum_{j=o}^{2N-1}\bar{Y}_{nm}^{\beta ij}\bar{Y}_{rs}^{\alpha ij} = 0 \qquad \text{if } \alpha \neq \beta \text{ or } n \neq r \text{ or } m \neq s \qquad (4.45)$$

is imposed so that (4.44) becomes

$$C_{rs}^{\alpha} = \frac{1}{\gamma(r-1)}\left\{\sum_{i=o}^{N-1}\sum_{j=o}^{2N-1}\frac{(\bar{Y}_{rs}^{\alpha ij})^2}{\Delta\sigma_i}\right\}^{-1}\sum_{i=o}^{N-1}\sum_{j=o}^{2N-1} dg_{ij}\bar{Y}_{rs}^{\alpha ij}. \qquad (4.46)$$

Condition (4.45) (in integral form) is automatically fulfilled only if the sampling is continuous (infinitely small sampling interval). Hence, for surface harmonics of the same degree and order, one should expect that departures of their inner products from zero would decrease with decreasing sampling interval.

Note that in view of (4.35) and (4.40) the condition (4.45) reduces to

$$\sum_{i=o}^{N-1}\sum_{j=o}^{2N-1}\bar{Y}_{nm}^{\alpha ij}\bar{Y}_{rm}^{\alpha ij} = 0, \qquad \text{if } n-r \text{ even.} \qquad (4.47)$$

If further the condition that

$$\sum_{i=o}^{N-1}\sum_{j=o}^{2N-1}\frac{(\bar{Y}_{rs}^{\alpha ij})^2}{\Delta\sigma_i} = 4\pi \qquad (4.48)$$

is imposed then from (4.46) one gets

$$C_{rs}^{\alpha} = \frac{1}{4\pi\gamma(r-1)}\sum_{i=o}^{N-1}\sum_{j=o}^{2N-1} dg_{ij}\bar{Y}_{rs}^{\alpha ij} \qquad (4.49)$$

which is recognized to be identical to the quadrature formulas (without quadrature weights q_ℓ) used for the determination of potential coefficients from discrete mean values. Accordingly, quadrature formulas represent a least squares solution provided that:

(i) A complete (Nx2N) set of gravity data dg_{ij} is defined on a sphere.
(ii) The weight function for these data is defined by $p_{ij} = c\Delta\sigma_i$ with c being any positive constant.
(iii) Conditions (4.47) and (4.48) are imposed on the adjustment.

Condition (4.47) amounts to setting all off-diagonal elements of the normal matrix N equal to zero, while (4.48) enforces the diagonal elements to take values

$$N_{C_{nm}^{\alpha}} = 4\pi\gamma^2(n-1)^2 \qquad (4.50)$$

Since these conditions are externally imposed on the system, the quadrature formulas will fail to recover a set of coefficients C_{nm}^{α} from synthetic data dg_{ij} that have been computed from these coefficients [Rapp, 1986].

Colombo (1981) has introduced "quadrature weights" q_ℓ and has modified equation (4.49) to

$$C_{rs}^{\alpha} = \frac{1}{4\pi\gamma(r-1)q_\ell} \sum_{i=0}^{N-1} \sum_{j=0}^{2N-1} \bar{Y}_{rs}^{\alpha ij} dg_{ij}. \qquad (4.51)$$

He has also investigated numerically the definition of q_ℓ in an optimum manner (ibid, p. 76), so that the estimator of the harmonic coefficients defined in (4.51) minimizes the sum of squares of the coefficient errors.

To illustrate these aspects the following numerical tests have been performed.

We started with the Rapp (1981) potential coefficient set complete from $N_{min} = 2$ to $N_{max} = 36$, and computed a complete set (64800 values) of 1°x1° mean anomalies on a sphere of radius R=6378137 m, using the

SSYNTH program of Colombo (ibid, p. 101). From these synthetic data (zero noise) we have attempted to recover the potential coefficients using the following procedures:

(1) Least squares adjustment with weight matrix P = I
(2) Least squares adjustment with weights $p_{ij} = \Delta\sigma_i$
(3) By applying equation (4.46)
(4) By applying equation (4.49), i.e. using quadrature formulas without optimum quadrature weights.

In all cases the entire set of anomalies was used as input. The recovered coefficients from each procedure were then compared to the original ones. The criteria used in the comparisons were the percentage difference by degree and cumulatively, and the anomaly and undulation differences by degree and cumulatively (see also Section 5.2.3 for the definition of these quantities). In Table 4 the results of these comparisons are given. Along with the results of the four methods above, for certain degrees, the results of a corresponding comparison performed by Rapp (1986, p. 378, Table 2) where the recovery of coefficients was attempted using equation (4.51) with q_ℓ defined by Colombo (1981, p. 76) are listed under "Method 5".

Table 4. Comparison of Input and Output Potential Coefficient Sets

	METHOD														
	(1)			(2)			(3)			(4)			(5)		
n	δN	δg	P	δN	δg	P	δN	δg	P	δN	δg	P	δN	δg	P
2	.00	.00	.00	.00	.00	.00	.10	.00	.01	.20	.00	.01	.10	.00	.01
6	.00	.00	.00	.00	.00	.00	.10	.00	.02	.50	.00	.09			
10	.00	.00	.00	.00	.00	.00	.10	.00	.05	.60	.01	.24	.10	.00	.06
12	.00	.00	.00	.00	.00	.00	.10	.00	.09	.40	.01	.34			
18	.00	.00	.00	.00	.00	.00	.10	.00	.16	.50	.01	.74			
24	.00	.00	.01	.00	.00	.01	.10	.00	.32	.50	.02	1.32			
30	.00	.00	.01	.00	.00	.01	.10	.01	.40	.70	.03	2.06	.20	.01	.47
36	.00	.00	.01	.00	.00	.01	.10	.01	.47	.70	.04	2.87			
to 30													.80	.02	.20
to 36	.00	.00	.00	.00	.00	.00	1.00	.02	.22	.30	.12	1.07			

Note: Units of δN are cm; units of δg are mgals; units of P is %

The numerical results shown above merely confirm the conclusions that can be drawn from the theory, i.e.

(i) The least squares adjustment procedure is able to recover exactly the original coefficients; the small percentage differences at degrees 24, 30 and 36 are to be attributed to numerical noise.

(ii) In the case of simulated data (zero noise) the least squares solution is independent of the selection of the weight matrix P. This is expected since in such cases all residuals become identically zero, so that $v^T P v$ reaches its absolute minimum ($v^T P v$ is a quadratic form), regardless of the selection of P. In case of real data, of course, the selection of P influences the final result (we do not consider here an overall scaling of P which does not affect the least squares solution but only its covariance matrix).

(iii) The quadrature formulas, as expected, fail to recover the original coefficients. The discrepancies found in method (3) indicate the effect of condition (4.47), while comparing the results of (3) and (4), one can see the additional effect of imposing condition (4.48). A comparison of the results of methods (3) and (5) reveals that the introduction of q_ℓ as defined in [Colombo, 1981, p. 76], almost compensates the effect of (4.48). However, as expected, the omission of the terms

$$\sum_{i=0}^{N-1} \sum_{j=0}^{2N-1} \bar{Y}_{nm}^{\alpha i j} \bar{Y}_{rm}^{\alpha i j}$$

with n-r even, implied by (4.47) cannot be offset, by the use of quadrature weights. Reversing the argument here, we can view equation (4.46) as an alternative way of defining the quadrature formulas. Such a definition will certainly not relieve one from the distortions of the spectrum caused by the enforcement of condition (4.47), but at least it will not introduce the additional distortions caused by (4.48) which is not needed for the development of equation (4.46). Note that, for computational purposes, the evaluation of the terms

$$\sum_{i=0}^{N-1} \sum_{j=0}^{2N-1} \frac{(\bar{Y}_{rs}^{\alpha i j})^2}{\Delta\sigma_i}$$

appearing in (4.46) is required. Although it is certainly more demanding than the evaluation of q_ℓ, it only depends on the blocksize and the maximum degree of the expansion, so that, it can be performed once with its results stored and used repeatedly in subsequent applications.

Finally, to obtain a quantitative feeling for the effect of condition (4.47), we have formed a set of normals corresponding to an expansion up to $N_{max} = 12$ from a global set of 1°x1° data assumed to refer to the surface of the reference ellipsoid. From this normal matrix the corresponding correlation matrix was then computed. The maximum (absolute) correlation was found to be 48% referring to $\bar{C}^*_{10,0}$ and $\bar{C}^*_{12,0}$.

Let us now return to the problem of the combination solution. We assume that a complete set (Nx2N values) of gravity anomalies are defined on the surface of a sphere. These data now contain noise and are of varying accuracy. In addition a set of potential coefficient estimates is given, obtained from the analysis of satellite observations. This set is accompanied by its covariance matrix. The combination solution can be carried out in two ways which, following Rapp's (1986) notation will be denoted as:

Method A: The estimates of potential coefficients from terrestrial data are obtained from quadrature formulas.
Method B: The estimates of potential coefficients from terrestrial data are obtained from a least squares adjustment.

It is formally shown in Appendix B that in both cases the satellite information enters the combination solution in the same manner (compare equations B.13 and B.33). Hence, any differences in the final result of these methods has to be attributed to the different ways of obtaining the terrestrial estimates of the coefficients. These differences will be

due to:

(i) The different minimization principle used in the least squares adjustment and the quadrature formulas. The minimazation principle in the least squares adjustment uses a weight function $p_{ij} = c/\sigma_{ij}^2$ where σ_{ij}^2 is the variance of each observation and c is any positive constant, while in the quadrature formulas $p_{ij} = c\Delta\sigma_i$. Accordingly quadrature formulas will yield coefficients that tend to reproduce the data regardless of their accuracy variations.

(ii) The introduction of the conditions (4.47) and (4.48) in the case of quadrature formulas. Since these conditons are not fulfilled by area-mean samples of finite blocksize they will distort the spectrum of the field obtained from the terrestrial data analysis.

Unfortunately, the only numerical comparison of the results obtained from the two combination methods, given the same input data, was performed by Rapp (1969) when the gravity data available were much fewer and less accurate as compared to the data available now. It would be of great interest to repeat such a comparison, based on more complete data and more refined modeling techniques.

CHAPTER V

NUMERICAL RESULTS AND COMPARISONS

5.1 The Computational Task - Organization of the Numerical Analysis

Based on the mathematical modeling and the estimation method presented in Chapters II and IV respectively, and using the data described in Chapter III, this study aims to accomplish the following computational goal:

> Form a set of normal equations corresponding to a low degree ($\leq$ 50) harmonic expansion of the geopotential, in an optimum manner.

This set is then to be combined with the corresponding normal equations obtained from satellite data analysis at NASA (Goddard Space Flight Center) for the development of an optimum global gravity model to be used for the TOPEX/POSEIDON mission [Marsh et al, 1987].

In terms of the notation used in Chapter IV, the end product of this work consists of the matrix N_T and the vector U_T appearing in equation (4.8). Obviously, in this analysis we have not restricted ourselves to the formation of the normal equations, but, for each set of normals formed, the adjustment of the terrestrial data was completed by evaluating the adjusted coefficients $\hat{X}_T$, the residuals, as well as the associated statistics ($v^T P v$, $\Sigma_{\hat{X}}$, etc.). These information are essential for comparison purposes, in order to validate our results, identify

potential problems and investigate alternative ways of facing these problems. On the other hand, validation of our results cannot be considered complete unless the quality of the final result of the combination solution is also examined, by performing various comparisons (satellite orbit fits, Doppler undulation comparisons etc.).

The computational effort involved in this study can be roughly divided into four parts:

(i) Software Development

The necessary software to perform the adjustment of the surface gravity data has been developed and thoroughly tested on the IBM-3081 at the Ohio State University.

By far, the most demanding part of the calculation (both in terms of storage and time), is the formation of the matrix N_T and the vector U_T. For a scalar processor it becomes practically impossible to form the normal system for degrees of expansion greater than about 20, even if high speed large machines, such as the IBM-3081 are to be used. For the computations to become feasible the use of a vector processor is necessary. All the normal equation sets discussed in the following were formed on the CRAY X-MP/48 at the Pittsburgh Supercomputing Center (PSC). The software developed was optimized in order to take maximum advantage of vectorization on the CRAY. In Table 5 CPU times related to the performance of the software on the CRAY are given, for various degrees of expansion (N_{max}). For a solution to $N_{max} = 6$ the formation of the normals on the IBM-3081 takes 181.71 seconds. Hence, as it can be seen from Table 5, a speedup of about 60 was achieved by using the CRAY. It was estimated that the formation of normals up to $N_{max} = 50$, which takes less than 2.5 CPU hours on the CRAY, would have taken more than 7 CPU days on the IBM-3081.

Table 5. CPU Times for the CRAY X-MP/48 at PSC

		CPU Time (seconds)	
N_{max}	Number of Unknowns	Formation of the Normals	Inversion
6	46	2.98	.0043
12	166	35.58	.0677
18	358	148.97	.4265
24	622	431.67	1.8640
36	1366	2118.51	16.3983

(ii) Network Setup

From the previous discussion it is clear that the completion of this work involves three research and/or computation centers:

(a) The Ohio State University (OSU), where the preparation of the terrestrial databases, the design of experiments related to the formation of the "terrestrial" normals and the analysis of results from the "terrestrial" point of view (anomaly and undulation comparisons etc.) are being performed.
(b) The Pittsburgh Supercomputing Center (PSC), where the "terrestrial" adjustments are being carried out.
(c) The Goddard Space Flight Center (NASA/GSFC), where the "satellite" normals, the combination solutions and the related comparisons (orbit fits etc.) are being performed.

For that reason it was essential to establish efficient procedures for communication and data exchange between these centers. In Figure 16 the topology of the network established and the activities of each center are schematically presented.

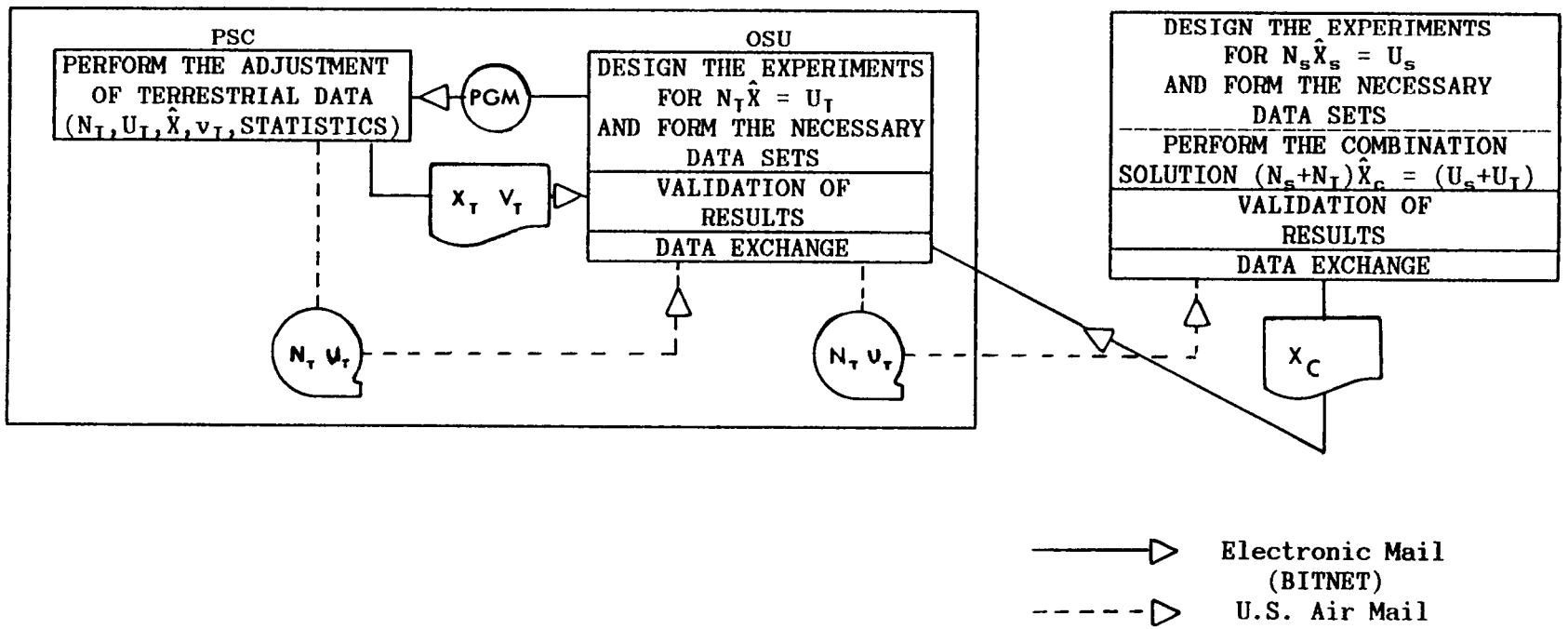

Figure 16. Network Topology.

(iii) Preliminary Investigations

These constitute the main part of the numerical analysis performed in this study. A number of numerical experiments were carried out in order to investigate various aspects of the problem, and to improve the procedures used in the normal equation formation. In Section 5.2 the numerical results and the conclusions drawn from these investigations are presented.

(iv) Validation

The investigation related to this study is still undergoing. Hence, any results to be presented, by no means should be interpreted as "final". Although at present a number of combination solutions have been performed at NASA/GSFC, which include normal equations formed from surface gravity (see Table 7); it would be unfair to comment on these results since they are still under testing. Hence, in Section 5.3 we will attempt to draw some conclusions regarding the quality of our results from comparisons of the terrestrial only solutions with other existing geopotential models.

All the results to be presented refer to expansions up to N_{max} = 36. Although a set of normals up to N_{max} = 50 has been developed recently from surface gravity, it will not be included in the presentation since additional tests and comparisons are still to be performed regarding this set.

5.2 Preliminary Investigations

In the following paragraphs the results of a number of experiments performed in this study are presented and discussed. To simplify the presentation, avoid unnecessary repetitions and provide an easy reference, we will begin with a collective description of the datasets involved in the computations, the setup for each experiment and the criteria adopted for some of the comparisons made.

5.2.1 Description of the Datasets Used

The basic datasets involved in the computations are listed on Table 6 along with the notation adopted for their content. All these datasets contain values corresponding to a 1°x1° equi-angular grid on the ellipsoid. A brief descritpion of these datasets is given next.

(1)-(3)

Synthetic area-mean gravity anomalies computed from the December 1981 potential coefficient set [Rapp, 1981], complete from N_{min} = 2 to N_{max} = 12, 36 and 180 respectively. These values refer to the surface of the reference ellipsoid defined by the GRS '80 geometric constants [Moritz, 1984], whose reference field is defined by the dynamical constants of the same system.

(4)

Contains the surface mean free-air anomalies of the June 1986 gravity data base (48955 values), discussed in Section 3.1.1.

(5)-(9)

These datasets contain the contribution to the 1°x1° mean free-air anomaly from various spectral bands, as computed from different geopotential models. The names used are rather self explanatory of the content of each data set. The reference values used in the formation of all these datasets are the ones used in the development of the OSU86 series of potential coefficient sets [Rapp and Cruz, 1986a, p. 4].

Table 6. Datasets Used in the Numerical Analysis

No.	Dataset Name	Notation
1	DEC81.TO12	sg_1
2	DEC81.TO36	sg_2
3	DEC81.TO180	sg_3
4	JUN86	dg
5	DEC81.FROM37.TO180	hf_1
6	OSU86D.FROM37.TO180	hf_2
7	OSU86F.FROM37.TO180	hf_3
8	OSU86F.FROM181.TO360	hf_4
9	OSU86F.FROM37.TO360	hf_5
10	ELLCORR	ell_1
11	TERRAIN	tc
12	FLAGSWITH	f_1
13	FLAGSWOUT	f_2
14	TUG86	elv_1
15	TUG87	elv_2
16	OSU86F.FROM37.TO360.TOPEX	hf_6
17	ELLTERMS	ell_2

(10)

Contains 1°x1° mean values of the sum of the ellipsoidal correction terms,

$$\hat{IE}_h^{ij} + \hat{IE}_\gamma^{ij}$$

as defined in equations (2.111) and (2.112), computed from the OSU86F geopotential model complete from $N_{min} = 2$ to $N_{max} = 180$. The OSU86 reference values [ibid, p. 4] have been used for this computation.

(11)

Contains 466 values of 1°x1° mean terrain corrections in the continental United States. These data were recevied from the Defence Mapping Agency/Aerospace Center in March 1987. The locations of these data are shown in Figure 17. Their use is discussed in Section 5.2.7.

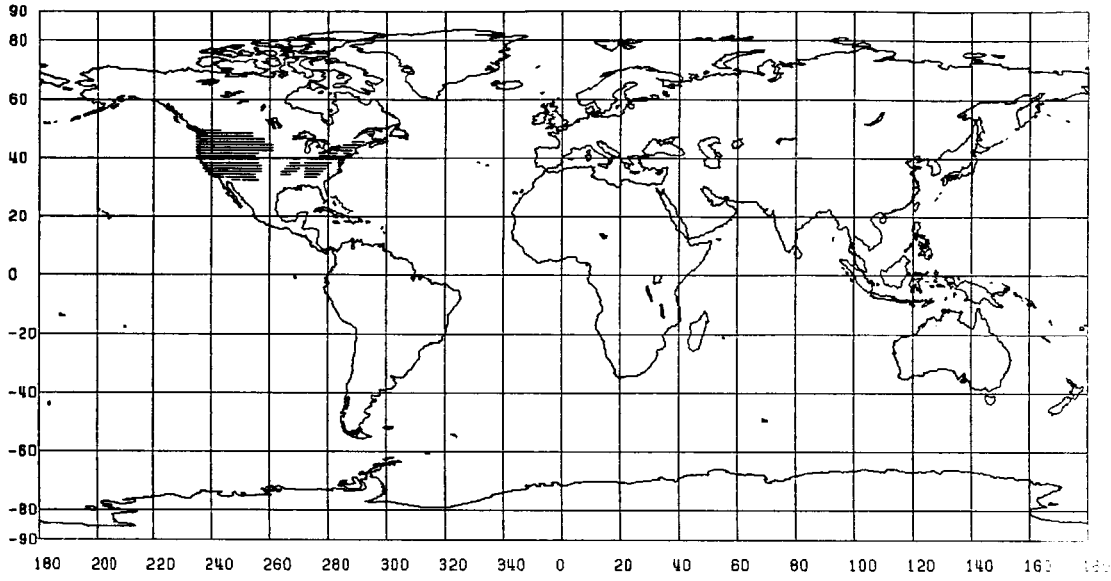

Figure 17. Location of the 466 1°x1° Mean Terrain Corrections Received from DMA/AC.

(12)

This dataset was formed for weighting purposes. To each 1°x1° block a "flag" f_1 is assigned as follows

$$f_1 = \begin{cases} 1 \text{ if } \left| \overline{\Delta g}_{1^\circ \times 1^\circ \text{OSU86F}_{2 \to 36}} - \overline{\Delta g}_{1^\circ \times 1^\circ \text{ADJUST2O}} \right| > 10 \text{ mgals} \\ 0 \text{ otherwise} \end{cases} \quad (5.1)$$

That is, the absolute difference of the 1°x1° mean anomaly implied by the OSU86F geopotential model complete from N_{min} = 2 to N_{max} = 36, and the corresponding adjusted value of the anomaly implied by the terrestrial only solution ADJUST20 (see Table 7), is compared against a threshold value of 10 mgals. The comparison was made only for the locations of the 48955 blocks of Figure 8.

The rationale for the use of this information is discussed in Section 5.3.3.

(13)

Same as above but now the comparison is between the OSU86E and the ADJUST40 (see Table 7) implied anomalies. The comparison was performed only in the locations of the 43271 blocks of Figure 10.

(14)-(15)

Contain the two 1°x1° mean elevation data sets discussed in Section 3.1.2.

(16)

Same as (9) but computed using the TOPEX constants defined in equation (3.3).

(17)

Contains 1°x1° mean values of the quantity

$$\hat{IE}_h^{ij} + \hat{IE}_\gamma^{ij} + \hat{IE}_p^{ij}$$

(see Section 2.3.6), computed from the OSU86F set of potential coefficients complete from N_{min} = 2 to N_{max} = 180. The TOPEX set of constants was used in this computation.

With the exception of (4) and (11), all other datasets listed on Table 6 are complete sets of 64800 values.

Computations of synthetic anomalies and ellipsoidal correction terms were made using the SSYNTH subroutine of Colombo (1981).

5.2.2 The Experiments to be Presented

In Table 7 some of the experiments performed for this study are listed, along with the relevant information concerning the setup of each experiment. With respect to this table the following comments need to be made:

(i) Under the fourth column, the number of data used in each experiment takes three possible values with the following meaning:
64800: applies only in cases where synthetic data are used, since in none of our solutions we have used fill-in anomaly values.
48955: applies in both synthetic and real data experiments and implies that the data used refer to the locations where a gravity anomaly estimate is available in the June 1986 data base (see Figure 8).
43271: as above, but now data referring to the locations of Figure 10 where geophysically predicted data are excluded.

(ii) In the fifth column an entry zero implies that the adjustment was carried out on the ellipsoid. The case of ADJUST30 will be discussed separately in Section 5.2.7.

(iii) In the sixth column an entry 1 implies that unit weight matrix is used. An entry 10 implies that the standard deviation of all anomalies was set to 10 mgals, while σ_{JUN86} implies that the standard deviations of the June 1986 data base were used for the formation of the weight matrix ($p_{ij} = \sigma_{ij}^{-2}(JUN86)$). The entries (20,38), (20,38,f_1) and (20,38,f_2) will be separately discussed in Sections 5.2.6 and 5.3.3.

Table 7. The Experiments to be Presented

No.	Name	Input Data d =	Number of Data Used	Elevation elv =	Standard Deviations	Reference Values Used	Reference	Used in Combined Solutions
1	ADJ020	sg_2	64800	0	1	GRS'80	Sect. 5.2.4	
2	ADJ021	sg_2	48955	0	1	GRS'80	Sect. 5.2.4	
3	SOLV18	sg_3	64800	0	1	GRS'80	Sect. 5.2.4	
4	SOLV19	sg_3	48955	0	1	GRS'80	Sect. 5.2.4	
5	SOLV01	$dg-hf_2$	48955	elv_1	10	OSU86	Sect. 5.2.6	
6	SOLV02	$dg-hf_2$	48955	elv_1	σ_{JUN86}	OSU86	Sect. 5.2.6	
7	SOLV03	$dg-hf_2$	48955	elv_1	(20,38)	OSU86	Sect. 5.2.5 Sect. 5.2.6	
8	SOLV04	$dg-hf_1$	48955	elv_1	(20,38)	OSU86	Sect. 5.2.5	
9	ADJUST02	$dg-hf_3-ell_1$	48955	elv_1	(20,38)	OSU86	Sect. 5.2.5	
10	ADJUST20	$dg-hf_5-ell_1$	48955	elv_1	(20,38)	OSU86	Sect. 5.2.5 Sect. 5.3	PGS3265
11	ADJUST30	$dg-hf_5-ell_1$ tc	48955	$elv_1/0$	(20,38)	OSU86	Sect. 5.3	
12	ADJUST40	$dg-hf_5-ell_1$	43271	elv_1	(20,38)	OSU86	Sect. 5.3	PGS3226 PGS3238
13	ADJUST65	$dg-hf_5-ell_1$	48955	elv_2	$(20,38,f_1)$	TOPEX	Sect. 5.3	PGS3296
14	ADJUST71	$dg-hf_5-ell_1$	43271	elv_2	$(20,38,f_2)$	TOPEX	Sect. 5.3	PGS3297
15	ADJUST81	$dg-hf_6-ell_1$	48955	elv_2	$(20,38,f_1)$	TOPEX	Sect. 5.3	

Finally, we should mention that in the cases where real data were used in the adjustment, the atmospheric correction, the second order vertical gradient correction δg_h^2 (Section 3.1.1) and the conversion of the gravity data from GRS'67 to the reference system used, were applied by the adjustment program. The only systematic reductions that need to be precomputed are the ellipsoidal corrections and the high frequency content of the anomaly data.

5.2.3 Criteria Adopted for the Comparisons

The analysis of the results obtained from the experiments listed above, involved, in most cases, intercomparisons between different sets of potential coefficients. For these intercomparisons a set of criteria established and used by Rapp (1986) has been adopted. These criteria are defined as follows:

(1) The root mean square (RMS) undulation difference by degree and cumulatively.

(a) By degree

$$\delta N_\ell = R\Big[\sum_{m=0}^{\ell}\sum_{\alpha=0}^{1}(\Delta C_{\ell m}^{\alpha})^2\Big]^{1/2} \qquad (5.2)$$

where R is a mean earth radius

(b) Cumulatively

$$\delta N = \Big[\sum_{\ell=2}^{Nmax}\delta N_\ell^2\Big]^{1/2} \qquad (5.3)$$

(2) The root mean square anomaly difference by degree and cumulatively

(a) By degree

$$\delta g_\ell = \gamma(\ell-1)\Big[\sum_{m=0}^{\ell}\sum_{\alpha=0}^{1}(\Delta C_{\ell m}^{\alpha})^2\Big]^{1/2} \qquad (5.4)$$

where γ is an average value of gravity.

(b) Cumulatively

$$\delta g = \left[\sum_{\ell=2}^{Nmax} \delta g_\ell^2\right]^{1/2} \tag{5.5}$$

(3) The percentage differences of the coefficients by degree and cumulatively

(a) By degree

$$P_\ell = \left[\frac{\sum_{m=0}^{\ell}\sum_{\alpha=0}^{1}(\Delta C_{\ell m}^{\alpha})^2}{\sum_{m=0}^{\ell}\sum_{\alpha=0}^{1}(C_{\ell m}^{\alpha})^2}\right]^{1/2} 100 \tag{5.6}$$

(b) Cumulatively (average percentage difference)

$$P = \frac{\sum_{\ell=0}^{Nmax} P_\ell}{N_{max} - 1} \tag{5.7}$$

Note that P_ℓ and P depend on which of the two sets to be compared is used as a reference (denominator of equation (5.6)). In the following presentations the adopted convention is that the set used as reference is always listed first in the pair of coefficient sets being compared.

Another two quantities that can be used to compare two coefficient sets are the average correlation by degree and cumulatively as defined by (Rapp, 1986). In our comparisons these quantities were only cursorily examined.

5.2.4 Recovery of Harmonic Coefficients and Aliasing Effects

The experiments to be discussed next were designed and performed in order to investigate how the recovery of potential coefficients is affected by the frequency content of the sampled signal in conjunction with the completeness or sparsity of the sampling.

The solutions performed for this purpose are ADJ020, ADJ021, SOLV18 and SOLV19, all referring to the recovery of a complete set of coefficients from N_{min} = 2 to N_{max} = 36. In all cases the anomaly data used were noiseless. The setup for these experiments has as follows:

(1) ADJ020: The signal contains the same harmonics as the ones to be recovered and the sampling is complete (64800 values).
(2) ADJ021: The signal contains the same harmonics as the ones solved for, but only 48955 values corresponding to the locations of the anomalies in the June 1986 field are sampled.
(3) SOLV18: The signal contains harmonics from N_{min} = 2 to N_{max} = 180 and the sampling is as in (1).
(4) SOLV19: The signal is as in (3) and the sampling as in (2).

The recovered coefficients from each solution were then compared to the original coefficients which were taken from the December 1981 [Rapp, 1981] gravity model. These comparisons are given on Tables 8 and 9.

Examining the results from ADJ020 (Table 8) we verify that the least squares adjustment recovers exactly the coefficients, if the harmonics contained in the signal are the same as the harmonics estimated, and the sampling is complete.

The results from the comparison of ADJ021 to the original coefficients should be carefully interpreted. First of all they indicate that if 1°x1° mean anomalies are sampled at the 48955 locations corresponding to the locations of the June 1986 data base (Figure 8),

and if these samples are noiseless and contain harmonics from $N_{min} = 2$

Table 8. Comparison of the Coefficients Obtained From Solutions ADJ020 and ADJ021 With the Original Coefficients (December 1981 Field).

		DEC81 -VS- ADJ020			DEC81 -VS- ADJ021		
DEGREE	# OF COEFFS	% DIFF.	UND. DIFF. (METERS)	ANOM. DIFF. (MGALS)	% DIFF.	UND. DIFF. (METERS)	ANOM. DIFF. (MGALS)
2	5	0.00	0.000	0.00	0.00	0.000	0.00
3	7	0.00	0.000	0.00	0.00	0.000	0.00
4	9	0.00	0.000	0.00	0.00	0.000	0.00
5	11	0.00	0.000	0.00	0.00	0.000	0.00
6	13	0.00	0.000	0.00	0.00	0.000	0.00
7	15	0.00	0.000	0.00	0.00	0.000	0.00
8	17	0.00	0.000	0.00	0.00	0.000	0.00
9	19	0.00	0.000	0.00	0.00	0.000	0.00
10	21	0.00	0.000	0.00	0.00	0.000	0.00
11	23	0.00	0.000	0.00	0.00	0.000	0.00
12	25	0.00	0.000	0.00	0.01	0.000	0.00
13	27	0.00	0.000	0.00	0.00	0.000	0.00
14	29	0.01	0.000	0.00	0.01	0.000	0.00
15	31	0.00	0.000	0.00	0.01	0.000	0.00
16	33	0.00	0.000	0.00	0.00	0.000	0.00
17	35	0.00	0.000	0.00	0.01	0.000	0.00
18	37	0.01	0.000	0.00	0.01	0.000	0.00
19	39	0.00	0.000	0.00	0.01	0.000	0.00
20	41	0.01	0.000	0.00	0.01	0.000	0.00
21	43	0.01	0.000	0.00	0.01	0.000	0.00
22	45	0.00	0.000	0.00	0.01	0.000	0.00
23	47	0.01	0.000	0.00	0.01	0.000	0.00
24	49	0.01	0.000	0.00	0.01	0.000	0.00
25	51	0.01	0.000	0.00	0.01	0.000	0.00
26	53	0.01	0.000	0.00	0.01	0.000	0.00
27	55	0.01	0.000	0.00	0.01	0.000	0.00
28	57	0.01	0.000	0.00	0.01	0.000	0.00
29	59	0.01	0.000	0.00	0.01	0.000	0.00
30	61	0.01	0.000	0.00	0.01	0.000	0.00
31	63	0.01	0.000	0.00	0.01	0.000	0.00
32	65	0.01	0.000	0.00	0.01	0.000	0.00
33	67	0.01	0.000	0.00	0.01	0.000	0.00
34	69	0.01	0.000	0.00	0.01	0.000	0.00
35	71	0.01	0.000	0.00	0.01	0.000	0.00
36	73	0.01	0.000	0.00	0.01	0.000	0.00
AVERAGE % DIFF.		0.00			0.01		
RMS UNDULATION DIFF.			0.00			0.00	
RMS ANOMALY DIFF.				0.00			0.00

to $N_{max} = 36$, then these samples are sufficient for an almost perfect recovery of these coefficients. It should be emphasized here that this result pertains only for the particular blocksize used here (1°x1°), the particular number and location of the data gaps and the particular degree of expansion. If any of these "components" of the system changes, one should expect changes in the agreement of the recovered coefficients to the original ones as well, and this is due to the fact that the effect of data gaps is interrelated with the above

"components". For example, if we keep the blocksize and the location and number of data gaps constant, and we start increasing the

Table 9. Comparison of the Coefficients Obtained From Solutions SOLV18 and SOLV19 With the Original Coefficients (December 1981 Field).

		DEC81 -VS- SOLV18			DEC81 -VS- SOLV19		
DEGREE	# OF COEFFS	% DIFF.	UND. DIFF. (METERS)	ANOM. DIFF. (MGALS)	% DIFF.	UND. DIFF. (METERS)	ANOM. DIFF. (MGALS)
2	5	0.14	0.026	0.00	14.08	2.522	0.39
3	7	0.12	0.023	0.01	11.17	2.112	0.65
4	9	0.12	0.012	0.01	18.76	1.809	0.83
5	11	0.16	0.012	0.01	17.49	1.294	0.80
6	13	0.15	0.009	0.01	20.07	1.148	0.88
7	15	0.19	0.009	0.01	18.74	0.911	0.84
8	17	0.23	0.007	0.01	31.44	0.970	1.04
9	19	0.28	0.008	0.01	30.19	0.817	1.01
10	21	0.29	0.006	0.01	36.95	0.834	1.15
11	23	0.41	0.007	0.01	42.23	0.719	1.11
12	25	0.58	0.006	0.01	59.85	0.632	1.07
13	27	0.44	0.006	0.01	43.62	0.633	1.17
14	29	0.68	0.006	0.01	63.69	0.550	1.10
15	31	0.75	0.006	0.01	64.68	0.522	1.12
16	33	0.62	0.006	0.01	49.47	0.469	1.08
17	35	0.78	0.006	0.01	69.33	0.524	1.29
18	37	0.86	0.006	0.02	76.28	0.531	1.39
19	39	0.93	0.006	0.02	82.63	0.516	1.43
20	41	1.30	0.006	0.02	108.05	0.511	1.49
21	43	1.16	0.006	0.02	89.50	0.455	1.40
22	45	1.09	0.007	0.02	77.82	0.465	1.50
23	47	1.33	0.006	0.02	86.32	0.395	1.34
24	49	1.73	0.007	0.03	92.87	0.381	1.35
25	51	1.47	0.006	0.02	84.43	0.369	1.36
26	53	2.34	0.008	0.03	106.05	0.360	1.38
27	55	2.22	0.007	0.03	109.34	0.348	1.39
28	57	2.53	0.009	0.04	87.32	0.317	1.32
29	59	2.56	0.008	0.04	104.11	0.333	1.44
30	61	3.21	0.011	0.05	81.21	0.285	1.27
31	63	3.85	0.011	0.05	114.96	0.319	1.47
32	65	5.79	0.015	0.07	98.85	0.260	1.24
33	67	5.33	0.015	0.08	94.22	0.272	1.34
34	69	6.91	0.023	0.11	65.42	0.214	1.09
35	71	29.88	0.087	0.45	76.60	0.222	1.16
36	73	45.12	0.111	0.59	67.45	0.165	0.89
AVERAGE % DIFF.		3.59			65.58		
RMS UNDULATION DIFF.			0.15			5.02	
RMS ANOMALY DIFF.				0.77			7.06

maximum degree of the harmonics we estimate, (increasing consistently the frequency content of the sampled data), we would experience a degrading in the agreement between the recovered and the original coefficients as the maximum degree increases. In fact, at some point the normal system will become singular, even though the number of observations would still exceed the number of unknowns. The

particular degree at which the singularity will occur depends on the number and locations of the empty blocks.

Such behavior will not be seen if the data grid is full. In that case we will always be able to recover the coefficients exactly (inside the limits of the numerical noise), as long as the maximum degree (and order) of the complete set of estimated coefficients, does not reach or exceed the Nyquist frequency implied by the data sampling. If the maximum degree becomes equal to the Nyquist frequency the normal system becomes singular, although again, the number of observations is larger than the number of unknowns. This is formally proved by Colombo (1981, p. 11).

The results from the comparisons of SOLV18 and SOLV19 with the original coefficients, given in Table 9, serve as an example of the aliasing effect discussed in Section 4.2.1.

In SOLV18, although the Nyquist frequency is not exceeded by the estimated coefficients, and although the sampling is regular and complete, the recovered coefficients are distorted with respect to the original ones. This is due to the fact that the signal has power beyond $N_{max} = 36$ and the correlations between the coefficients from 2 to 36 with the coefficients from 37 to 180 are neglected in SOLV18 (as well as in SOLV19). Schematically we can represent the normal system as follows

$$\begin{bmatrix} N_{11} & N_{12} \\ 2\rightarrow 36 & \\ \hline & N_{22} \\ & 37\rightarrow 180 \end{bmatrix} \begin{bmatrix} \hat{X}_1 & 2 \downarrow 36 \\ \hline \hat{X}_2 & 37 \downarrow 180 \end{bmatrix} = \begin{bmatrix} U_1 \\ \hline U_2 \end{bmatrix} \qquad (5.8)$$

The exact recovery of the harmonics from 2 to 36 would have been given by [Uotila, 1986, p. 155]

$$\hat{X}_1 = (N_{11} - N_{12}N_{22}^{-1}N_{12}^T)^{-1}(U_1 - N_{12}N_{22}^{-1}U_2) \qquad (5.9)$$

while SOLV18 (as well as SOLV19) represent the solution

$$\hat{X}_1^d = N_{11}^{-1}U_1 \qquad (5.10)$$

Since N_{12} is a non-zero matrix, $\hat{X}_1^d$ will be different from the original coefficients represented by $\hat{X}_1$. However, in SOLV18 the only non-zero elements in N_{12} are the ones corresponding to C_{nm}^{α} and C_{rm}^{α} with n-r even (see equation (4.41)). It is thus expected that the distortion of the spectrum from 2 to 36 will be increasing with the degree and in general will be small. Severe distortion occurs close to the "cut-off boundary", as expected. In contrast the introduction of data gaps in SOLV19 masks the diagonal dominance of the normals. The cross-covariance matrix N_{12} diverges far from the zero matrix (see also Figures 15a, 15c), so that its omission in (5.10) causes severe distortions of the spectrum. The particular degrees affected most, are now a function of the number and location of data gaps and the distortion of the spectrum does not necessarily increase with increasing degree any more, as it is verified from Table 9.

5.2.5 Removal of High Frequency Content of the Gravity Anomalies

From the results presented in the previous section it becomes clear, that in order to obtain estimates of the harmonic coefficients from an incomplete set of anomalies, without suffering large distortions of the spectrum due to aliasing effects, the contribution to the anomaly data from all frequencies beyond the ones estimated has to be removed.

In principle, to do so we need to devise an ideal low-pass filter that will effectively eliminate all the high frequency content of the data without distorting the spectrum of the lower frequencies. In practice, to construct such a filter is impossible since the exact

frequency content of each 1°x1° mean value of the gravity anomaly is unknown. There are two alternatives that can be used to approximate such a process:

(1) Based on the 1°x1° mean free-air anomalies, predict mean anomaly values over larger blocks (e.g. for expansions up to N_{max} = 36, use 5°x5° blocks), in an attempt to reduce the high frequency content of the data.
(2) Use an existing geopotential model (which extends beyond the maximum degree and order for which the current solution is attempted), in order to estimate the contribution of the higher frequencies to each 1°x1° mean anomaly, which then can be subtracted from each data value.

Method (1) has the disadvantage that a covariance function between the 1°x1° mean values and the larger blocksize (5°x5°) mean values has to be estimated, for global application, in such a way that it eliminates the power from all frequencies above the ones estimated, and causes the minimum distortion of the lower part of the spectrum. The difficulties involved in such a task are rather obvious. However, it should be mentioned, that if such a goal is achieved, the computational effort to form the normal system would be significantly reduced since much fewer "observations" would be used in the adjustment (for 5°x5° blocks, 2592 values provide global coverage).

In contrast, method (2) leaves the computational effort for the normal equation formation unchanged, but provides much better control over the frequencies which are eliminated and is in general "cleaner" in terms of additonal assumptions and approximations with respect to method (1). For these reasons we have decided to proceed using method (2) in this study. However, before using this procedure we had to investigate and clarify some important aspects. These are:

(a) The sensitivity of the results of the least squares adjustment, with respect to the geopotential model used for the removal of the high

frequency content of the data.

(b) The maximum degree (and order) up to which the high frequency contribution should be computed.

To numerically investigate the first problem we have performed three solutions in each one of which a different high degree field has been used for the removal of the high frequency contribution to the anomalies. In all cases this contribution was computed from harmonic sets complete from N_{min} = 37 to N_{max} = 180. These solutions have as follows:

SOLV04: Removal using the December 1981 field [Rapp, 1981].
SOLV03: Removal using the OSU86D field [Rapp and Cruz, 1986a].
ADJUST02: Removal using the OSU86F field [Rapp and Cruz, 1986b].

The intercomparisons of the results obtained form these solutions are given on Table 10. Before we comment on these results let us first list two properties that the high degree expansion is desirable to have for the purpose that we want to use it:

(i) The surface gravity data used for the high degree expansion should be as consistent as possible with the surface gravity data used in the current solutions. Ideally we would like the high degree expansion to have been developed based on the same surface data with the ones used here. Unfortunately most of the existing high degree fields (e.g. OSU86 series of high degree expansions), have used, in the oceanic regions, primarily altimeter derived anomalies rather than ship-track estimates which are used in this study.

(ii) The high degree expansion should contain a minimum of satellite information so that we do not introduce significant correlations between our reduced observables and the observables used in the orbital perturbation analysis. For this reason it is preferable not to use high degree fields where a large number of satellite derived fill-in values has been used in their development (e.g.

OSU86C or OSU86E).

Returning now to the results of Table 10 we observe that both solutions SOLV03 and ADJUST02 have a substantial and about equal difference from the results of SOLV04. This is expected because OSU86D and OSU86F are almost identical in the range of degrees 37 to 180 (see also [Rapp and Cruz, 1986b, p. 12, Figure 4]), since they have been developed from consistent surface gravity data, while the December 1981 field has been developed from a substantially different set of surface anomalies both in terms of number of data and in terms of quality.

Table 10. Intercomparison of Terrestrial Only Solutions Where Different High Degree Models Were Used for the Removal of the High Frequency Content of the Gravity Anomalies

		SOLV04 -VS- SOLV03			SOLV04 -VS- ADJUST02		
DEGREE	# OF COEFFS	% DIFF.	UND. DIFF. (METERS)	ANOM. DIFF. (MGALS)	% DIFF.	UND. DIFF. (METERS)	ANOM. DIFF. (MGALS)
2	5	2.10	0.385	0.06	3.85	0.707	0.11
3	7	4.40	0.867	0.27	4.02	0.793	0.24
4	9	4.97	0.523	0.24	5.29	0.558	0.26
5	11	7.92	0.532	0.33	7.74	0.520	0.32
6	13	7.77	0.410	0.32	7.81	0.412	0.32
7	15	8.66	0.414	0.38	8.24	0.394	0.36
8	17	12.12	0.375	0.40	12.70	0.393	0.42
9	19	10.77	0.309	0.38	11.48	0.329	0.41
10	21	15.50	0.372	0.51	16.43	0.394	0.55
11	23	15.45	0.344	0.53	16.14	0.359	0.55
12	25	27.34	0.359	0.61	28.48	0.374	0.63
13	27	18.17	0.296	0.55	19.20	0.313	0.58
14	29	29.20	0.285	0.57	29.52	0.288	0.58
15	31	20.17	0.217	0.47	21.08	0.226	0.49
16	33	15.07	0.174	0.40	17.06	0.197	0.46
17	35	19.62	0.203	0.50	21.18	0.219	0.54
18	37	24.73	0.208	0.54	25.69	0.216	0.57
19	39	24.94	0.195	0.54	27.25	0.213	0.59
20	41	30.48	0.185	0.54	34.06	0.207	0.60
21	43	24.34	0.180	0.55	26.08	0.193	0.59
22	45	23.16	0.166	0.54	25.37	0.182	0.59
23	47	23.17	0.156	0.53	24.38	0.164	0.55
24	49	26.48	0.158	0.56	27.33	0.163	0.58
25	51	26.29	0.149	0.55	27.02	0.154	0.57
26	53	27.18	0.135	0.52	28.01	0.139	0.53
27	55	29.88	0.124	0.50	30.15	0.125	0.50
28	57	26.77	0.123	0.51	27.63	0.127	0.53
29	59	31.07	0.130	0.56	30.45	0.127	0.55
30	61	26.68	0.121	0.54	26.01	0.118	0.53
31	63	29.30	0.127	0.59	29.88	0.130	0.60
32	65	29.30	0.107	0.51	29.51	0.108	0.51
33	67	28.44	0.106	0.52	28.43	0.106	0.52
34	69	17.83	0.076	0.38	18.59	0.079	0.40
35	71	22.37	0.094	0.49	22.41	0.094	0.49
36	73	18.18	0.061	0.33	18.59	0.062	0.33
AVERAGE % DIFF.		20.28			21.06		
RMS UNDULATION DIFF.			1.76			1.86	
RMS ANOMALY DIFF.				2.84			2.95

Comparison between ADJUST02 and SOLV03 yields an overall percentage difference of 3.52%, while the RMS undulation and anomaly differences are 0.58 m and 0.46 mgals respectively. However, part of this discrepancy is due to the fact that in ADJUST02 ellipsoidal correction terms have been included, in contrast to SOLV03.

From the point of view of the desirable properties listed before, either one of the two fields OSU86D and OSU86F can be equally well used for the removal of the high frequency content of the data. In the following solutions we have used OSU86F for this removal.

The decision regarding the maximum degree up to which the removal should take place was greatly facilitated by an examination of the residuals obtained from the adjustment of the surface anomalies. In Figure 18 the geographical distribution of the 11404 residuals, obtained from ADJUST02, which exceed (in absolute value) 10 mgals is shown.

Examination of this figure indicates that the residuals are highly correlated with the high frequency content of the anomaly field (observe their signature in the area of the Andes). This observation leads to the following two conclusions:

(i) The frequency content of the 1°x1° mean values of the June 1986 field extends beyond degree 180.

(ii) The neglected correlations between the coefficients from degrees 2 to 36 and the coefficients beyond 181 (see also equation (5.9)) are so small that the contribution of these coefficients to the anomaly data does not contaminate (at least extensively) our solution. Rather this contribution manifests itself in the form of residuals of the adjustment.

Based on the above we have decided in the following solutions to remove from the data the high frequency part corresponding to the harmonics from 37 to 360. This part has been evaluated from the OSU86F set of potential coefficients [Rapp and Cruz, 1986b].

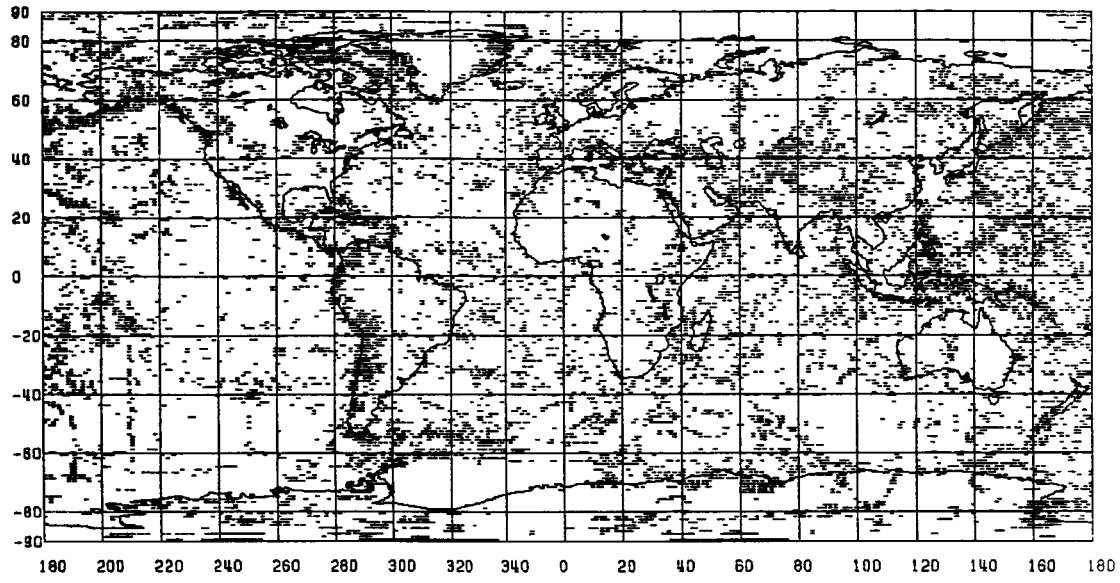

Figure 18. Locations of the 11404 Residuals in ADJUST02 Exceeding in Absolute Value 10 mgals.

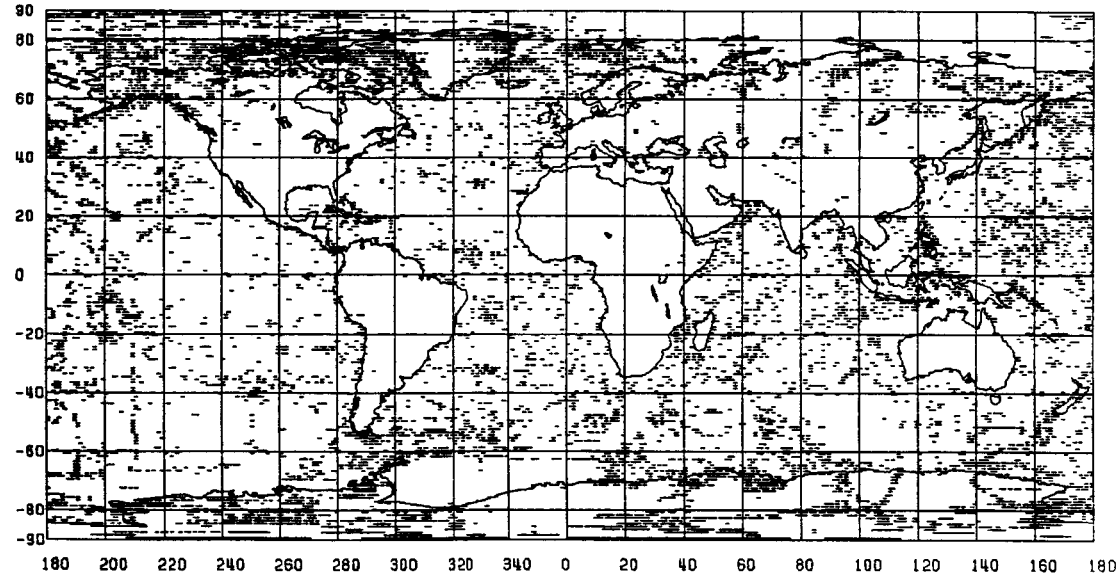

Figure 19. Locations of the 9416 Residuals in ADJUST20 Exceeding in Absolute Value 10 mgals.

A solution of this type is ADJUST20. In Figure 19 the locations of the 9416 residuals from ADJUST20 whose values exceed (in absolute value) 10 mgals are shown. It is interesting to note that in the land regions where the data used in ADJUST20 are consistent with the data in OSU86F, the least squares adjustment yields a remarkable fit.

On the other hand the comparison between ADJUST02 and ADJUST20 yields an overall percentage difference of 8.7% with the RMS undulation and anomaly differences being 0.74 m and 1.15 mgals respectively. When the two solutions ADJUST02 and ADJUST20 are compared to a common standard (the OSU86F field), they yield practically the same differences as it can be seen from the results given on Table 11. These numbers substantiate the argument made in (ii) above.

An additional comment should be made regarding the computation of the contribution of the higher frequencies to the anomaly data. As it can be seen from equation (4.10) this contribution has to be evaluated at the surface level ($r = \bar{r}_{ij}$) in order to be consistent with the anomaly data which refer to the surface of the earth. However, the elevation introduces a long wavelength effect which can be neglected here since we are interested in the high frequency part of the spectrum. Accordingly, in this study, the terms $(\bar{\delta g}_{hf})_{ij}$ were evaluated on the surface of the ellipsoid ($r = r_{Ei}$).

5.2.6 Weighting of the Surface Gravity Data

There are two basic problems associated with the estimation of the error properties of the surface gravity data and their influence on the results of combination solutions:

(a) The assumption that the errors of the surface gravity data are uncorrelated

Table 11. Comparison of Solutions ADJUST02 and ADJUST20 to the OSU86F Geopotential Model

		OSU86F -VS- ADJUST02			OSU86F -VS- ADJUST20		
DEGREE	# OF COEFFS	% DIFF.	UND. DIFF. (METERS)	ANOM. DIFF. (MGALS)	% DIFF.	UND. DIFF. (METERS)	ANOM. DIFF. (MGALS)
2	5	21.26	3.808	0.59	20.18	3.615	0.56
3	7	12.86	2.434	0.75	13.60	2.573	0.79
4	9	19.98	1.928	0.89	20.41	1.970	0.91
5	11	18.23	1.349	0.83	17.92	1.327	0.82
6	13	19.25	1.100	0.85	19.05	1.088	0.84
7	15	21.05	1.008	0.93	20.41	0.978	0.90
8	17	35.00	1.077	1.16	34.22	1.054	1.13
9	19	31.21	0.841	1.03	28.81	0.776	0.95
10	21	34.04	0.762	1.06	33.49	0.750	1.04
11	23	51.33	0.871	1.34	50.33	0.854	1.31
12	25	45.46	0.515	0.87	45.08	0.511	0.86
13	27	37.97	0.548	1.01	36.85	0.532	0.98
14	29	63.66	0.569	1.14	65.76	0.588	1.18
15	31	63.65	0.480	1.03	64.40	0.486	1.05
16	33	71.08	0.572	1.32	70.36	0.566	1.31
17	35	78.48	0.537	1.32	81.36	0.556	1.37
18	37	66.41	0.465	1.22	68.78	0.482	1.26
19	39	71.95	0.449	1.24	76.81	0.479	1.33
20	41	82.13	0.392	1.14	81.40	0.388	1.13
21	43	91.39	0.422	1.30	92.92	0.430	1.32
22	45	68.60	0.372	1.20	67.75	0.368	1.19
23	47	70.15	0.315	1.07	73.55	0.330	1.12
24	49	77.24	0.301	1.06	74.61	0.290	1.03
25	51	61.00	0.298	1.10	61.67	0.302	1.11
26	53	79.36	0.266	1.02	78.80	0.264	1.02
27	55	56.09	0.186	0.74	56.60	0.188	0.75
28	57	51.13	0.198	0.82	49.66	0.192	0.80
29	59	68.49	0.227	0.98	70.15	0.233	1.00
30	61	50.78	0.196	0.88	53.19	0.206	0.92
31	63	53.34	0.177	0.81	5[illegible].00	0.182	0.84
32	65	42.41	0.140	0.67	43.79	0.144	0.69
33	67	46.34	0.160	0.79	48.00	0.166	0.82
34	69	38.21	0.143	0.73	40.37	0.151	0.77
35	71	38.94	0.135	0.71	39.13	0.136	0.71
36	73	37.13	0.111	0.60	38.75	0.116	0.62
AVERAGE % DIFF.		50.73			51.23		
RMS UNDULATION DIFF.			5.89			5.82	
RMS ANOMALY DIFF.				5.91			5.95

(b) The need for an appropriate relative weighting scheme, so that an optimum combination of the satellite and terrestrial normal equations can be achieved.

It was mentioned before (Section 3.1.1) that the assumption of uncorrelated noise for the surface anomalies is an unrealistic one. We recognize that especially for data belonging to the same source common systematic errors in the observations or the compilation procedures used for their estimation may be present, causing error correlations between such data. Weber and Wenzel (1982) have investigated

estimation of error covariance functions for a limited area in Europe based on the existing differences between dual or multiple data sources referring to this area.

However, implementation of the same technique on a global basis is not possible at present, due to the lack of redundant data and the inhomogeneity of the quantity and quality of available data from one area to another.

In an attempt to compensate for the omission of the existing correlations between the surface anomaly estimates Rapp and Cruz (1986a) have rescaled (increased) the variances of the anomaly estimates provided in the June 1986 data base, and constrained their values in a specified range, in order to obtain moderate weight ratios. The particular rescaling and the range of the variances selected have been determined in an empirical fashion heavily dependant on numerical experimentation [Rapp and Cruz, 1986a, Sections 6.1, 6.3].

Numerical experimentation is also employed for the determination of appropriate relative weights for the terrestrial and the satellite normals in combination solutions. The goal here is mainly to obtain realistic error degree variances for the potential coefficient estimates of the combined solution. To investigate the implications of different relative weighting schemes and facilitate the determination of optimum relative weights, a number of comparisons (potential coefficient error degree variances, RMS from satellite orbit fits, Doppler derived undulations) has been performed and examined in the development of the OSU86C/D geopotential models [Rapp and Cruz, 1986a, Section 6.3]. Corresponding comparisons provide also the means of determining optimal relative weights in the combination solutions performed by NASA/GSFC (see also [Marsh et al, 1987, p. 193, Table 8.1]).

In this study we have performed three test solutions (only from surface gravity data), in order to investigate the effect of different weighting schemes.

SOLV01: all anomaly standard deviations are set to 10 mgals

SOLV02: the anomaly standard deviations of the June 1986 field ($\sigma_{ij(JUN86)}$) are used.

SOLV03: the standard deviation σ_{ij} of the data value dg_{ij} is defined as follows

$$\sigma_{ij} = \begin{cases} \max(20,\ 2.5\sigma_{ij(JUN86)}) \\ \min(2.5\sigma_{ij(JUN86)},\ 38) \end{cases} \qquad (5.11)$$

Such a weighting scheme was used in the development of the OSU86C/D gravity models [Rapp and Cruz, 1986a].

The weights in all three solutions are assigned by

$$p_{ij} = \sigma_0^2/\sigma_{ij}^2 \qquad (5.12)$$

where σ_0^2 denotes the a priori variance of unit weight and has always been set equal to 1 (unitless).

On Table 12 the results from the comparisons of these solutions with the OSU86F potential coefficient set are given. These results indicate no significant change on the solutions due to the various weights used.

The same behavior was seen by examining the classification in terms of magnitude and the geographical distribution of the residuals from these solutions. It is interesting to note the values of the a posteriori variance of unit weight ($\hat{\sigma}_0^2$) resulting from these solutions. We have

SOLV01: $\hat{\sigma}_0^2 = 1.22$

SOLV02: $\hat{\sigma}_0^2 = 2.51$

SOLV03: $\hat{\sigma}_0^2 = 0.15$

Table 12. Comparison of Solutions SOLV01, SOLV02 and SOLV03 to the OSU86F Geopotential Model.

		OSU86F -VS- SOLV01			OSU86F -VS- SOLV02			OSU86F -VS- SOLV03		
DEGREE	# OF COEFFS	% DIFF.	UND. DIFF. (METERS)	ANOM. DIFF. (MGALS)	% DIFF.	UND. DIFF. (METERS)	ANOM. DIFF. (MGALS)	% DIFF.	UND. DIFF. (METERS)	ANOM. DIFF. (MGALS)
2	5	22.38	4.008	0.62	17.43	3.121	0.48	20.15	3.610	0.56
3	7	12.64	2.391	0.74	13.44	2.542	0.78	12.61	2.386	0.73
4	9	20.90	2.017	0.93	18.66	1.801	0.83	20.12	1.942	0.90
5	11	18.70	1.384	0.85	18.67	1.382	0.85	18.47	1.367	0.84
6	13	21.30	1.217	0.94	18.10	1.034	0.80	19.12	1.092	0.84
7	15	22.55	1.080	1.00	21.78	1.043	0.96	20.38	0.976	0.90
8	17	37.54	1.156	1.24	32.27	0.993	1.07	34.97	1.077	1.16
9	19	32.57	0.877	1.08	30.28	0.815	1.00	30.91	0.832	1.02
10	21	36.57	0.819	1.13	31.83	0.713	0.99	34.00	0.761	1.05
11	23	52.02	0.883	1.36	51.31	0.871	1.34	51.48	0.874	1.34
12	25	48.72	0.552	0.93	39.88	0.452	0.76	44.94	0.509	0.86
13	27	41.29	0.596	1.10	34.41	0.497	0.92	38.39	0.554	1.02
14	29	69.36	0.620	1.24	63.41	0.567	1.13	62.80	0.561	1.12
15	31	72.54	0.548	1.18	57.67	0.435	0.94	64.56	0.487	1.05
16	33	76.27	0.613	1.41	69.67	0.560	1.29	72.04	0.579	1.34
17	35	87.25	0.597	1.47	71.88	0.491	1.21	79.36	0.543	1.34
18	37	72.24	0.506	1.32	62.24	0.436	1.14	66.54	0.466	1.22
19	39	80.06	0.499	1.38	64.76	0.404	1.12	71.35	0.445	1.23
20	41	88.52	0.422	1.23	75.63	0.361	1.05	83.04	0.396	1.16
21	43	98.45	0.455	1.40	86.13	0.398	1.22	92.85	0.425	1.31
22	45	76.22	0.414	1.34	63.46	0.344	1.11	69.35	0.376	1.22
23	47	77.89	0.350	1.18	66.10	0.297	1.00	71.37	0.320	1.08
24	49	81.82	0.318	1.13	72.41	0.282	1.00	78.35	0.305	1.08
25	51	62.12	0.304	1.12	59.75	0.292	1.08	61.51	0.301	1.11
26	53	79.55	0.267	1.03	75.05	0.252	0.97	79.81	0.268	1.03
27	55	59.16	0.196	0.78	55.82	0.185	0.74	55.35	0.183	0.73
28	57	51.70	0.200	0.83	51.73	0.200	0.83	50.27	0.195	0.81
29	59	67.77	0.225	0.97	62.51	0.208	0.89	67.32	0.223	0.96
30	61	56.64	0.219	0.98	47.84	0.185	0.83	50.56	0.196	0.87
31	63	56.04	0.186	0.86	51.05	0.169	0.78	54.05	0.179	0.83
32	65	41.96	0.138	0.66	47.37	0.156	0.74	42.52	0.140	0.67
33	67	48.82	0.169	0.83	48.39	0.167	0.82	46.11	0.159	0.78
34	69	40.99	0.154	0.78	37.36	0.140	0.71	37.82	0.142	0.72
35	71	41.62	0.144	0.76	41.16	0.143	0.75	39.73	0.138	0.72
36	73	41.44	0.124	0.67	41.46	0.124	0.67	36.88	0.110	0.59
AVERAGE % DIFF.		54.16			48.60			50.80		
RMS UNDULATION DIFF.			6.15			5.41			5.74	
RMS ANOMALY DIFF.				6.32			5.66			5.92

From the point of view of internal consistency the 10 mgal standard deviation for the gravity data appears to yield the best results, while the June 1986 and (20,38) weighting schemes indicate optimistic and pessimistic estimates for the accuracies respectively.

The similarity of the results from these solutions regardless of the weights used should be expected. The effects of different weighting schemes for the anomalies will become apparent only when the dual satellite information is introduced in the combined solution.

However, in our case we did not have the ability to perform combined solutions and examine the effect of different relative weighting schemes. Hence, we decided to relay on the results of Rapp and Cruz (1986a) and adopt (at least in the beginning) the (20,38) weighting scheme used in the OSU86C/D solutions. The fact that such a selection was not an inappropriate one was verified later, when the first preliminary results from combined solutions were made available to us [E. Pavlis, private communication]. According to these results the "calibration scale factors" (see [Marsh et al, 1987, p. 264 for definitions) by degree and by order obtained for PGS3226 (see Table 7) were 0.97 and 0.93 respectively with their ideal values being 1.00.

From the discussion given above it becomes apparent that the treatment of the error properties of the data is currently based on empirical methods heavily based on numerical experimentation. Although numerical experimentation (to some extent) will probably remain necessary as a tool guiding the analysis and the making of decisions, it would be highly desirable to further investigate, also from the theoretical point of view, the estimation of error properties for global surface anomaly data bases.

5.2.7 The Use of Terrain Corrections

In order to numerically investigate the influence of the use of terrain corrections on our results we have performed the solution ADJUST30 with the following setup:

ADJUST30: the "observations" which are input to the adjustment are defined by (see Table 7)

$$d_{ij} = dg_{ij} - (hf_s)_{ij} - (e\ell\ell_1)_{ij} + tc_{ij} \qquad (5.12)$$

for the locations corresponding to the 466 blocks of Figure 17, and as

$$d_{ij} = dg_{ij} - (hf_s)_{ij} - (e\ell\ell_1)_{ij} \qquad (5.13)$$

for the rest of the 48955 blocks of Figure 8. In the cases corresponding to (5.12), dg_{ij} is assumed to refer to the surface of the reference ellipsoid (elevation is set to zero), in agreement with the formulation presented in Section 2.4.

With the exception of the use of terrain corrections this solution is identical in terms of setup with ADJUST20 (weighting scheme, high frequency content removal etc), as it can be seen from Table 7. Hence, the effect of the terrain corrections is examined by an intercomparison of the results from these two solutions.

The average percentage difference of ADJUST30 as compared to ADJUST20 was found to be 1.74%, while the RMS undulation and anomaly differences between the two solutions were 0.51 m and 0.27 mgals respectively. However, these figures are representative of the differences between the two fields in a global sense. Of greater interest here are the differences between the two solutions in the area where the terrain corrections were applied.

Figure 20 illustrates the undulation differences between the two solutions ($N_{ADJUST20}$ - $N_{ADJUST30}$) in the region of interest (ϕ = 30° to ϕ = 50° and λ = -130° to λ = -70°).

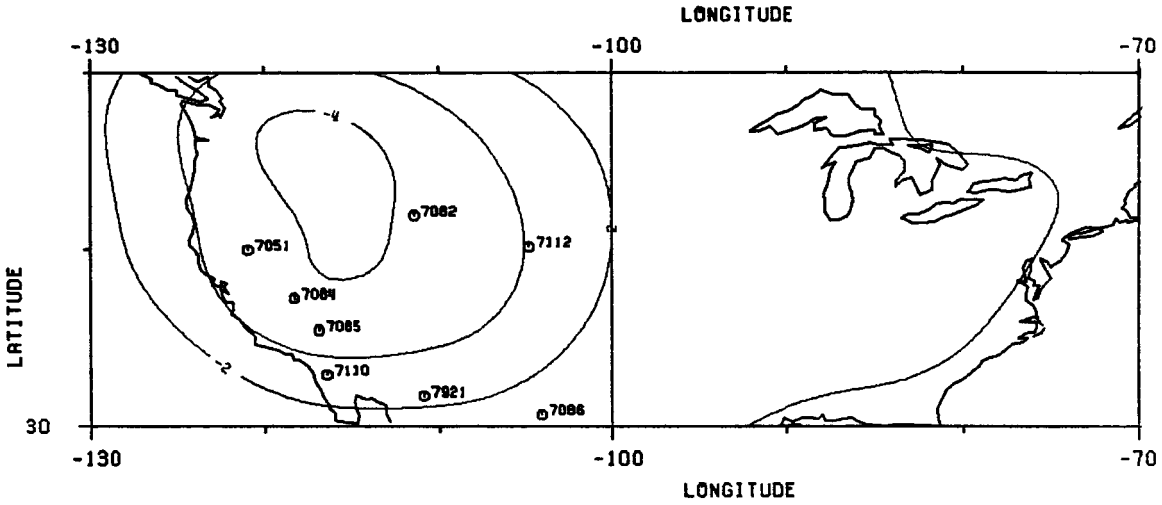

Figure 20. Undulation Differences - ADJUST20 Minus ADJUST30 (Contour Interval is 1 m, Based on a 2°x2° Grid) Superimposed are the Locations of Selected Laser Stations.

Comparing Figure 20 with Figure 17 it becomes clear that the terrain corrections have left a long wavelength signature on the field in the area where they were applied. The fact that such a signature is an erroneous one was verified through comparisons of the undulations computed from the two solutions with the undulations at 13 laser stations in the above area. The latter, denoted by N_G, were given by Despotakis (1987, p. 46, Table 10), and have been computed by differencing the ellipsoidal and orthometric heights at these stations. They refer to an ellipsoid with parameters

$$\left.\begin{aligned} a &= 6378136.0 \text{ m} \\ 1/f &= 298.257222101 \end{aligned}\right\} \qquad (5.14)$$

The locations of these stations are also, shown in Figure 20. For the purpose of this comparison we have formed two geopotential models both up to N_{max} = 360 as follows:

model F20: $ADJUST20_{2\rightarrow36}$ augmented by $OSU86F_{37\rightarrow360}$
model F30: $ADJUST30_{2\rightarrow36}$ augmented by $OSU86F_{37\rightarrow360}$

The undulations implied by F20 and F30 (denoted N_{20} and N_{30} respectively) at the locations of the 13 laser stations were computed and compared with N_G. The results of this comparison are given on Table 13. Comparing the differences given in columns five and six we verify that ADJUST20 is in good agreement with the "ground truth" while ADJUST30 suffers from the long wavelength errors shown in Figure 20. The last column serves as a double check of the values shown in Figure 20.

At this point we have no answer to what causes the problem identified before. Possible causes for this problem may be:

(a) The omission of the terms (2.148) and (2.152) may not be permissible for the degree of expansion we use here (36). In [Moritz, 1966, p. 105] it is postulated that such omission is justifiable up to degree about 5. In our application such a guideline is certainly being violated.
(b) The use of the terrain corrections only in a limited area.

Further investigation is required in order to elucidate the appropriate use of terrain corrections in global geopotential modeling.

5.3 Validation

During the course of this study five major sets of normal equations have been developed from surface gravity data, to be used in combination solutions at NASA/GSFC. These normal sets (and the corresponding terrestrial only solutions) are denoted

Table 13. Undulation Comparisons at Laser Stations in the Western United States

ID	N_G	N_{20}	N_{30}	N_G-N_{20}	N_G-N_{30}	$N_{20}-N_{30}$
7051	-22.57	-22.08	-18.49	-0.48	-4.07	-3.59
7109	-22.59	-22.09	-18.50	-0.50	-4.09	-3.59
7062	-32.47	-32.64	-30.17	0.16	-2.30	-2.46
7110	-30.86	-31.19	-28.60	0.33	-2.26	-2.59
7082	-12.58	-12.54	-8.62	-0.04	-3.96	-3.91
7084	-24.90	-24.46	-20.69	-0.44	-4.21	-3.77
7114	-24.84	-24.46	-20.70	-0.38	-4.15	-3.77
7085	-29.68	-29.92	-26.44	0.24	-3.24	-3.48
7115	-29.58	-30.08	-26.65	0.50	-2.93	-3.43
7086	-20.78	-19.56	-17.97	-1.22	-2.81	-1.59
7885	-20.83	-19.56	-17.97	-1.27	-2.86	-1.59
7112	-17.40	-15.68	-12.73	-1.72	-4.67	-2.95
7921	-29.47	-27.75	-25.60	-1.72	-3.88	-2.15

Units are meters

(1) ADJUST20: 48955 observations (include geophysical data)
(2) ADJUST40: 43271 observations (exclude geophysical data)
(3) ADJUST65: 48955 observations (include geophysical data)
(4) ADJUST71: 43271 observations (exclude geophysical data)
(5) ADJUST81: 48955 observations (include geophysical data)

The first two solutions were developed based on the same setup as far as weighting, removal of high frequency content of the anomalies etc. are concerned, as it can be seen from Table 7. The difference between them is the exclusion of geophysically predicted anomalies in the second set.

The second pair of solutions differs from the first by the use of the improved elevation data (TUG87), and the use of a different weighting scheme which will be discussed in Section 5.3.3. Again this pair consists of one solution where geophysical data are included in the adjustment, and one where they are excluded.

Finally, in the last set the systematic reduction δg_{h^2} discussed in Section 3.1.1, was applied to the anomaly data, in contrast to the previous solutions. This solution reflects the optimum procedure for the analysis of surface gravity data, suggested by this study.

The first four normal equation sets already have been used in combination solutions performed at NASA/GSFC.

The majority of the comparions and tests to be presented in the sequel refers to solutions (1) and (2). However, as it can be seen from Table 7 and as it will be discussed in the following, the differences between corresponding solutions (using the same number of observations), are rather minor, so that the conclusions drawn from these comparisons pertain also to the cases of (3), (4) and (5).

The evaluation of the quality of our results will be mainly based on comparisons with two geopotential models. The GEMT1 [Marsh et al, 1987] which is a satellite only field complete to degree and order 36, and the OSU86F [Rapp and Cruz, 1986b] which is a combined high degree geopotential model complete up to 360.

5.3.1 Comparisons With Existing Geopotential Models

Before we attempt any comparisons of our results with satellite only or combined solutions, it is important to compare the input of our adjustment, i.e. the surface gravity data, with the values implied for these data from the satellite solutions. Such a comparison will indicate the agreement between the gravity field as this is sensed by the satellites and the gravity field which is implied by the surface measurements. In addition it will provide us with a fairly good idea of what we should expect from the comparisons of our results with satellite only solutions, since the output of any adjustment primarily reflects the characteristics of its input. For that purpose the following comparisons were performed:

(a) A set of 48955 1°x1° anomaly values were computed as (see Table 6)

$$dg_{in} = dg - hf_s \qquad (5.15)$$

These values essentially represent the input of our adjustment since the systematic correction terms (ellipsoidal corrections etc.) are of very small magnitude.

(b) A global set of 1°x1° mean anomalies was formed using the GEMT1 coefficient set complete from N_{min}= 2 to N_{max} = 36. These anomalies are denoted $\bar{\Delta}g_{GEM}$.

The differences between $\bar{\Delta}g_{GEM}$ and dg_{in} were then evaluated in the areas where the June 1986 field contains an anomaly estimate (Figure 8). In Figure 21 the locations where the absolute value of such differences is larger than or equal to 10 mgals are shown. From this figure it becomes apparent that systematic discrepancies between the satellite implied and terrestrial field exist in large continental areas. Since the extent of many of these areas exceeds the minimum wavelength recoverable by an expansion up to 36, it is expected that the results of terrestrial only solutions will reflect these inconsistencies.

It is also interesting to examine if the above discrepancies are related to geophysically predicted data in the June 1986 field. The results of a corresponding comparison peformed only over the 43271 locations of Figure 10 are illustrated in Figure 22. Although some of these inconsistencies are associated with geophysically predicted data (USSR, China), Figure 22 indicates that such inconsistencies exist also in areas where observed gravity data are available (Africa, South America).

With the above as a background, we next performed the corresponding comparisons between $\bar{\Delta}g_{GEM}$ and the adjusted values of the gravity anomalies obtained from the solution ADJUST20 and ADJUST40 (see Table 7), denoted $\bar{\Delta}g_{A20}$ and $\bar{\Delta}g_{A40}$ respectively. The results from these comparisons are illustrated in Figures 23 and 24 respectively.

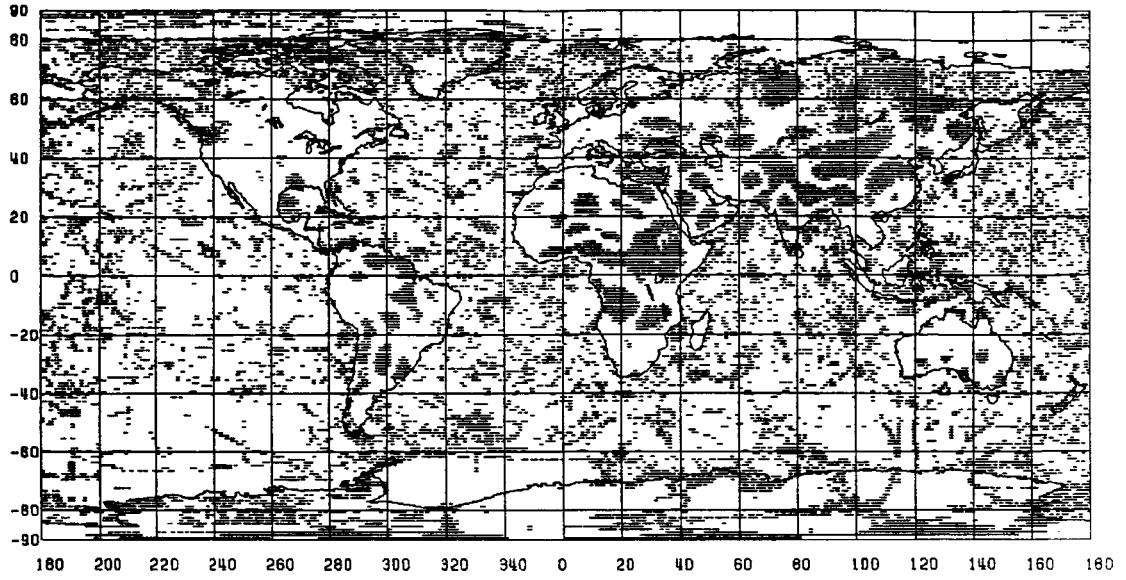

Figure 21. Locations of the 17082 1°x1° Blocks Where $|\bar{\Delta}g_{GEM} - dg_{in}| >$ 10 mgals (Geophysical Data are Included in the Comparison).

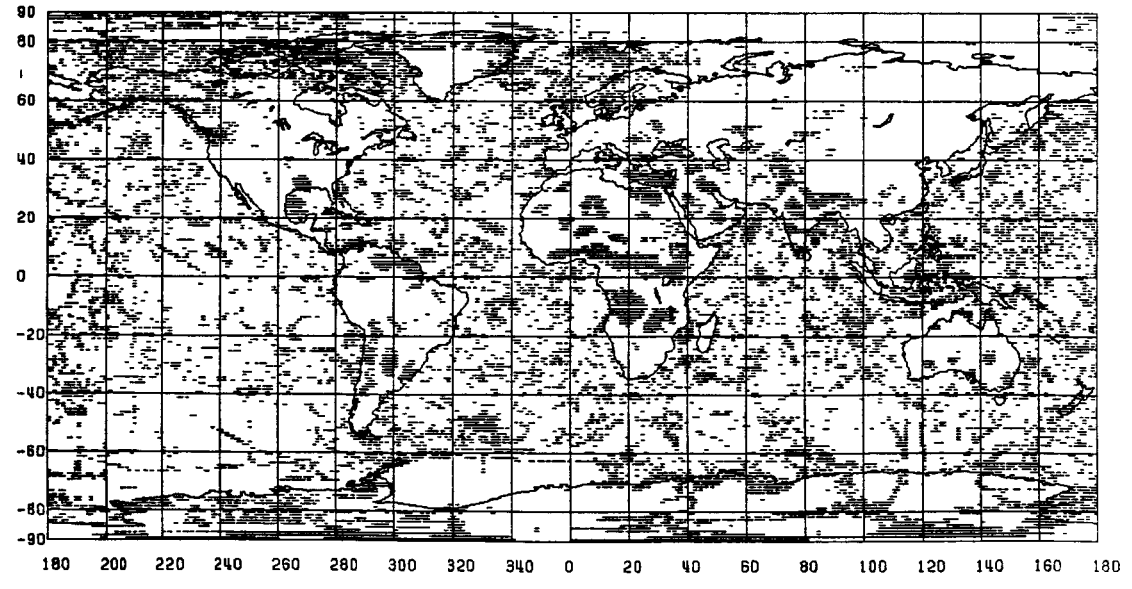

Figure 22. Locations of the 14412 1°x1° Blocks Where $|\bar{\Delta}g_{GEM} - dg_{in}| >$ 10 mgals. (Geophysical Data are Excluded from the Comparison).

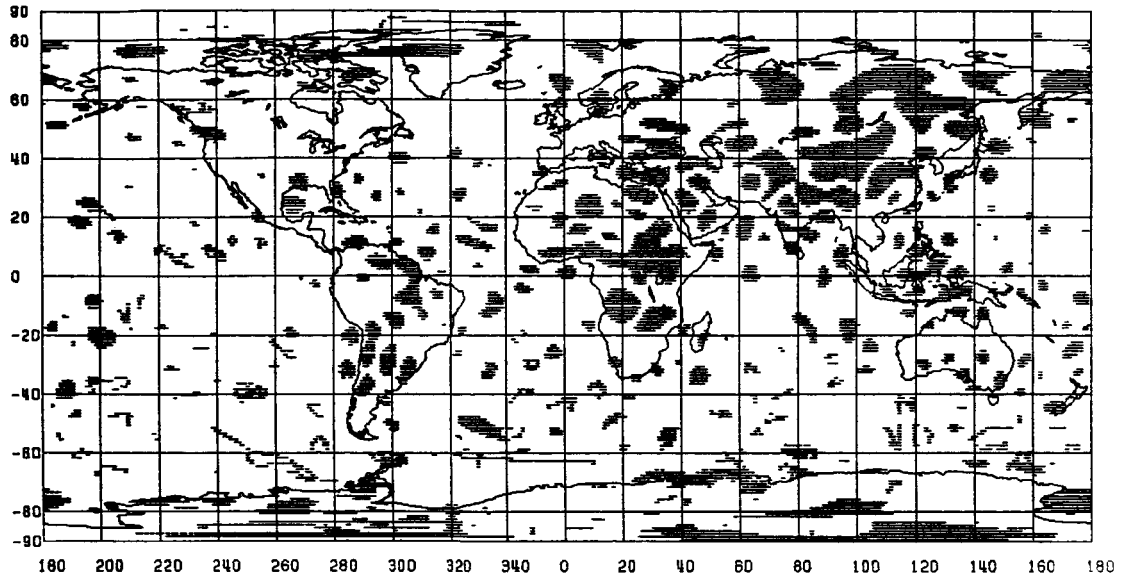

Figure 23. Locations of the 9745 1°x1° Blocks Where $|\bar{\Delta}g_{GEM} - \bar{\Delta}g_{A20}| >$ 10 mgals (Locations Corresponding to Geophysical Data are Included in the Comparison).

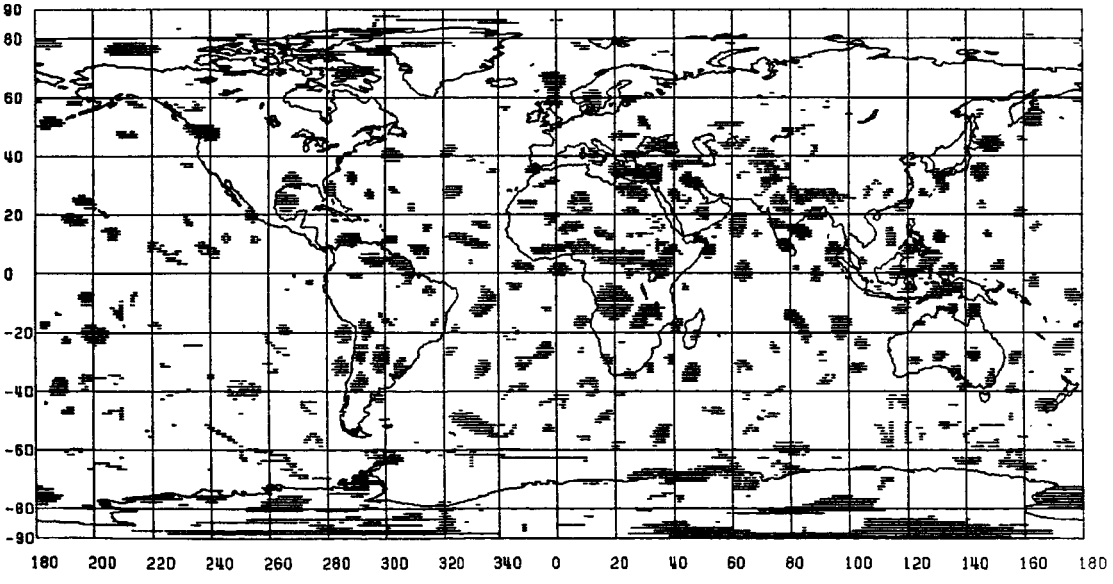

Figure 24. Locations of the 7545 1°x1° Blocks Where $|\bar{\Delta}g_{GEM} - \bar{\Delta}g_{A40}| >$ 10 mgals (Locations Corresponding to Geophysical Data are Excluded from the Comparison).

There are two main observations to be made with respect to these figures.

(i)

As expected the inconsistencies between the satellite implied and terrestrial fields, that were observed over extended geographical regions are also reflected (with remarkable exactness) in the results of terrestrial only solution (compare Figures 21 and 23 or 22 and 24).

(ii)

The behavior of the least squares adjustment in areas where the inconsistencies between the satellite implied and terrestrial fields are localized is rather interesting. Typical examples of such cases occur in oceanic regions. From the examination of Figures 19, 21 and 23 it becomes apparent that the discrepancies between the two sources of information in such cases are closely related to the residuals of the terrestrial only solution. In fact it appears that the terrestrial adjustment yields adjusted anomalies that are closer to the satellite field implied anomalies than to the surface observations!

Before we attempt to explain why such behavior is observed we will present a comparison that clarifies the issue. We consider the residuals of the solution ADJUST20, denoted v_{20}, and we form the following differences:

$$a = \bar{\Delta}g_{GEM} - dg_{in} \tag{5.16}$$

and

$$b = v_{20} - a \tag{5.17}$$

Note that (see also Table 6 and equation (5.15)),

$$b = dg_{in} + v_{20} - \bar{\Delta}g_{GEM} \approx \bar{\Delta}g_{A20} - \bar{\Delta}g_{GEM} \tag{5.18}$$

hence, apart from the small systematic correction terms, b represents the differences between the adjusted anomalies from ADJUST20 and the GEMT1 implied anomalies.

Based on the values a and b we then identify the locations where

$$|a| \geq 10 \text{ mgals } \underline{\text{and}} \ |b| < 10 \text{ mgals} \tag{5.19}$$

and where

$$|a| \geq 10 \text{ mgals } \underline{\text{and}} \ |b| > 10 \text{ mgals.} \tag{5.20}$$

Locations where the conditions (5.19) are simultaneously fulfilled indicate the cases where, although the input of our adjustment differs from the GEMT1 implied anomaly substantially (with respect to the threshold value of 10 mgals), the output is closer to the satellite implied anomaly than to the terrestrial one (again with respect to the 10 mgal threshold value). The cases where the opposite occurs are indicated by the simultaneous fulfillment of conditions (5.20). Figures 25 and 26 illustrate the geographical distribution of the blocks where conditions (5.19) and (5.20) are fulfilled respectively. These figures verify that the speculation made in (ii) above about the behavior of the terrestrial solution in the cases of isolated (localized) discrepancies between the satellite and terrestrial information is indeed a fact. It remains now to explain how the terrestrial solution (which has no information about the satellite implied field) can yield in these cases results that agree better with the satellite information than with its own input. The explanation is rather obvious. The least squares adjustment does not yield values agreeing better with the satellite implied anomalies; what it does though for these isolated blocks, is that it yields values that are in agreement with the anomaly values of the broader neighborhood of these blocks (which happen to be in good agreement with the satellite implied anomalies). The underlying cause of such behavior of the least squares adjustment is the sampling interval in conjunction with the maximum estimated degree of the expansion. The $1^{\circ}x1^{\circ}$ interval provides enough data

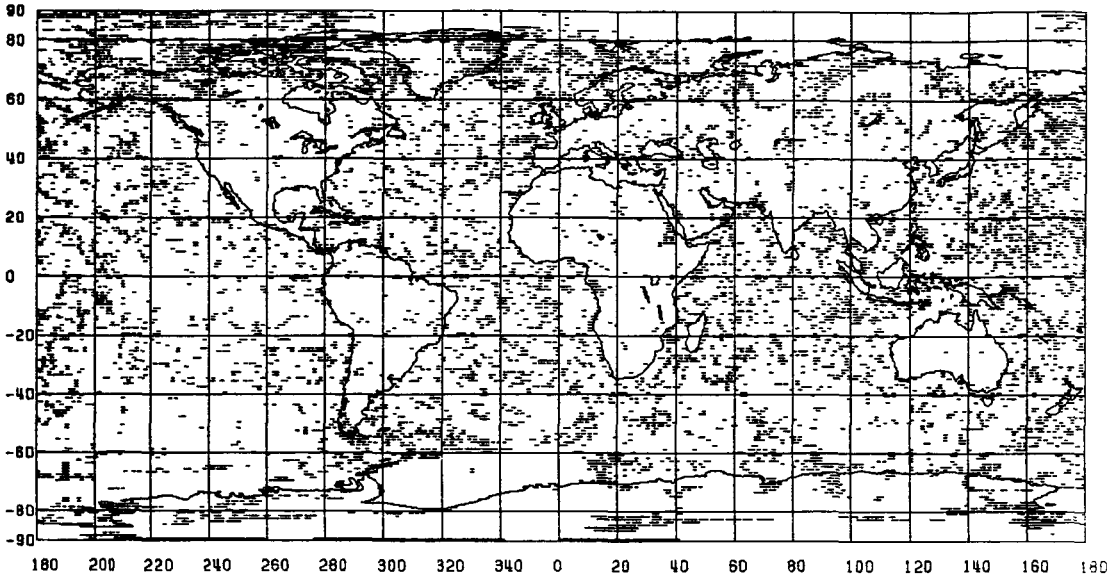

Figure 25. Locations of the 10149 1°x1° Blocks Where Conditon (5.19) is Fulfilled. (Locations Corresponding to Geophysical Data are Included in the Comparison).

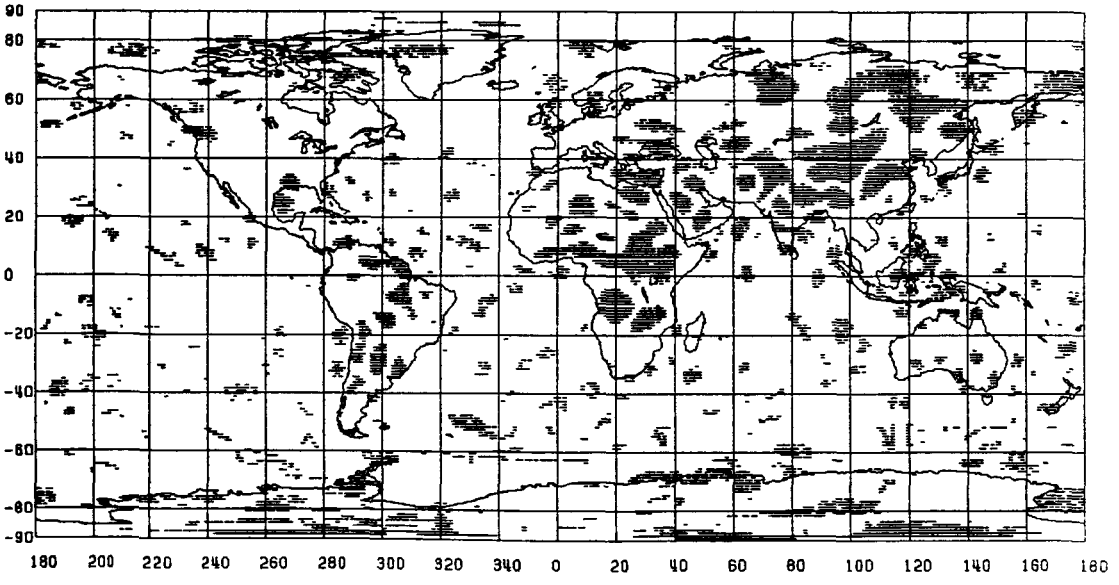

Figure 26. Locations of the 6933 1°x1° Blocks Where Conditon (5.20) is Fulfilled. (Locations Corresponding to Geophysical Data are Included in the Comparison).

redundancy to enable the least squares adjustment to isolate (by assigning them large residuals), observations which do not comply with the more general pattern implied by their broader region (outliers). An illustrative example explaining the above can be given if we consider a least squares fit of a straight line into sampled data (Figure 27), for two different sampling patterns. In Figure 27a all the data sampled are used. Point P, which does not comply with information implied by its neighboring points will be characterized by a large residual. If now

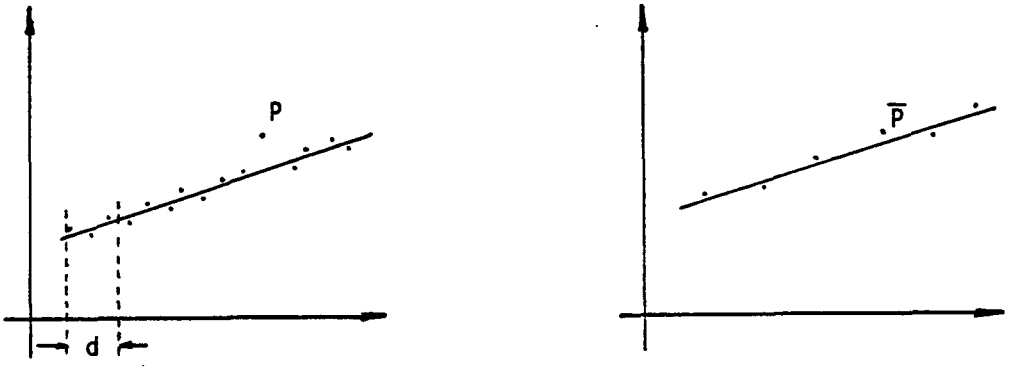

(a) (b)

Figure 27. The Least Squares Adjustment and the Data Sampling.

the previous observations are averaged over some interval d and the same fit is attempted (Figure 27b), the point $\bar{P}$ which represents the mean value in the region of P will be characterized by a much smaller residual and the quality of the fit in the region of $\bar{P}$ will not differ much from the quality of the fit on the other points. On the other hand if we keep the sampling as in Figure 27a but we start increasing the degree of the polynomial to be fitted to the data, the corresponding residuals for P will decrease eventually making P appear as a valid observation.

From the above discussion it becomes clear that there is an additional good reason for preferring the 1°x1° sampling with the removal of the high frequency content from the data, over the

alternative use of 5°x5° averages. If 5°x5° averages were used we would have no way to identify very localized inconsistencies between the satellite and terrestrial solutions.

Up to now all we have determined is the existence of inconsistencies between the satellite implied field and the terrestrial one. The next step, of course, is to try to determine which of the two sources provides a more accurate estimate of the gravity field. To facilitate the investigation in this direction we have to employ comparisons with external sources of information. We will distinguish between the case of the oceanic regions where the inconsistencies found were more of local character, and the continental areas where more regional problems were experienced. In the oceanic regions, anomalies obtained from altimetric observations will provide the external source, while in the continental regions (which will be discussed in the next section) Doppler derived undulations will be used as independent source of information.

Figure 28 illustrates the locations of the 6833 1°x1° blocks where (see Table 6)

$$|dg - \bar{\Delta}g_{alt}| > 10 \text{ mgals} \qquad (5.21)$$

with $\bar{\Delta}g_{alt}$ denoting the 1°x1° anomaly implied from the altimetric observations. These anomalies were estimated from the combined GEOS3/SEASAT altimeter data [Rapp, 1985]. In contrast Figure 29 illustrates the locations of the 3574 1°x1° blocks where (see Table 6)

$$|\bar{\Delta}g_{GEM} - (\bar{\Delta}g_{alt} - hf_s)| > 10 \text{ mgals} \qquad (5.22)$$

Figure 29 shows a good agreement between the GEMT1 implied anomalies and the altimetry derived anomalies. Hence, the discrepancies shown in Figure 28 are most probably due to erroneous ship-track measurements.

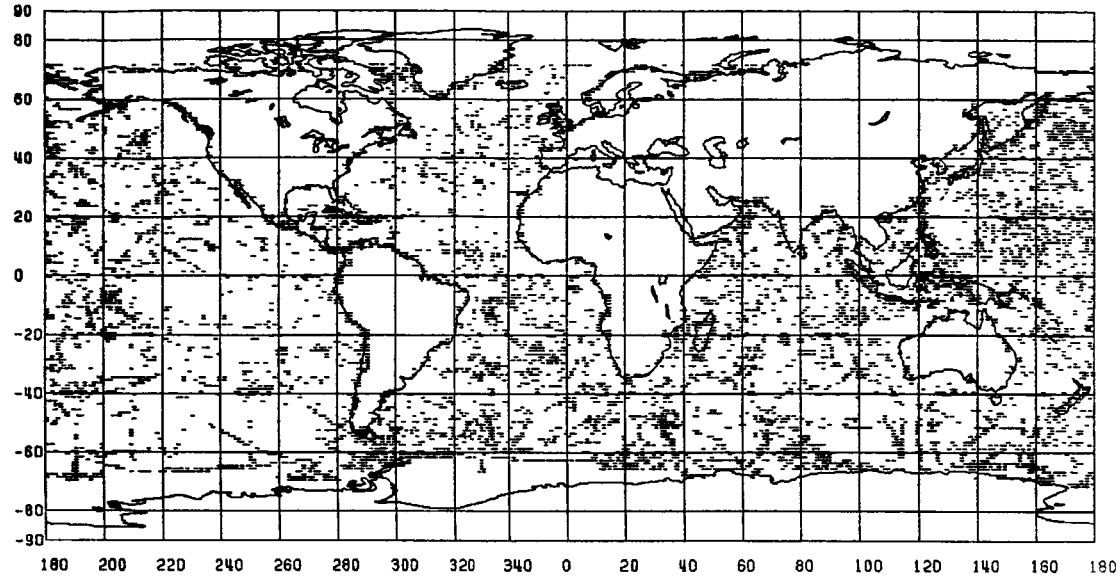

Figure 28. Locations of the 6833 1°x1° Blocks Where $|dg - \bar{\Delta}g_{alt}| \geq 10$ mgals.

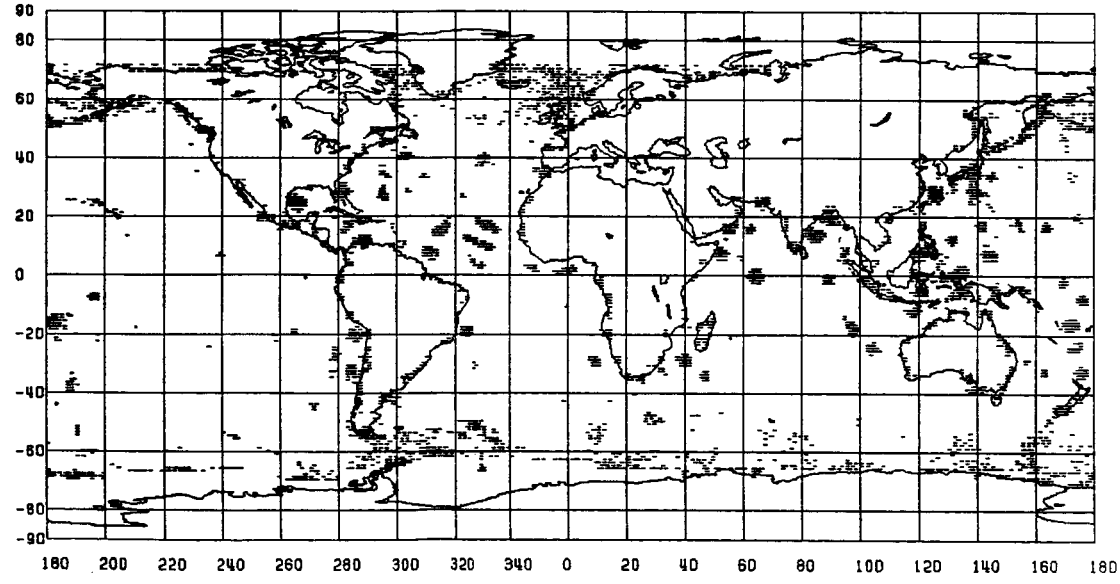

Figure 29. Locations of the 3574 1°x1° Blocks Where $|\bar{\Delta}g_{GEM} - (\bar{\Delta}_{alt} - hf_5)| > 10$ mgals.

Comparisons as the ones discussed above provide information about the geographical distribution and the number of the 1°x1° blocks where inconsistencies between the satellite-implied and the terrestrial data are observed. However, they do not provide information about the magnitude of these discrepancies (other than the crude information provided by the threshold value used). In order to obtain such information we have plotted global undulation and anomaly difference maps between the satellite only field (GEMT1) and the terrestrial only solutions.

In Figures 30 and 31 the gravity anomaly and undulation differences between GEMT1 and ADJUST20 are illustrated. Note that examination of such plots should always take into account the data coverage used in the development of the terrestrial only solutions, in order to discriminate between areas where large discrepancies occur due to lack of terrestrial data (South Pacific, Antarctic region) and areas where systematic inconsistencies between satellite and terrestrial data exist (Soviet Union, Mongolia, China, Africa and Brazil).

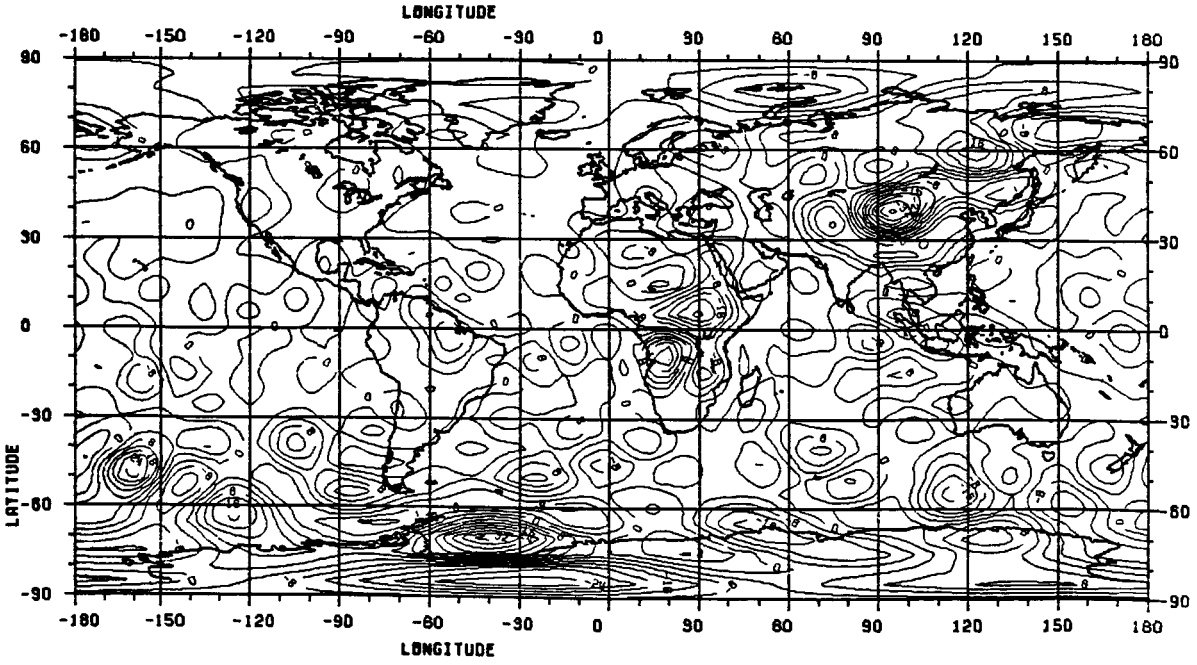

Figure 30. Gravity Anomaly Differences: GEMT1 Minus ADJUST20 Based on a 5°x5° Grid (Contour Interval is 4 mgals).

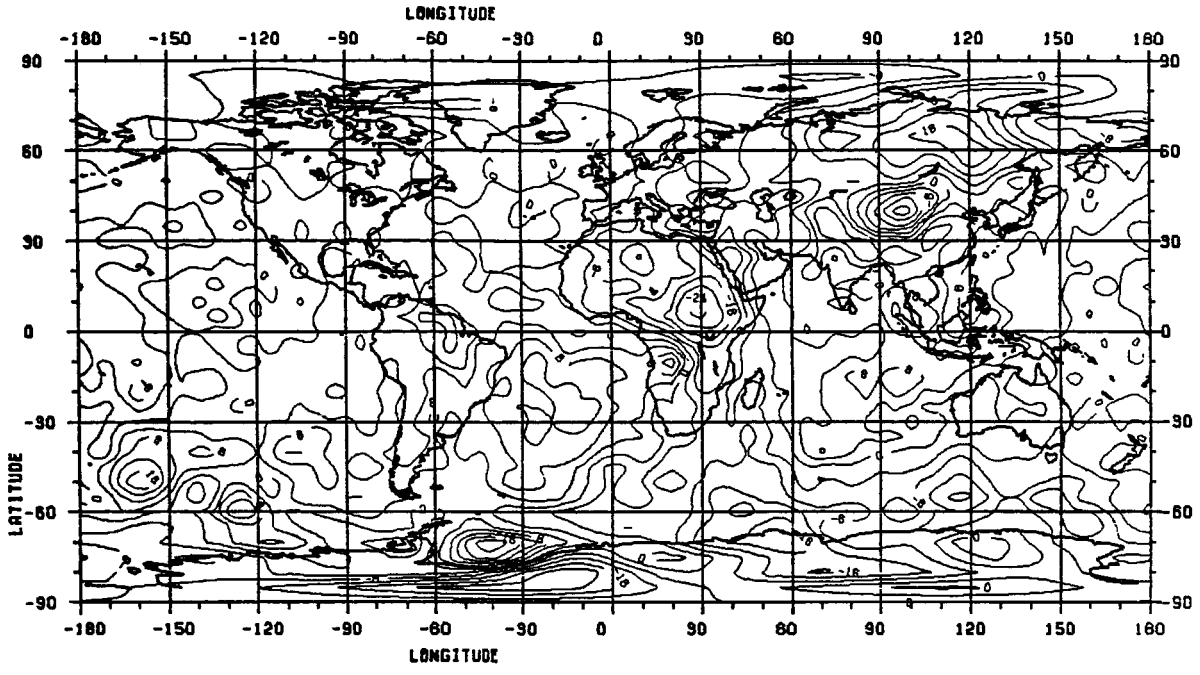

Figure 31. Undulation Differences: GEMT1 Minus ADJUST20 Based on 5°x5° Grid (Contour Interval is 4 m).

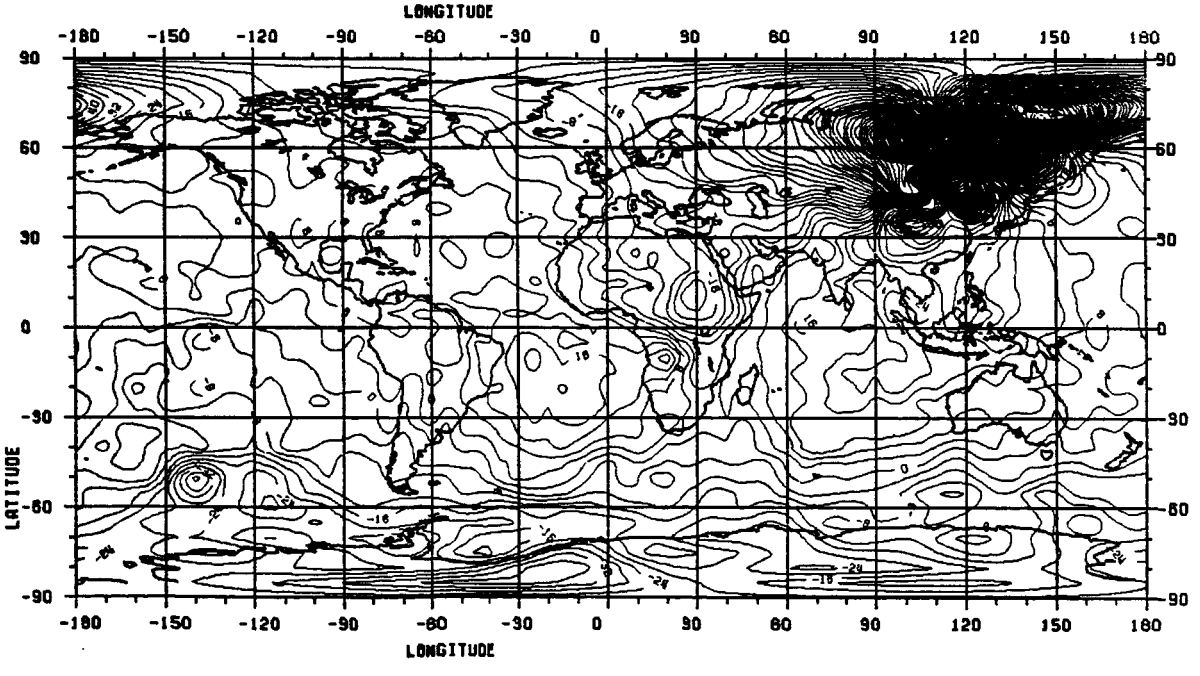

Figure 32. Undulation Differences: GEMT1 Minus ADJUST40 Based on a 5°x5° Grid (Contour Interval is 4 m).

A comparison in terms of undulations between GEMT1 and ADJUST40 is shown in Figure 32. As it can be seen from this plot, large oscillations of the terrestrial only solution occur in the extended gap generated by the exclusion of geophysical data. In addition a comparison of Figures 31 and 32 indicates that ADJUST40 is characterized by more long wavelength differences with respect to GEMT1 than ADJUST20. This should be expected since the exclusion of geophysical data, which cover extended regions, degrades the estimability of long wavelength features of the gravity field.

In Figures 33 and 34 the corresponding comparisons are given between the OSU86F combined solution (up to N_{max} = 36) and the solution ADJUST20. Although these plots are very similar to 30 and 31 respectively, there is an important difference to be noted from the comparison of 30 with 33 (or 31 to 34). The differences between ADJUST20 and OSU86F have less power in the high frequencies as compared to the differences between ADJUST20 and GEMT1.

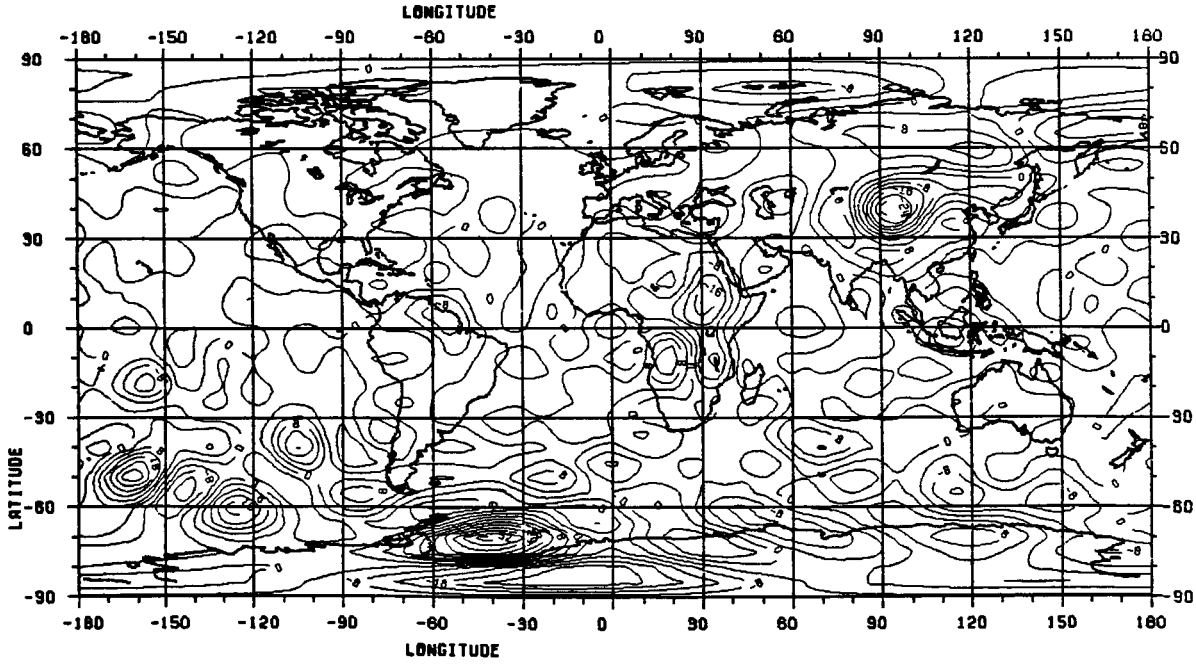

Figure 33. Gravity Anomaly Differences: OSU86F Minus ADJUST20 Based on a 5°x5° Grid (Contour Interval is 4 mgals).

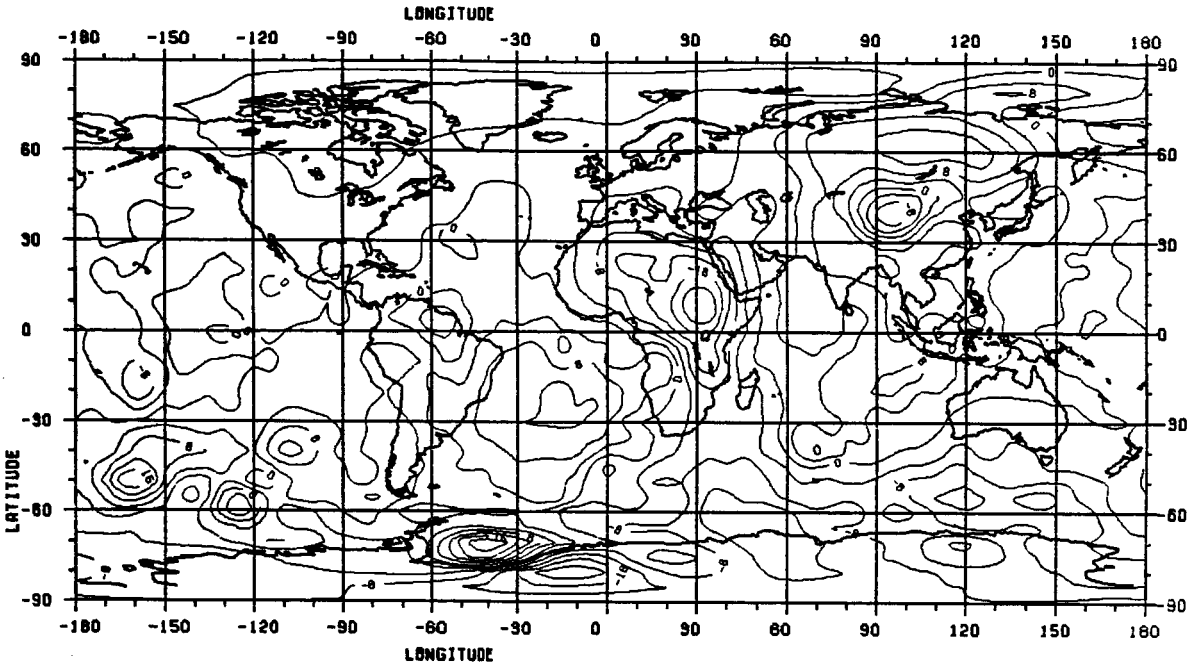

Figure 34. Undulation Differences: OSU86F Minus ADJUST20 Based on a 5°x5° Grid (Contour Interval is 4 m).

Such behavior should be expected since GEMT1 fails to recover high frequency features of the gravity field, while the opposite is true for OSU86F and ADJUST20. In Figure 35 this aspect is illustrated in a better way. In this figure the percentage differences of PGS3041 (a pre GEMT1 satellite only solution), and ADJUST20, with respect to OSU86F are plotted. At low degrees (<6) OSU86F and PGS3041 show an excellent agreement which is expected since OSU86F has used GEML2′ [Lerch et al, 1982a] to control these coefficients, and PGS3041 is not expected to have large discrepancies with GEML2′.

For the same degrees, in the case of ADJUST20 the percentage differences are larger, a fact which expresses the inability of the terrestrial only solution to recover long wavelength features of the geopotential. However, at degree about 20, the picture changes, and PGS3041 departs from OSU86F, while the discrepancies of ADJUST20 with OSU86F start to drop. This is due to the inadequacy of a

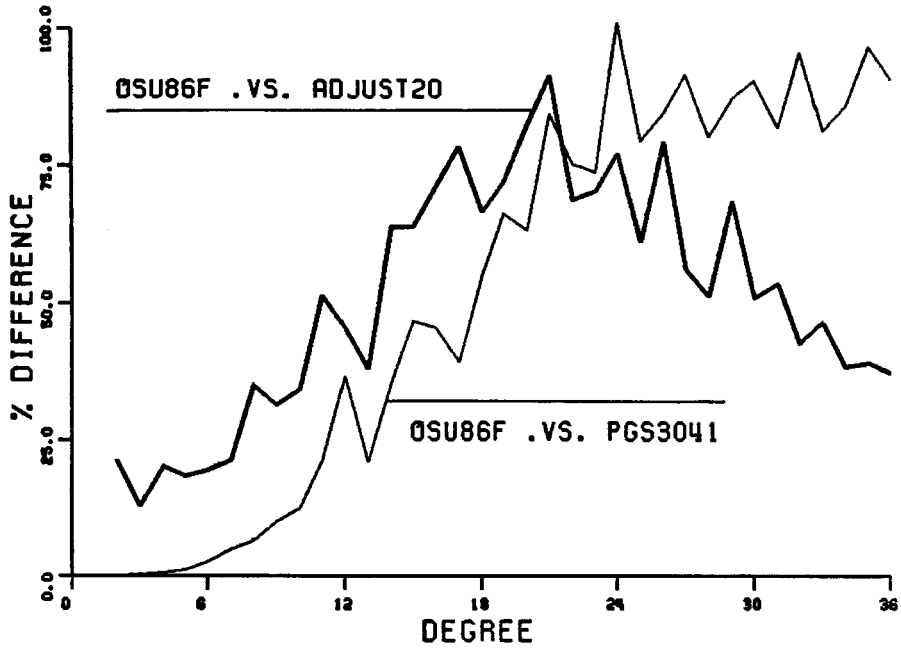

Figure 35. Percentage Differences Between OSU86F Versus ADJUST20 and OSU86F Versus PGS3041.

satellite solution to recover high frequency features of the geopotential. Figure 35 can be used to describe in a compact and clear manner the whole idea and purpose behind the combination solutions. It also suggests that when Figures such as 30 or 31 are examined, very long wavelength biases should not be considered a problem, since they merely reflect the inability of the terrestrial only solutions to recover low degree coefficients. However, systematic differences such as the ones occuring in Africa, constitute a problem, since their extent corresponds to wavelengths which should be recoverable by terrestrial only solutions.

5.3.2 Systematic Inconsistencies Between Satellite Only and Terrestrial Only Solutions

One of the continental regions where systematic inconsistencies between the satellite and terrestrial solutions are observed is Africa. We have decided to further investigate the problem in this area for two reasons:

(a) The discrepancies in this area are quite large (e.g. 24 m undulation differences are observed in Figure 31), and
(b) A fairly well distributed set of Doppler Stations covering the area in question was available, providing an independent standard for comparison.

Large systematic differences occur also in Asia (see Figure 31), however no redundant information for comparisons is available in these regions.

In Figure 36 a more detailed anomaly difference contour map is given for the area in question. It can be seen from this figure that the differences reach values of 24 mgal.

On the other hand, Figure 37 shows that the undulation differences in this area reach values of -24 m. Figure 37 shows also the locations of some of the 32 Doppler stations that were used in the following comparison:

(a) We started with a set of 32 "Doppler undulations" denoted by N_D and evaluated by

$$N_D = h_D - H \qquad (5.23)$$

where h_D (the Doppler derived ellipsoidal height) was first converted from the Doppler reference frame to a geocentric, properly scaled reference frame using the translation and scale

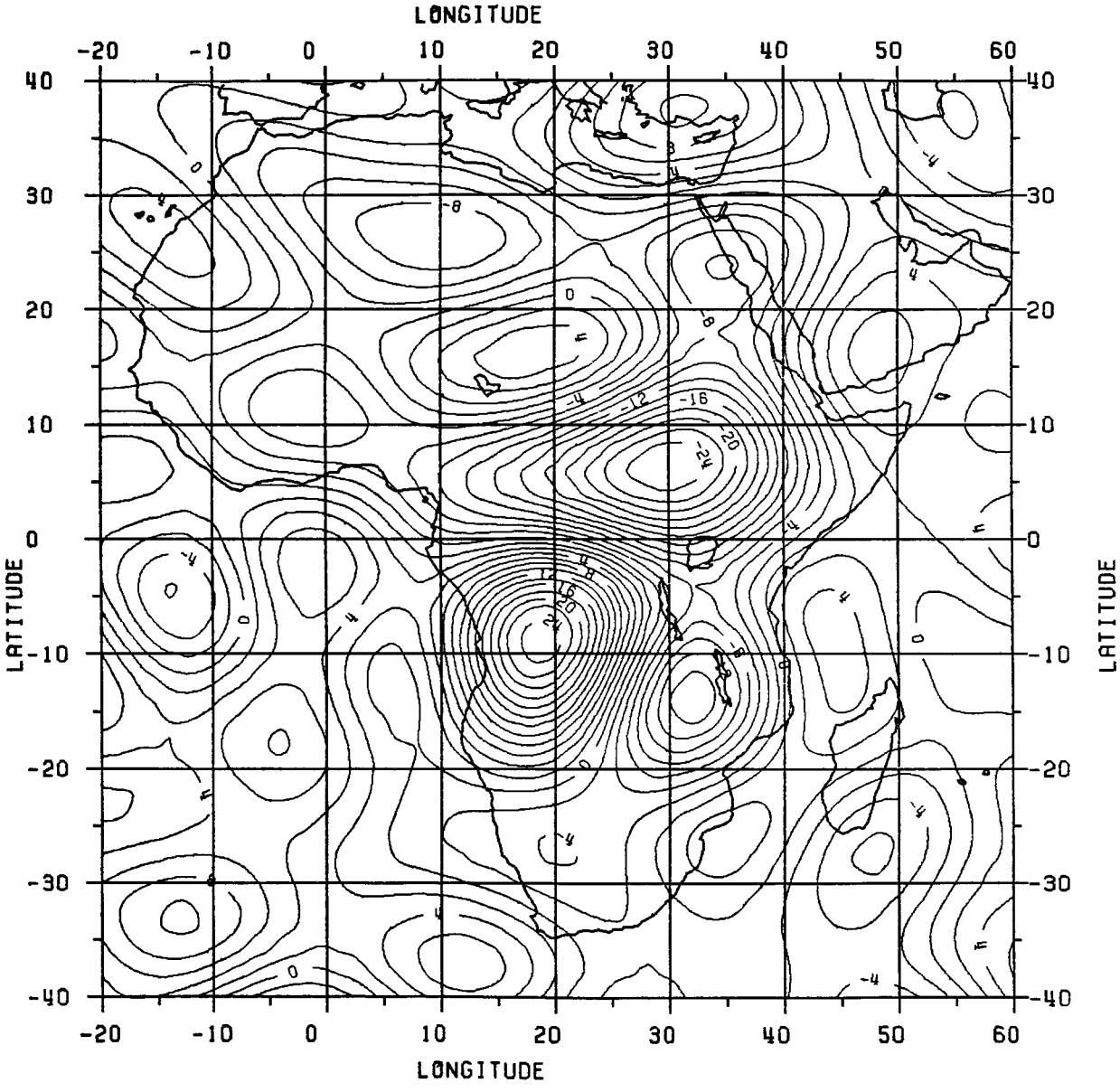

Figure 36. Gravity Anomaly Differences: GEMT1 Minus ADJUST20 Based on a 2°x2° Grid (Contour Interval 2 mgals).

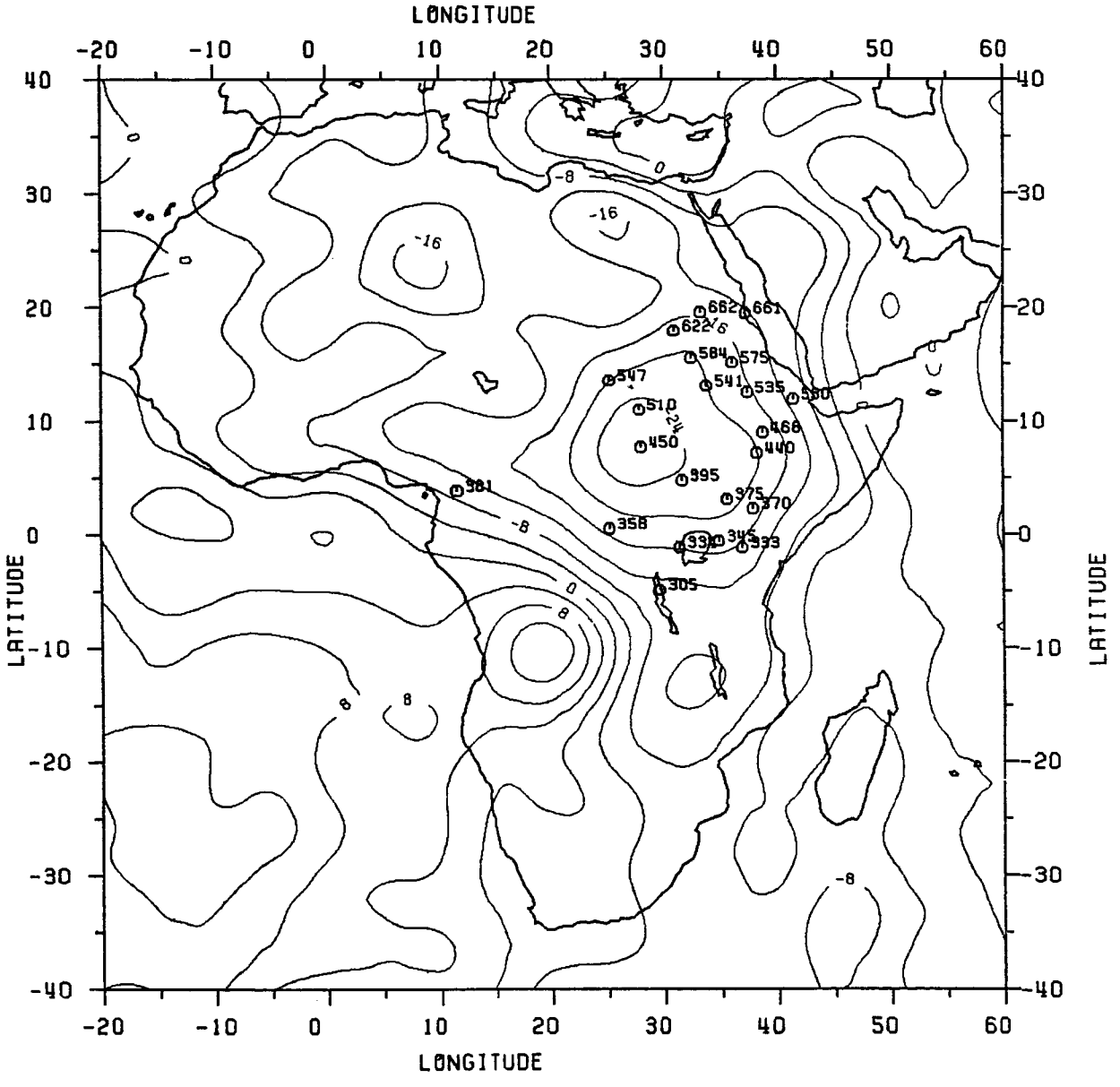

Figure 37. Undulation Differences: GEMT1 Minus ADJUST20 Based on a 2°x2° Grid (Contour Interval 4 m). Superimposed are Selected Doppler Station Locations.

Table 14. Undulation Comparisons at Doppler Stations in Africa.

SELECTED DOPPLER STATIONS IN AFRICA

N* : DOPPLER UNDUL. - UNDUL. IMPLIED BY OSU86F (NMIN=37,NMAX=360)
NT1 : UNDUL. IMPLIED BY GEMT1 (NMIN=2,NMAX=36)
NA20 : UNDUL. IMPLIED BY ADJUST20 (NMIN=2,NMAX=36)
DN1 = N* - NT1
DN2 = N* - NA20
DN3 = DOPPLER UNDUL. - UNDUL. IMPLIED BY OSU86F (NMIN=2,NMAX=360)

STN.	LAT	LON	H(ELL)	N*	NT1	NA20	DN1	DN2	DN3
305	-4.86634	29.63628	907.830	-13.77	-12.62	-1.66	-1.16	-12.11	0.03
333	-1.16821	36.94086	1518.052	-16.49	-20.35	-5.04	3.87	-11.45	0.99
334	-1.13384	31.38364	1314.780	-13.84	-13.68	2.53	-0.17	-16.38	-1.13
345	-0.57266	34.85817	1999.122	-13.58	-17.16	0.34	3.57	-13.92	0.87
358	0.51367	25.18820	392.320	-17.16	-17.52	-0.48	0.35	-16.68	-2.43
370	2.26306	37.90152	1406.962	-15.37	-19.55	-1.77	4.18	-13.60	0.35
373	2.71574	36.68937	368.812	-13.37	-17.38	2.59	4.01	-15.95	0.36
375	3.11495	35.60518	486.552	-11.68	-15.76	5.50	4.08	-17.17	1.15
379	3.51501	38.55354	678.762	-16.49	-18.57	-0.53	2.09	-15.95	-2.15
381	3.84124	11.52424	767.720	15.67	14.03	23.33	1.64	-7.67	0.36
394	4.59185	13.68789	715.800	13.32	9.94	22.39	3.38	-9.08	0.93
395	4.75553	31.63069	630.020	-8.32	-11.17	12.16	2.85	-20.48	1.90
440	7.17102	38.30381	2202.210	-9.15	-11.45	8.78	2.30	-17.93	-1.54
450	7.69683	28.00029	445.630	-0.03	-7.30	19.58	7.28	-19.60	2.40
462	8.72038	38.88549	1904.012	-9.67	-9.53	9.07	-0.14	-18.74	-3.02
468	8.98466	38.78894	2316.122	-6.19	-8.94	9.54	2.75	-15.73	0.23
471	9.08775	36.58082	2159.125	-2.48	-6.37	14.19	3.88	-16.67	3.26
510	10.99886	27.83403	429.510	0.99	-2.47	22.76	3.47	-21.77	0.11
512	11.08385	39.71495	1853.680	-8.09	-7.14	7.73	-0.95	-15.82	-1.34
530	11.93986	41.45189	409.380	-9.44	-9.04	1.86	-0.39	-11.30	0.14
535	12.51986	37.43329	1959.740	-1.99	-2.02	14.61	0.03	-16.61	1.29
538	12.73172	43.11202	53.260	-9.75	-10.89	-3.81	1.14	-5.95	2.73
541	13.10689	33.85169	428.375	-1.68	-0.55	19.57	-1.13	-21.24	-0.18
543	13.43213	22.43807	815.550	6.67	8.83	24.81	-2.16	-18.14	-2.67
547	13.56639	25.22098	802.260	8.04	6.08	25.91	1.96	-17.87	0.38
575	15.14766	36.10997	481.653	2.27	1.61	18.83	0.66	-16.55	1.31
584	15.53997	32.48451	397.589	2.96	2.92	23.29	0.04	-20.33	-0.55
585	15.61135	32.53878	404.400	2.57	3.02	23.33	-0.45	-20.76	-1.05
594	16.16405	32.75606	430.011	3.85	3.85	23.71	0.00	-19.86	-0.64
622	17.93626	30.96552	304.768	8.27	8.31	25.75	-0.03	-17.47	0.75
661	19.50155	37.26091	4.417	3.77	3.46	15.84	0.30	-12.07	1.36
662	19.58522	33.31354	362.118	7.46	7.83	23.19	-0.36	-15.72	0.64

parameters derived by Boucher and Altamimi (1985)

(b) We removed the high frequency contribution to these undulations using the OSU86F model [Rapp and Cruz, 1986b] from N_{min} = 37 to N_{max} = 360

(c) We computed the undulations implied by GEMT1 and ADJUST20 for the locations of these stations.

The results from these computations are given on Table 14. The last column of this table shows the differences between N_D and the

undulations implied by OSU86F (from N_{min} = 2 to N_{max} = 360), as an indicator of the agreement of N_D with undulations implied by a high degree geopotential model.

As it can be seen from this table, the undulations implied by GEMT1 are in good agreement with the Doppler derived undulations (the RMS of the differences $N_D - N_{GEMT1}$ is 2.6 m), while the undulations implied by ADJUST20 are systematically biased with respect to the Doppler undulations (the RMS difference $N_D - N_{ADJUST20}$ is about 16 m).

This comparison indicates that the problem in Africa is due to erroneous surface gravity values. This was also verified by another comparison performed between 10° equal area mean gravity anomalies obtained from Satellite-to-Satellite Tracking (SST) techniques given by Kahn et al (1982) with the corresponding 10° equal area mean values computed from the June 1986 1°x1° anomalies by area averaging. The results of this comparison are given on Table 15.

Table 15. 10° Equal Area Gravity Anomaly Comparisons in Africa.

Border of 10° ea. Block			10° e.a. Mean Anomaly Δg (mgals)			
ϕ_N	ϕ_s	λ_w	λ_E	SST	GEMT-1	JUNE86
-5°	-15°	10:8825	21:0375	10.9	8.2	-8.9
15°	5°	31:1925	41:3475	7.1	7.2	22.7

The 10° e.a. anomalies implied by GEMT1 (computed by area averaging of the 1°x1° equi-angular implied anomalies) agree well with the SST derived anomalies, while the terrestrial anomalies show large differences. In both the cases of June 1986 as well as of GEMT1, the 1°x1° equi-angular blocks used to define the 10° equal area gravity anomaly were determined by rounding the 10° block longitude borders

to the nearest degree.

The regional inconsistencies between the anomalies implied from satellite only geopotential models and the terrestrial measurements were identified also in previous investigations [Kahn et al, 1982], [Mainville and Rapp, 1985]. Possible causes for these biases (in the cases where observed gravity data exist) are:

(i) Systematic biases in gravity base stations
(ii) Systematic errors introduced in the collection or compilation of the gravity data (gravity formula etc)
(iii) Systematic biases of the vertical datums of these regions (see also Section 2.3.5).

In the region of Africa, examination of the differences between the TUG86 and the TUG87 1°x1° mean elevations has not shown any systematic differences in the region that could account for the anomaly differences detected. However, this is only to be interpreted as an indication since we have no information about the elevations used for the compilation of the 1°x1° mean anomalies in that region.

On the other hand, in the areas of geophysically predicted anomalies, the biases may be due to inappropriate modeling and estimation techniques used to estimate these values.

Finally, it should be mentioned that the regional inconsistencies detected here have also been experienced in previous combination solutions. Figure 26 is very similar (over continental regions) with the Figure 11 given in [Rapp and Cruz, 1986a, p. 46] which illustrates the locations of residuals exceeding 7 mgals in the OSU86D combined solution.

5.3.3 Downweighting of Selected Terrestrial Gravity Data

Three alternative procedures can be used in order to compensate for the regional inconsistencies discussed in the previous section.

(1)

In areas where it is identified that the problem is caused due to vertical datum inconsistencies, introduce additional parameters in the modeling as it was discussed in Section 2.3.5.

(2)

In areas where redundant information is available (e.g. Doppler undulations), introduce additional observations in the adjustment.

(3)

Downweight the anomalies in regions where it is identified that the satellite information provides a more accurate description of the gravity field.

Method (1) suffers the disadvantage that the existing correlations in the normal matrix may cause contamination of other parameters instead of resolving vertical datum biases. In any case the use of such a method requires thorough investigation that is beyond the scope of this study.

Method (2) is limited by the fact that redundant information is seldomly available. For example, no Doppler undulations are available in the regions of the Soviet Union or China where large regional biases were detected. In addition, introduction of sparse point undulation data in a global adjustment has to be studied carefully. Parameterization of these observations should not include the very low degree harmonics since the sparse distribution of these data will degrade the estimability of long wavelength features of the gravity field. In an experimental solution where a limited set of point Doppler undulations was used in Africa as additional observations, a reduction

of the undulation differences (GEMT1 minus terrestrial solution), by 4 m was obtained. However, in this solution only coefficients above degree 20 have been parameterized in the undulation observations and a very small relative weight (0.01) was used in the combination of the normal equations obtained from the undulations with the normals obtained from the anomalies.

Such a solution was made only for experimental purposes since we recognize that the use of heterogeneous data (both in terms of nature and in terms of distribution), is a problem that could not be addressed in the time frame of this work.

Consequently, we have decided to attempt to compensate for the inconsistencies using method (3). The regions where the data would be downweighted were defined through the following comparisons:

$$\text{(a)}\quad |\bar{\Delta g}_{1^\circ\times 1^\circ \text{OSU86F}_{2\to 36}} - \bar{\Delta g}_{1^\circ\times 1^\circ \text{ADJUST20}}| > 10 \text{ mgals} \qquad (5.24)$$

$$\text{(b)}\quad |\bar{\Delta g}_{1^\circ\times 1^\circ \text{OSU86E}_{2\to 36}} - \bar{\Delta g}_{1^\circ\times 1^\circ \text{ADJUST40}}| > 10 \text{ mgals} \qquad (5.25)$$

The locations of these blocks are shown in Figures 38 and 39 respectively.

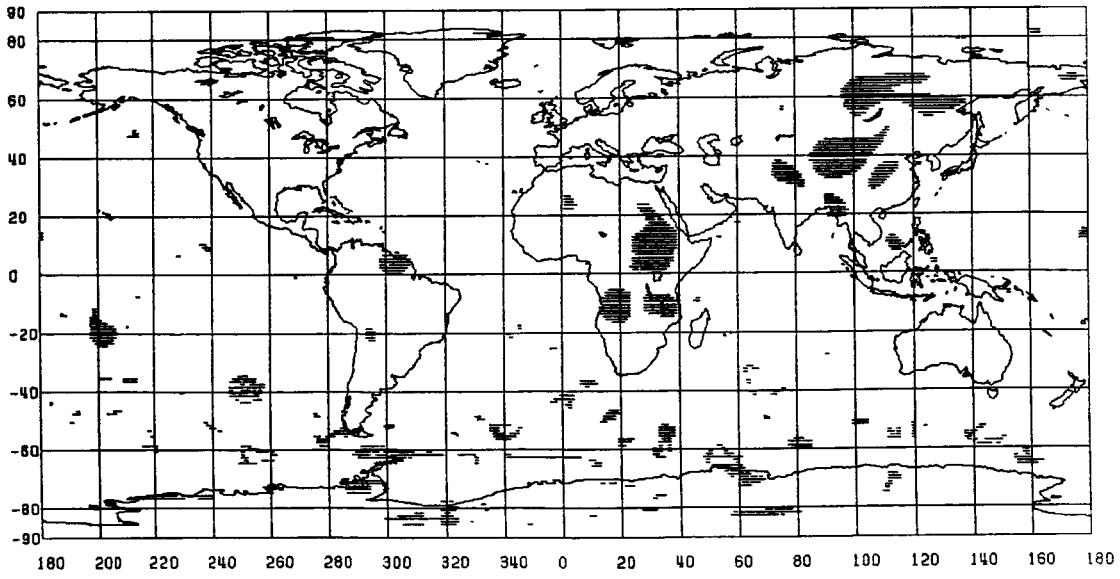

Figure 38. Locations of the 2550 1°x1° Blocks Where $|\bar{\Delta g}_{1^\circ\times 1^\circ \text{OSU86F}_{2\to 36}} - \bar{\Delta g}_{1^\circ\times 1^\circ \text{ADJUST20}}| > 10$ mgals.

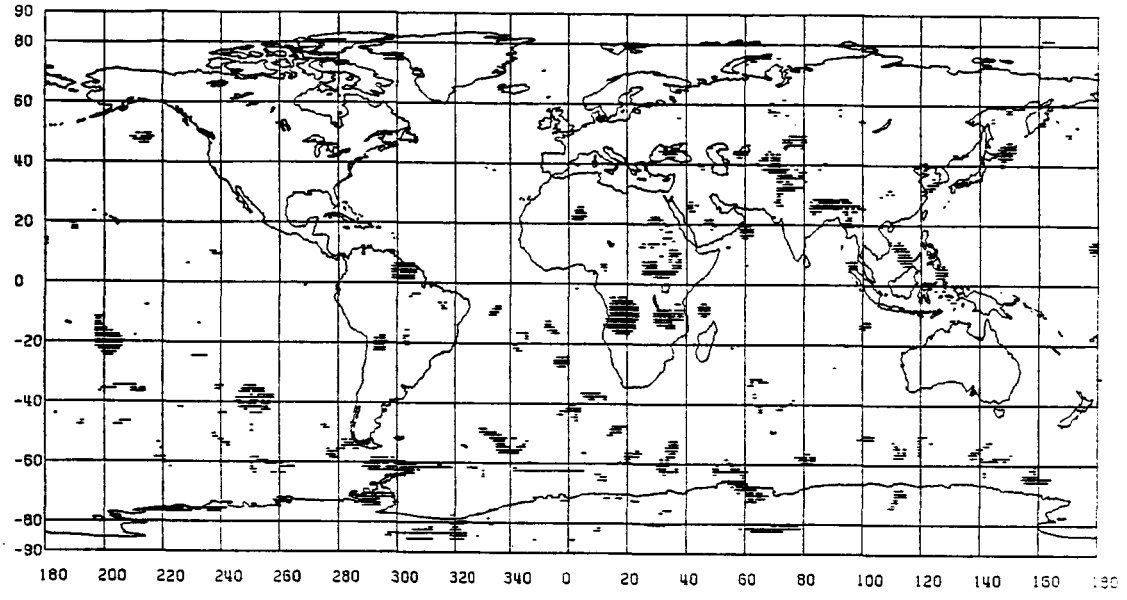

Figure 39. Locations of the 1985 1°x1° Blocks Where $|\bar{\Delta g}_{1°\times 1°\,OSU86E\,2\to 36} - \bar{\Delta g}_{1°\times 1°\,ADJUST\,40}| > 10$ mgals.

The OSU86E/F implied 1°x1° anomalies used in the comparisons contained the part of the spectrum only up to $N_{max} = 36$.

Two files containing "flags" indicating these locations have been constructed (see also Section 5.2.1). The standard deviations of the anomalies in these locations were defined by

$$\sigma_{ij} = \begin{cases} \max(30,\ 2.5\sigma_{ij(JUN86)}) \\ \min(60,\ 2.5\sigma_{ij(JUN86)}). \end{cases} \qquad (5.26)$$

In the case corresponding to Figure 38, the area average standard deviation of the 46405 blocks which do not fulfill (5.24) (these standard deviations are assigned according to (5.11)), is 28.8 mgals. The area average of the standard deviations of the 2550 blocks (assigned according to (5.26)) is 44.2 mgals. Hence, a downweighting of about 2.5

is performed for the areas where inconsistencies occur.

Two solutions performed according to this weighting scheme are the ADJUST65 (including geophysical data) and ADJUST71 (excluding geophysical data) (see also Table 7). The comparison of these solutions to the corresponding solutions ADJUST20 and ADJUST40 gave the overall results shown on Table 16.

As it is expected the downweighting affects more the solution where geophysical data are excluded because in that case the total number of available observations is substantially smaller than when geophysical data are included.

In addition, the comparison of ADJUST65 against the GEMT1 field in terms of global undulation and anomaly maps did not show substantial changes over the corresponding comparison of ADJUST20. This is due to the fact that the effect of downweighting cannot become apparent unless redundant information is introduced for the regions in question in the combination solution with the satellite normal equations.

Table 16. Overall Comparison Between Terrestrial-Only Solutions Without and With Downweighting of Selected Anomaly Data

	ADJUST20 versus ADJUST65	ADJUST40 versus ADJUST71
Average % Diff	8.67	10.49
RMS Undulation Diff (m)	0.60	3.67
RMS Anomaly Diff (mgals)	1.16	6.29

We recognize here that the procedure adopted to compensate for the regional inconsistencies between satellite-implied and terrestrial anomaly data, is not an optimum one. These problems should be considered in a more systematic manner in future updates of global anomaly data bases.

5.3.4 Computation of Anomaly Degree Variances

Concluding this chapter an important issue related to the computation of anomaly degree variances from coefficients obtained from a least squares adjustment of an incomplete set of gravity anomaly data will be discussed.

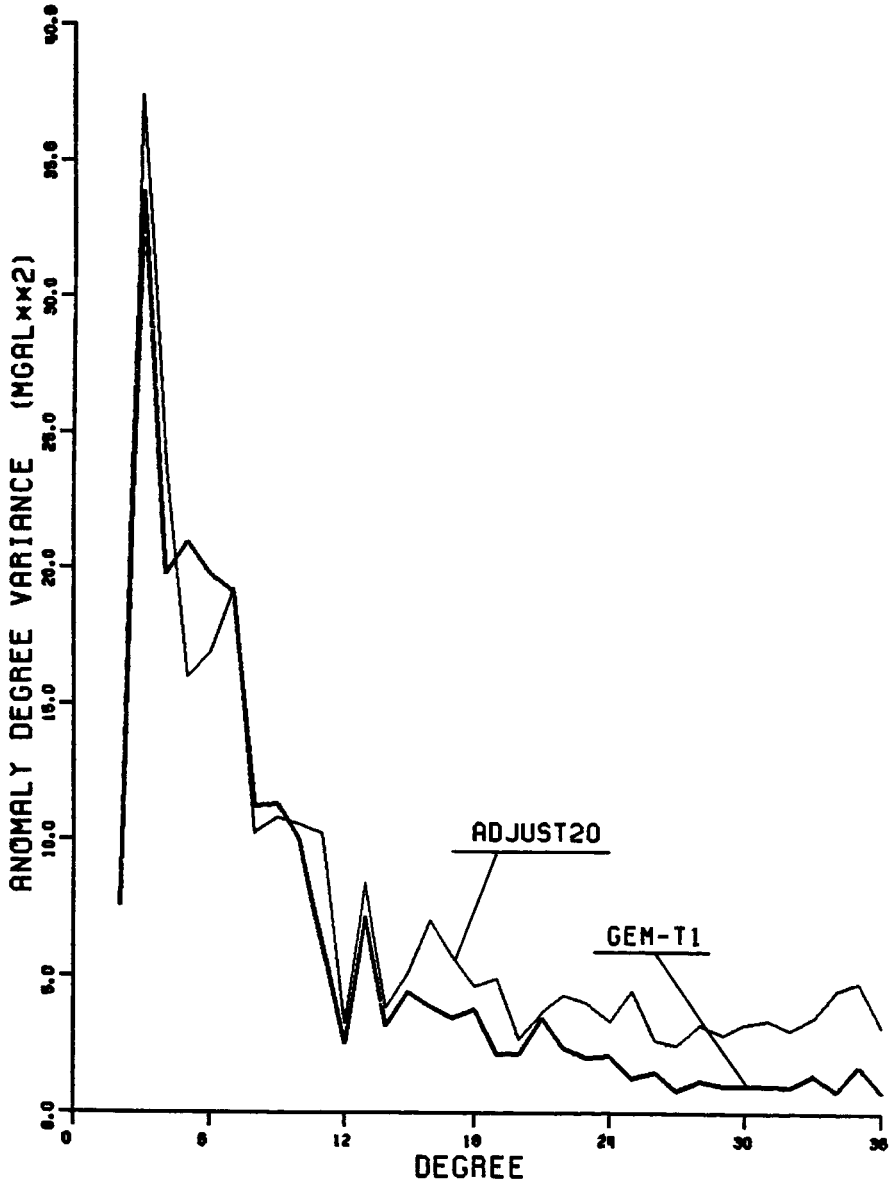

Figure 40. Anomaly Degree Variances Implied by GEMT1 and ADJUST20.

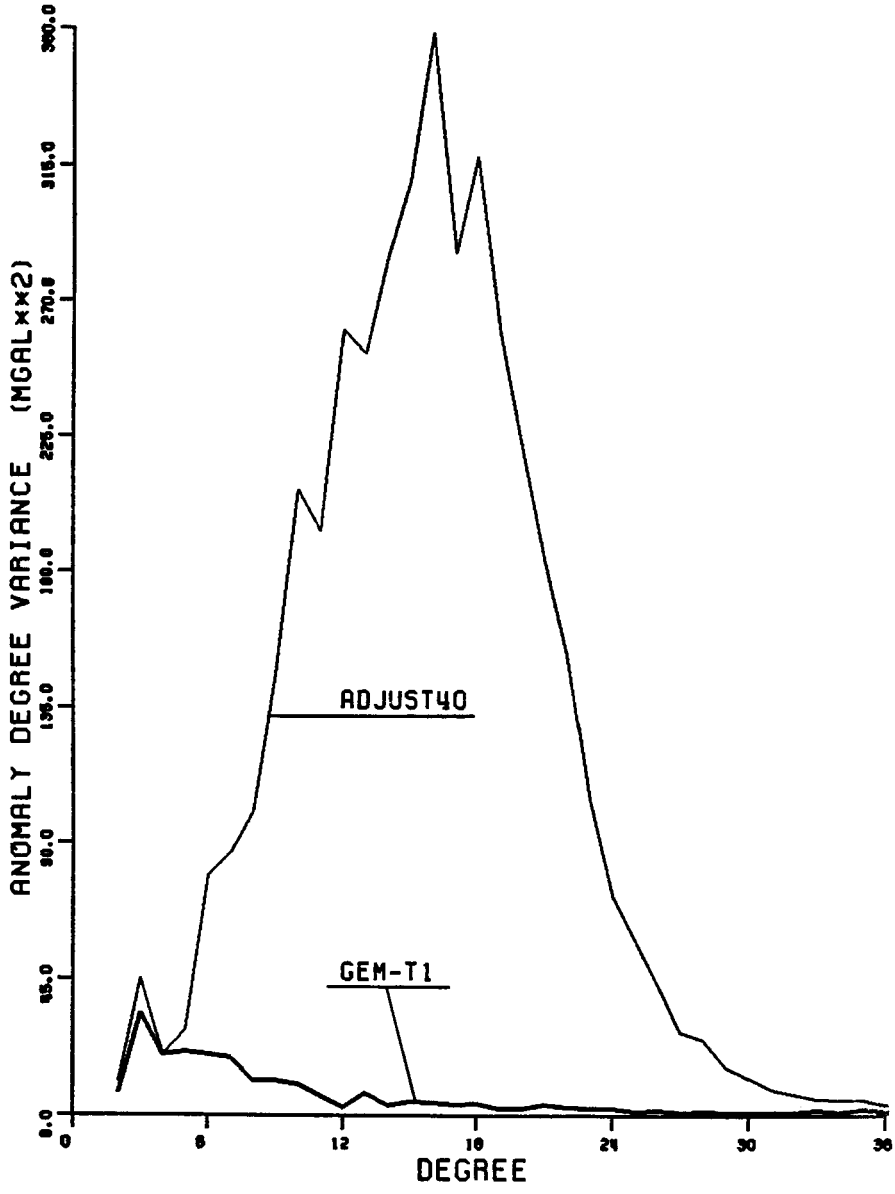

Figure 41. Anomaly Degree Variances Implied by GEMT1 and ADJUST40.

The anomaly degree variances implied by a given potential coefficient set were computed according to

$$c_n = \gamma^2(n-1)^2 \sum_{m=0}^{n} (\bar{C}^{*2}_{nm} + \bar{S}^{2}_{nm}) \qquad (5.27)$$

where

$$\gamma = \frac{GM}{a^2} \, . \qquad (5.28)$$

The values of GM, a used were the ones given in (3.3), while the even degree zonal coefficients of the normal potential (J_2, J_4, J_6), used to define $\bar{C}^{*}_{nm}$ (see equation (3.10)), were the ones given in (3.13).

Figures 40 and 41 show the anomaly degree variances implied by the satellite only field GEMT1 and the terrestrial only fields ADJUST20 and ADJUST40.

Examining Figure 40 we observe that the solution ADJUST20 gives anomaly degree variances which are in good agreement with those implied by GEMT1. Also, as it should be expected the terrestrial solution appears to have more power at higher degrees (above degree about 20), than the satellite one.

On the other hand, a first look of Figure 41 suggests that ADJUST40 yields coefficients totally unrealistic. However, the awkward shape of the spectrum implied by ADJUST40 is due to the fact that in the computation of degree variances, the assumption is inherent that the potential coefficients are uncorrelated. In the case of ADJUST20 the correlations between the coefficients which are neglected are small as it can be deduced from Figure 15a or 15c. However in case of ADJUST40 as it can be deduced from Figures 15b or 15d, the correlations between the coefficients cannot be omitted.

Degree variances, in theory, cannot be defined for any set of coefficients estimated from gridded data (point or mean values) of finite gridsize, even if the data grid is complete, according to what was discussed in Sections 4.2.1 and 4.2.2. However as it can be seen from the above the omission of the existing correlations between the coefficients effects the results severely only in cases where the

coverage is quite limited.

Computation of "degree variances" can be done if we diagonalize the normal matrix associated with the coefficients. However, the base functions that will be defined from the diagonalization will be linear combinations of surface harmonics not necessarily of the same degree. Hence, we would be able to compute the contribution to the anomaly from different coefficients but these coefficients will not necessarily be of the same degree.

CHAPTER VI

SUMMARY - CONCLUSIONS - RECOMMENDATIONS

The estimation of harmonic coefficients of the geopotential from surface gravity data was reexamined. The ultimate purpose was to investigate optimum modeling procedures and estimation techniques, in order to incorporate the information implied by the most up to date terrestrial gravity data, in combination solutions currently developed at NASA/Goddard Space Flight Center for use in the TOPEX/POSEIDON mission.

The modeling adopted is based on a form of the fundamental boundary condition of the linerarized Molodensky boundary value problem, which accounts for the effects of the earth's ellipticity to the order of the eccentricity squared.

The surface anomaly data were corrected for the effects of the atmosphere and the earth's ellipticity. The ellipsoidal correction terms were computed from an existing geopotential model, and applied to the surface anomaly data prior to the adjustment. In addition, examination of the procedures used for the numerical realization of the Molodensky surface free-air anomalies, lead to the conclusion that the term corresponding to the second order vertical gradient of the normal gravity (δg_h^2) is neglected in the evaluation of the surface anomalies. This term causes long wavelength systematic errors in the undulations that have an RMS magnitude of about 22 cm, with maximum values reaching 1.80 meters.

Consequently, the additional correction ($\delta g_h{}^2$) was applied to the surface anomalies to compensate for this effect.

The observation equations used to relate the unknown harmonic coefficients to the gravity data (properly reduced for the above systematic effects), consider the data lying on the physical surface of the earth. Hence, analytical continuation of the surface data to a bounding surface, is not required for the solution.

The estimation of harmonic coefficients from the surface anomalies was peformed using a least squares minimum variance estimator as proposed by Rapp (1967). The full normal matrix was formed and inverted to obtain the least squares solution. The advantage of this technique is that it does not require a complete set of anomaly data, and that it does not involve any assumptions regarding the orthogonality of area-mean samples of surface spherical harmonics. Hence, in contrast to the quadrature formulas, it enables exact recovery of a set of harmonic coefficients from simulated (noiseless) anomaly data computed from these coefficients.

An analytical comparison between the quadrature formulas and this technique, resulted in an alternative way which is proposed here for the definition and numerical evaluation of the quadrature formulas given in equation (4.46). Such a definition does not require the use of optimal quadrature weights.

In the application of the least squares adjustment procedure, an alternative approach to compensate for aliasing effects was proposed and used. Namely, instead of predicting mean anomalies of gridsize that corresponds to the maximum degree and order of the coefficients being estimated ($\Delta\lambda = \pi/N_{max}$), we use the original $1^\circ \times 1^\circ$ anomaly data and remove from them the frequency content beyond N_{max}. The high frequency content of the data is computed from an existing high degree geopotential model.

This procedure avoids the prediction of mean anomalies from the 1°x1° data, which would introduce additional approximations, and provides a better control over the frequency content of the data. In addition, the use of more dense data in low degree expansions enables the distinction of isolated erroneous data values, which are characterized by large residuals. From this point of view, such low degree expansions can be used as efficient tools for data editing in the compilation of global anomaly fields.

The comparison of low degree (N_{max} = 36) global gravity models obtained in this study from terrestrial data alone, with the satellite derived models, has indicated extended geographical regions (USSR, China, Africa) where systematic inconsistencies between the two sources of information occur. In the case of Africa comparisons with Doppler derived undulations verified that the problem lies with the terrestrial data. In an attempt to restrict the influence of the data from such regions in the combined solution, a downweighting of these anomalies was performed. It is recognized that this procedure is not really an optimum one and in future compilations of global anomaly fields special emphasis should be given in the improvement of the gravity material for these areas. Also, the techniques used for the estimation of gravity anomalies through geophysical correlation should be reexamined so that more reliable gravity anomaly estimates can be obtained from the application of these procedures.

The alternative use of gravity anomalies reduced to the ellipsoid through the application of terrain corrections was tested on a limited area. This procedure did not yield satisfactory results. Additional investigation is required in order to clarify the use of terrain corrections in the development of global geopotential models.

The nature of the topic of this study has introduced us to a number of related problems for which detailed investigation could not be conducted, inside the limits of this work. The estimation of error properties for global anomaly fields is certainly one of the problems

that should be investigated in the future. The study by Weber and Wenzel (1982) can serve as a starting point for such investigation.

The implementation of heterogeneous data (gravity anomalies, sea surface heights etc) in global geopotential modeling is another topic that deserves additional investigation. The ability to incorporate different and repeat data in the least squares adjustment, makes this estimation procedure a natural selection for solutions to the altimetry-gravimetry boundary value problem in mixed domains. Solutions as the one performed by Wenzel (1985), should be further investigated in an attempt to avoid some of the approximations used (e.g. formation of diagonal normal matrix).

Finally, the usefulness of the modern computational resources in the investigations related to global gravity modeling should be emphasized. This study serves as a perfect example of an investigation that was highly facilitated through the use of a supercomputer. Solutions which were carried out in a routine basis for this study were avoided 10 years ago due to their computational load. It is our sincere hope that these computational resources will make the term "computational limitations" to appear obsolete in a few years.

APPENDIX A

SYSTEMATIC EFFECTS

In this section the systematic effects arising from three causes are examined in terms of numerical values and spatial behavior. These are:

(a) ε_h: represents the effect on the boundary condition of the linear (first order) term in the Taylor series expansion of $\partial/\partial h$ around its "sperhical" value $\partial/\partial r$, and thus has its origin in the Taylor series expansion of the geometrical properties of the ellipsoid around their spherical values.

(b) ε_γ: represents the effect on the boundary condition of the linear term of the Taylor series expansion of the normal gravity γ and its gradient $\partial\gamma/\partial h$ around their spherical values. Hence, it originates from the Taylor series expansion of the dynamical properties of the ellipsoid around their spherical values.

(c) ε_r: represents the effect on the area-mean gravity anomaly caused by neglecting the variation of the geocentric radius over the block (omission of the second term in equation (2.99)).

The analytical expressions for the first two terms are

$$\varepsilon_h = e^2 \sin\theta\cos\theta \left(\frac{\partial T}{r\partial\theta}\right) \qquad (A.1)$$

$$\varepsilon_\gamma = \left[6J_2 \frac{a^2}{r^3} P_2(\cos\theta) - \frac{3\omega^2 r^2}{GM'} \sin^2\theta\right] T \qquad (A.2)$$

and the formulas for the computation of area-mean values IE_h and IE_γ of these terms are given in (2.111) and (2.112). The corresponding formula for ε_r is derived next to the $O(e^2)$. We have (see equation (2.99))

$$r(\phi) = \bar{r}_{ij} - \frac{1}{2} \frac{e^2 \sin 2\bar{\Phi}_i}{\bar{r}_{ij}} \bar{N}_i (\bar{M}_i + \bar{H}_{ij})(\phi - \bar{\Phi}_i) + \ldots \qquad (A.3)$$

so that

$$\frac{1}{r(\phi)} = \frac{1}{\bar{r}_{ij}} \left[1 + \frac{1}{2} \frac{e^2 \sin 2\bar{\Phi}_i}{\bar{r}_{ij}^2} \bar{N}_i (\bar{M}_i + \bar{H}_{ij})(\phi - \bar{\Phi}_i) + \ldots\right] \qquad (A.4)$$

and

$$\left(\frac{1}{r(\phi)}\right)^{n+2} = \left(\frac{1}{\bar{r}_{ij}}\right)^{n+2} \left[1 + \frac{(n+2)}{2} \frac{e^2 \sin 2\bar{\Phi}_i}{\bar{r}_{ij}^2} \bar{N}_i (\bar{M}_i + \bar{H}_{ij})(\phi - \bar{\Phi}_i) + \ldots\right] \qquad (A.5)$$

or

$$\left(\frac{1}{r(\phi)}\right)^{n+2} \approx \left(\frac{1}{\bar{r}_{ij}}\right)^{n+2} \left[1 + X(\phi)\right] \qquad (A.6)$$

with obvious notation.

However, we have

$$\Delta g(r,\theta,\lambda) = \frac{GM}{r^2} \sum_{n=2}^{\infty} (n-1) \left(\frac{a}{r}\right)^n \sum_{m=0}^{n} (\bar{C}^*_{nm} \cos m\lambda + \bar{S}_{nm} \sin m\lambda) \bar{P}_{nm}(\cos\theta) \qquad (A.7)$$

Setting

$$D_{nm} = \bar{C}^*_{nm} \cos m\lambda + \bar{S}_{nm} \sin m\lambda \qquad (A.8)$$

and

$$\bar{P}_{nm} = \bar{P}_{nm}(\cos\theta) \tag{A.9}$$

equation (A.7) can be written as

$$\Delta g = \frac{GM}{a^2} \sum_{n=2}^{\infty} (n-1)\left(\frac{a}{r}\right)^{n+2} \sum_{m=0}^{n} D_{nm}\bar{P}_{nm} \tag{A.10}$$

or according to (A.6)

$$\Delta g \approx \frac{GM}{a^2} \sum_{n=2}^{\infty} (n-1)\left(\frac{a}{\bar{r}_{ij}}\right)^{n+2} [1 + X(\phi)] \sum_{m=0}^{n} D_{nm}\bar{P}_{nm} \tag{A.11}$$

or

$$\Delta g \approx \frac{GM}{a^2} \sum_{n=2}^{\infty} (n-1)\left(\frac{a}{\bar{r}_{ij}}\right)^{n+2} \sum_{m=0}^{n} D_{nm}\bar{P}_{nm} +$$

$$\frac{GM}{a^2} \sum_{n=2}^{\infty} (n-1)\left(\frac{a}{\bar{r}_{ij}}\right)^{n+2} \sum_{m=0}^{n} D_{nm}X(\phi)\bar{P}_{nm} \tag{A.12}$$

so that

$$\Delta g = \Delta g^{\circ} + \varepsilon_r \tag{A.13}$$

where Δg° is the anomaly computed with the geocentric radius referring to the center of the block, and

$$\varepsilon_r = \frac{e^2 \sin 2\bar{\Phi}_i}{2\bar{r}_{ij}^4} \bar{N}_i(\bar{M}_i + \bar{H}_{ij})GM \sum_{n=2}^{\infty} (n-1)(n+2)\left(\frac{a}{\bar{r}_{ij}}\right)^{n} \sum_{m=0}^{n} D_{nm}(\phi - \bar{\Phi}_i)\bar{P}_{nm} \tag{A.14}$$

or

$$\varepsilon_r = c \sum_{n=2}^{\infty} (n-1)(n+2)\left(\frac{a}{\bar{r}_{ij}}\right)^{n} \sum_{m=0}^{n} D_{nm}(\phi - \bar{\Phi}_i)\bar{P}_{nm} \tag{A.15}$$

For small blocksizes (e.g. 1°x1°) we may write

$$(\phi - \bar{\phi}_i)^{rad} \approx \sin(\phi - \bar{\phi}_i) = \sin\phi\cos\bar{\phi}_i - \cos\phi\sin\bar{\phi}_i \qquad (A.16)$$

so that (A.15) becomes

$$\varepsilon_r = c\cos\bar{\phi}_i \sum_{n=2}^{\infty} (n-1)(n+2)\left(\frac{a}{\bar{r}_{ij}}\right)^n \sum_{m=0}^{n} D_{nm}\sin\phi\bar{P}_{nm}$$

$$- c\sin\bar{\phi}_i \sum_{n=2}^{\infty} (n-1)(n+2)\left(\frac{a}{\bar{r}_{ij}}\right)^n \sum_{m=0}^{n} D_{nm}\cos\phi\bar{P}_{nm} \qquad (A.17)$$

However, (see [Rapp, 1984, p. 26, equation 3.78])

$$\phi = \psi + m\sin 2\phi + \ldots \qquad (A.18)$$

or

$$\phi \approx \psi + \frac{e^2}{2}\sin 2\phi + \ldots \qquad (A.19)$$

where ψ denotes the geocentric latitude ($\psi = 90^\circ - \theta$). The last term in (A.19) will introduce terms of $O(e^4)$ when substituted in (A.17), hence it can be omitted. Accordingly (A.17) becomes

$$\varepsilon_r = c\cos\bar{\phi}_i \sum_{n=2}^{\infty} (n-1)(n+2)\left(\frac{a}{\bar{r}_{ij}}\right)^n \sum_{m=0}^{n} D_{nm}\cos\theta\bar{P}_{nm}$$

$$- c\sin\bar{\phi}_i \sum_{n=2}^{\infty} (n-1)(n+2)\left(\frac{a}{\bar{r}_{ij}}\right)^n \sum_{m=0}^{n} D_{nm}\sin\theta\bar{P}_{nm} \qquad (A.20)$$

From the recursive relations [Moritz, 1980, equation 39-45]

$$\cos\theta P_{nm}(\cos\theta) = \frac{n-m+1}{2n+1} P_{n+1,m} + \frac{n+m}{2n+1} P_{n-1,m} \qquad (A.21)$$

and [Ilk, 1983, equation Z.1.28]

$$\sin\theta P_{nm}(\cos\theta) = \frac{1}{2n+1}\left(P_{n+1,m+1} - P_{n-1,m+1}\right) \qquad (A.22)$$

we have

$$\cos\theta\bar{P}_{nm}(\cos\theta) = x_{nm}\bar{P}_{n+1,m} + y_{nm}\bar{P}_{n-1,m} \qquad (A.23)$$

$$\sin\theta\bar{P}_{nm}(\cos\theta) = z_{nm}\bar{P}_{n+1,m+1} - w_{nm}\bar{P}_{n-1,m+1} \qquad (A.24)$$

where

$$\left.\begin{aligned} x_{nm} &= \sqrt{\frac{(n-m+1)(n+m+1)}{(2n+1)(2n+3)}} && (a)\\ y_{nm} &= \sqrt{\frac{(n+m)(n-m)}{(2n+1)(2n-1)}} \qquad (n > 1) && (b)\\ z_{nm} &= \sqrt{\frac{(n+m+1)(n+m+2)}{(2n+1)(2n+3)}} && (c)\\ w_{nm} &= \sqrt{\frac{(n-m-1)(n-m)}{(2n+1)(2n-1)}} \qquad (n > 1) && (d) \end{aligned}\right\} \qquad (A.25)$$

Hence,

$$\begin{aligned} \varepsilon_r = c \Bigg\{ \cos\Phi_i \Bigg[& \sum_{n=2}^{\infty} (n-1)(n+2)\left(\frac{a}{\bar{r}_{ij}}\right)^n \sum_{m=0}^{n} D_{nm}x_{nm}\bar{P}_{n+1,m} \\ & + \sum_{n=2}^{\infty} (n-1)(n+2)\left(\frac{a}{\bar{r}_{ij}}\right)^n \sum_{m=0}^{n-1} D_{nm}y_{nm}\bar{P}_{n-1,m} \Bigg] \\ - \sin\Phi_i \Bigg[& \sum_{n=2}^{\infty} (n-1)(n+2)\left(\frac{a}{\bar{r}_{ij}}\right)^n \sum_{m=0}^{n} D_{nm}z_{nm}\bar{P}_{n+1,m+1} \\ & - \sum_{m=0}^{n} (n-1)(n+2)\left(\frac{a}{\bar{r}_{ij}}\right)^n \sum_{m=0}^{n-2} D_{nm}w_{nm}\bar{P}_{n-1,m+1} \Bigg] \Bigg\} \end{aligned} \qquad (A.26)$$

Evaluation of point values of ε_r can be made using (A.26), truncated to some finite degree N_{max}, from a given set of potential coefficients, while for area-mean values (IE_r), the above equation has to be modified in exactly the same manner as it was done in the case of ε_h and ε_γ (see equations (2.111) and (2.112)). As in the case of ε_h and ε_γ, the

evaluation of ε_r (or IE_r) may be made on the surface of the reference ellipsoid rather than on the physical surface of the earth without significant loss of accuracy.

For the numerical application , 1°x1° mean values of the terms IE_h, IE_γ and IE_r have been computed from the OSU86F potential coefficient set [Rapp and Cruz, 1986b] complete to N_{max} = 180, using the TOPEX constants.

A harmonic analysis was then performed to each one of the global sets containing the anomaly correction terms IE_h, IE_γ and IE_r. From the corresponding harmonic coefficient sets the implied undulation corrections were then computed. In Figures 42, 43 and 44 these undulation corrections are illustrated. These plots represent point values of the undulation on a 5°x5° grid, computed from harmonic coefficients complete to N_{max} = 36.

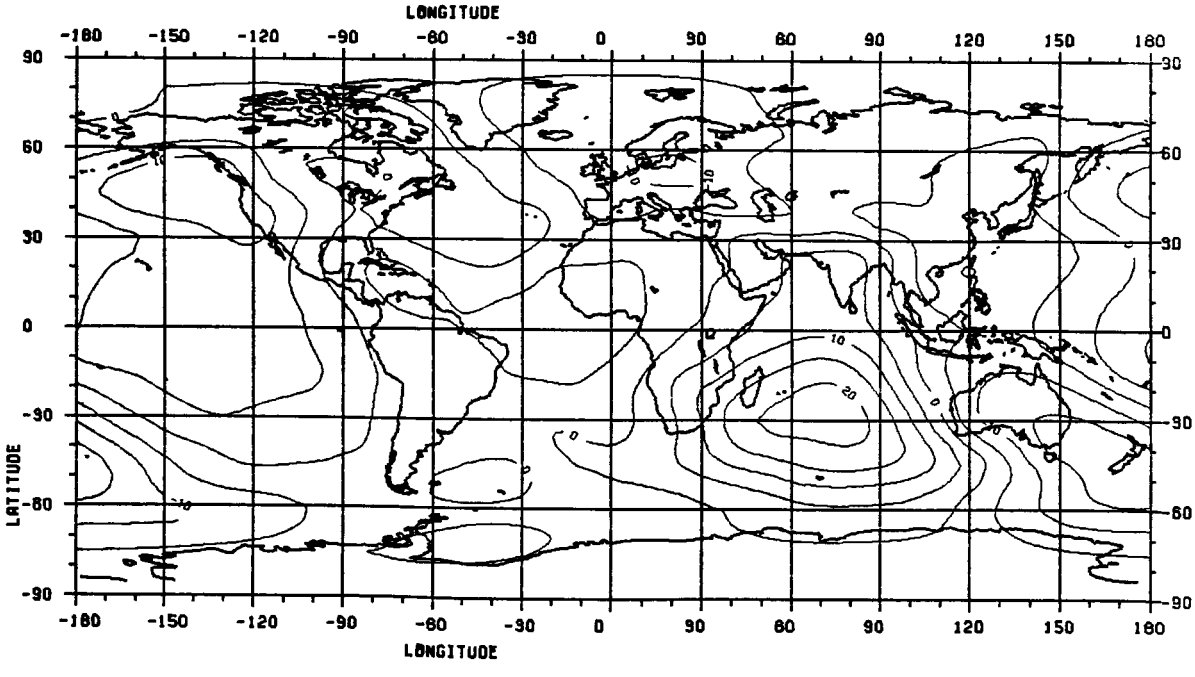

Figure 42. Undulation Corrections Implied by IE_h. (Contour Interval is 5 cm).

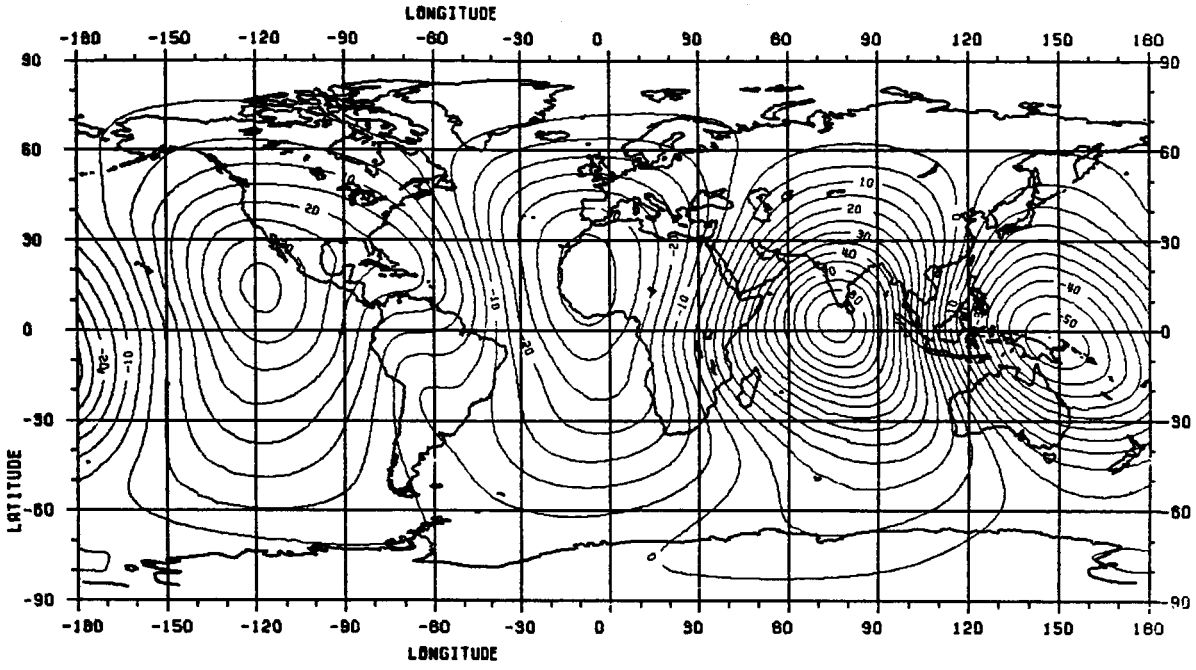

Figure 43. Undulation Corrections Implied by IE_γ. (Contour Interval is 5 cm).

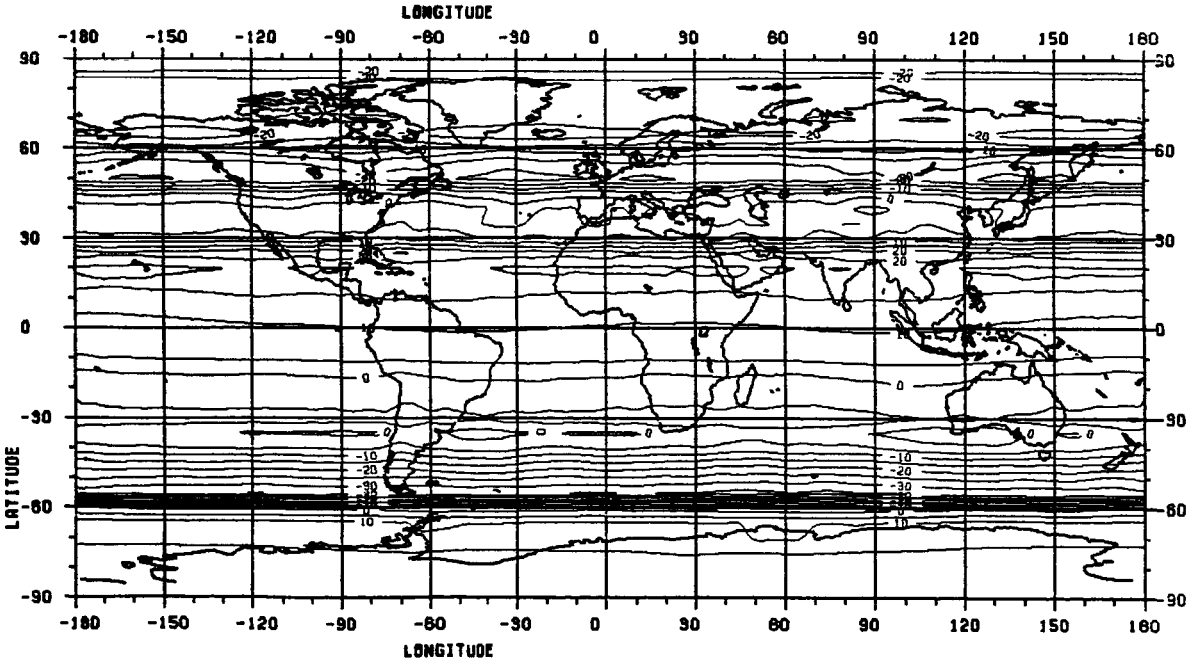

Figure 44. Undulation Corrections Implied by IE_r. (Contour Interval is 5 mm).

With respect to these plots the following comments are to be made

(a) The term ε_h is proportional to the meridional component of the deflection of the vertical, since

$$\varepsilon_h \approx e^2 \sin\theta\cos\theta\gamma\xi \qquad (A.27)$$

as it can be seen from (A.1). It is thus expected to take large values wherever the meridional slope of the geoid is large. An example of this behavior is the high observed in Figure 42 in the area of the Indian Ocean.

(b) The term ε_γ is proportional to the undulation as it can be seen from (A.2). This explains the similarity of Figure 43 with global plots of long wavelength geoids (compare, for example, with [Heiskanen and Moritz, 1967, Figure 3-21]).

Both Figures 42 and 43 are in perfect agreement with the corresponding Figures 1 and 2 in [Cruz, 1986, pp. 15, 16] verifying the equivalence of the two methods for the computation of the ellipsoidal effects.

(c) Figure 44 indicates that the undulation corrections implied by ε_r are almost exclusively a function of latitude, which is of course expected. It also indicates that the effect of ε_r can be safely neglected since the maximum undulation correction implied by this term is (in absolute value) about 3 cm.

APPENDIX B

COMBINATION SOLUTION ADJUSTMENT MODELS

Notation

X^a: theoretical values of parameters

L^a: theoretical values of observables

L^b: observed values of observables

$\hat{L}^a$: adjusted values of observables

X^o: approximate values of parameters (B.1)

$\hat{X}^a$: adjusted values of parameters

v : residuals

L_x: a set of observed parameters

$\hat{X}$: alteration vector (solution of normal equations)

$$\hat{X}^a = X^o + \hat{X} \tag{B.2}$$

$$\hat{L}^a = L^b + v \tag{B.3}$$

Identify:

L_x: potential coefficients obtained from satellite solution (B.4)

P_x: weight matrix associated with L_x (B.5)

L_T^b: area-mean gravity anomaly estimates, dg_{ij}, properly corrected for systematic errors (B.6)

P_ℓ: weight matrix associated with L_T^b (B.7)

Assume: L_x and L_T^b uncorrelated (B.8)

Set: $X^o = L_x$ (B.9)

Case I: Terrestrial estimates of potential coefficients obtained from quadrature formulas

Mathematical Model:

$$C_{nm}^{\alpha} = \frac{1}{4\pi\gamma(n-1)} \sum_{i=o}^{N-1} \bar{IP}_{nm}^{i} \sum_{j=o}^{2N-1} \begin{Bmatrix} IC_m^j \\ IS_m^j \end{Bmatrix} dg_{ij} \tag{B.10}$$

or

$$X^a = G(L^a) \tag{B.11}$$

Combination solution can be viewed as the sequential adjustment

$$\left.\begin{aligned} X^a &= G(L^a) \\ L_x &= X^a \end{aligned}\right\} \tag{B.12}$$

which reduces to the case of "observations in two groups with the same unknown parameters" [Uotila, 1986, Section 8], as long as we identify

$$\left.\begin{aligned} F_1(L_1^a, X^a) &= 0 \iff X^a - G(L^a) = 0 \\ F_2(L_2^a, X^a) &= 0 \iff L_x - X^a = 0 \end{aligned}\right\} \tag{B.13}$$

with $L_1^b = L_T^b$; $L_2^b = L_x$ (B.14)

Then,

$$A_1 = \frac{\partial F_1}{\partial X^a}\Big|_{\substack{L^a = L^b = I \\ X^a = X^o}} \tag{B.15}$$

$$B_1 = \frac{\partial F_1}{\partial L^a}\bigg|_{\substack{L^a = L^b \\ X^a = X^o}} = -\frac{\partial G}{\partial L^a}\bigg|_{\substack{L^a = L^b \\ X^a = X^o}} := B_\ell \tag{B.16}$$

$$W_1 = F_1\,(L_1^b, X^o) = L_x - G(L_T^b) := W \tag{B.17}$$

$$A_2 = \frac{\partial F_2}{\partial X^a}\bigg|_{\substack{L^a = L^b \\ X^a = X^o}} = -I \tag{B.18}$$

$$B_2 = \frac{\partial F_2}{\partial X^a}\bigg|_{\substack{L^a = L^b \\ X^a = X^o}} = I \tag{B.19}$$

$$W_2 = F_2(L_2^b, X^o) = L_x - L_x = 0 \tag{B.20}$$

Accordingly,

$$\left.\begin{aligned} A &= \begin{bmatrix} A_1 \\ A_2 \end{bmatrix} = \begin{bmatrix} I \\ -I \end{bmatrix} \;;\; B = \begin{bmatrix} B_1 & 0 \\ 0 & B_2 \end{bmatrix} = \begin{bmatrix} B_\ell & 0 \\ 0 & I \end{bmatrix} \\ L_b &= \begin{bmatrix} L_1^b \\ L_2^b \end{bmatrix} = \begin{bmatrix} L_T^b \\ L_x \end{bmatrix} \;;\; P = \begin{bmatrix} P_1 & 0 \\ 0 & P_2 \end{bmatrix} = \begin{bmatrix} P_\ell & 0 \\ 0 & P_x \end{bmatrix} \\ W &= \begin{bmatrix} W_1 \\ W_2 \end{bmatrix} = \begin{bmatrix} W \\ 0 \end{bmatrix} \;;\; v = \begin{bmatrix} v_1 \\ v_2 \end{bmatrix} = \begin{bmatrix} v_\ell \\ v_x \end{bmatrix} \end{aligned}\right\} \tag{B.21}$$

Hence,

$$M = BP^{-1}B^T = \begin{bmatrix} M_1 & 0 \\ 0 & M_2 \end{bmatrix} = \begin{bmatrix} B_\ell P_\ell^{-1} B_\ell^T & 0 \\ 0 & P_x^{-1} \end{bmatrix} \tag{B.22}$$

so that

$$M^{-1} = \begin{bmatrix} M_1^{-1} & 0 \\ 0 & M_2^{-1} \end{bmatrix} = \begin{bmatrix} (B_\ell P_\ell^{-1} B_\ell^T)^{-1} & 0 \\ 0 & P_x \end{bmatrix} \tag{B.23}$$

Thus

$$\hat{X} = -(A_1^T M_1^{-1} A_1 + A_2^T M_2^{-1} A_2)^{-1} (A_1^T M_1^{-1} W_1 + A_2^T M_2^{-1} W_2)$$

yields

$$\hat{X} = -[(B_\ell P_\ell^{-1} B_\ell^T)^{-1} + P_x]^{-1} (B_\ell P_\ell^{-1} B_\ell^T)^{-1} W \tag{B.24}$$

Also

$$v = P^{-1} B^T K \tag{B.25}$$

where K are the Lagrange multipliers. Hence

$$\begin{bmatrix} v_\ell \\ v_x \end{bmatrix} = \begin{bmatrix} P_\ell^{-1} & 0 \\ 0 & P_x^{-1} \end{bmatrix} \begin{bmatrix} B_\ell^T & 0 \\ 0 & I \end{bmatrix} \begin{bmatrix} K_1 \\ K_2 \end{bmatrix} \Rightarrow \begin{array}{l} v_\ell = P_\ell^{-1} B_\ell^T K_1 \\ v_x = P_x^{-1} K_2 \end{array} \Bigg\} \tag{B.26}$$

Now

$$\begin{bmatrix} K_1 \\ K_2 \end{bmatrix} = -M^{-1}(A\hat{X} + W) = -\begin{bmatrix} M_1^{-1} & 0 \\ 0 & M_2^{-1} \end{bmatrix} \left\{ \begin{bmatrix} I \\ -I \end{bmatrix} \hat{X} + \begin{bmatrix} W \\ 0 \end{bmatrix} \right\}$$

yields

$$\left.\begin{array}{l} K_1 = -(B_\ell P_\ell^{-1} B_\ell^T)^{-1} (\hat{X} + W) \\ K_2 = P_x \hat{X} \end{array}\right\} \tag{B.27}$$

From (B.26) and (B.27) we have

$$v_\ell = -P_\ell^{-1} B_\ell^T (B_\ell P_\ell^{-1} B_\ell^T)^{-1} (\hat{X} + W) \tag{B.28}$$

$$v_x = \hat{X} \tag{B.29}$$

Equation (B.29) in view of (B.24) yields

$$v_x = -[(B_\ell P_\ell^{-1} B_\ell^T)^{-1} + P_x]^{-1} (B_\ell P_\ell^{-1} B_\ell^T)^{-1} W \qquad (B.30)$$

Equation (B.30) is identical with equation (74) in [Rapp, 1984], while (B.28) is identical to [ibid, eq. 69] since $B_x = I$ in Rapp's notation.

Case II: Terrestrial estimates of potential coefficients obtained from least squares adjustment.

Mathematical Model

$$dg_{ij} = \frac{1}{\Delta\sigma_i} \frac{GM}{\bar{r}_{ij}^2} \sum_{\substack{n=0 \\ n\neq 1}}^{Nmax} (n-1) \left(\frac{a}{\bar{r}_{ij}}\right) \sum_{m=0}^{n} \sum_{\alpha=0}^{1} C_{nm}^{\alpha} \bar{Y}_{nm}^{\alpha ij} \qquad (B.31)$$

The combination solution can be viewed as the sequential adjustment

$$\left.\begin{aligned} L^a &= F(X^a) \\ L_x &= X^a \end{aligned}\right\} \qquad (B.32)$$

which again falls into the same category as before [Uotila, 1986, Section 8] as long as we identify

$$\left.\begin{aligned} F_1(L_1^a, X^a) = 0 &\iff L^a - F(X^a) = 0 \\ F_2(L_2^a, X^a) = 0 &\iff L_x - X^a = 0 \end{aligned}\right\} \qquad (B.33)$$

Following the same procedure as in Case I we now have

$$A_1 = -\frac{\partial F}{\partial X^a}\Bigg|_{\substack{L^a = L^b \\ X^a = X^0}} := A_x \qquad (B.34)$$

$$B_1 = I \qquad (B.35)$$

$$W_1 = F_1(L_1, X) = L_1^b - F(L_x) := W \qquad (B.36)$$

$$A_2 = -I \qquad (B.37)$$

$$B_2 = I \tag{B.38}$$

$$W_2 = 0 \tag{B.39}$$

Hence,

$$M = BP^{-1}B^T = \begin{bmatrix} I & 0 \\ 0 & I \end{bmatrix} \begin{bmatrix} P_\ell^{-1} & 0 \\ 0 & P_x^{-1} \end{bmatrix} \begin{bmatrix} I & 0 \\ 0 & I \end{bmatrix} = \begin{bmatrix} P_\ell^{-1} & 0 \\ 0 & P_x^{-1} \end{bmatrix} \tag{B.40}$$

and thus following exactly the same steps as in Case I we finally get

$$v_x = \hat{X} = -(A_x^T P_\ell A_x + P_x)^{-1} A_x^T P_\ell W \tag{B.41}$$

and

$$v_\ell = -(A_x \hat{X} + W) \tag{B.42}$$

Equations (B.41) and (B.42) become identical to equations (117) and (120) respectively of [Rapp, 1986, p. 388] once the proper changes of the notation are made.2

LIST OF REFERENCES

Boucher, C. and Z. Altamimi, Towards an Improved Realization of the BIH Terrestrial Frame, in Proc. of the Int. Conf. on Earth Rotation and Terrestrial Reference Frame, Dept. of Geodetic Science and Surveying, The Ohio State University, Columbus, Vol. 2, 1985.

Cappellari, J.O., C.E. Velez and A.J. Fuchs, Mathematical Theory of the Goddard Trajectory Determination System, Goddard Space Flight Center, X-582-76-77, Greenbelt, Maryland, 1976.

Colombo, O.L., Numerical Methods for Harmonic Analysis on the Sphere, Report No. 310, Dept. of Geodetic Science and Surveying, The Ohio State University, Columbus, 1981.

Cruz, J.Y., Disturbance Vector in Space From Surface Gravity Anomalies Using Complementary Models, Report No. 366, Dept. of Geodetic Science and Surveying, The Ohio State University, Columbus, August, 1985, AFGL-TR-85-0209, ADA 155730.

Cruz, J.Y., Ellipsoidal Corrections to Potential Coefficients Obtained from Gravity Anomaly Data on the Ellipsoid, Report No. 367, Dept. of Geodetic Science and Surveying, The Ohio State University, Columbus, August, 1986, AFGL-TR-86-0178.

Dermanis, A., The Geodetic Boundary Value Problem Linearized with Respect to the Somigliana-Pizzetti Normal Field, manuscripta geodaetica, Vol. 9, pp. 77-92, 1984 (Revised Version).

Despotakis, V., The Development of the June 1986 1°x1° and the August 30′x30′ Terrestrial Mean Free-Air Anomaly Data, Internal Report, Dept. of Geodetic Science and Surveying, The Ohio State University, Columbus, September 1986.

Despotakis, V., Geoid Undulation Computations at Laser Tracking Stations, Report No. 383, Dept. of Geodetic Science and Surveying, The Ohio State University, Columbus, September 1987.

Desrochers, G.A., A Study of the Aliasing Effect On Gravitational Potential Coefficients as Determined From Gravity Data, Report No. 160, Dept. of Geodetic Science, The Ohio State University, Columbus, December, 1971.

Hajela, D.P., Optimal Estimation of High Degree Gravity Field From a Global Set of 1°x1° Anomolies to Degree and Order 250, Report No. 358, Dept. of Geodetic Science and Surveying, The Ohio State University, Columbus, August, 1984.

Heiskanen, W.A., and H. Moritz, Physical Geodesy, Freeman, San Francisco, 1967.

International Association of Geodesy, Geodetic Reference System 1967, Special Publication of Bulletin Geodesique, Paris, 1971.

Jekeli, C., The Downward Continuation to the Earth's Surface of Truncated Spherical and Ellipsoidal Harmonic Series of the Gravity and Height Anomalies, Report No. 323, Dept. of Geodetic Science and Surveying, The Ohio State University, Columbus, 1981, AFGL-TR-81-0361.

Jet Propulsion Laboratory, National Aeronautics and Space Administration and Centre National d'Etudes Spatiales, TOPEX/POSEIDON Mission Description, JPL, California Institute of Technology, Pasadena, California, December, 1985.

Kahn, W.D., S.M. Klosko and W.T. Wells, Mean Gravity Anomalies From A Combination of Apollo/ATS6 and GEOS3/ATS6 SST Tracking Campaigns, J. Geophys. Res., Vol. 87, No. B4, pp. 2904-2981, April 1982.

Kaula, W.M., Theory of Satellite Geodesy, Blaisdell Publishing Co., Waltham, Mass., 1966a.

Kaula, W.M., Tests and Combination of Satellite Determinations of the Gravity Field with Gravimetry, J. Geophys. Res., Vol. 71, pp. 5303-5314, 1966b.

Krarup, T., Letters on Molodensky's Problem I-IV, Communication to the members of IAG Special Study Group 4.31, unpublished, 1973.

Lebedev, N.N., I.P. Skalskaya, Y.S. Uflyand, Worked Problems in Applied Mathematics, Dover Publications, Inc., New York, 1979.

Lerch, F.J., S.M. Klosko, R.E. Laubscher, and C.A. Wagner, Gravity Model Improvement using GEOS3 (GEM9 and 10), J. Geophys. Res., Vol. 84, No. B8, pp. 3897-3916, July 1979.

Lerch, F.J., B.H. Putney, C. A. Wagner, S.M. Klosko, Goddard Earth Models for Oceanographic Applications (GEM10B and 10C), Marine Geodesy, Vol. 5, No. 2, pp. 145-187, 1981.

Lerch, F.J., S.M. Klosko, and G.B. Patel, A Refined Gravity Model from Lageos (GEM-L2), Geophys. Res. Lett., Vol. 9, No. 11, pp. 1263-1266, November 1982a.

Lerch, F.J., J.G. Marsh, S.M. Klosko, and R.G. Williamson, Gravity Model Improvement for SEASAT, J. Geophys. Res., Vol. 87, No. C5, 1982b.

Mainville, A., The Altimetry-Gravimetry Problem Using Orthonormal Base Functions, Report No. 373, Dept. of Geodetic Science and Surveying, The Ohio State University, Columbus, December 1986.

Mainville, A., and R.H. Rapp, Detection of Regional Bias in 1°x1° Mean Terrestrial Gravity Anomalies, Bureau Gravimetrique International, Bulletin d'Information No. 57, December 1985.

Marsh, J.G. et al, An Improved Model of the Earth's Gravitational Field: GEM-T1, NASA Technical Memorandum 4019, July 1987.

Martin, T.V., W.F. Eddy, A. Brenner, B. Rosen, J. McCarthy, GEODYN System Description, Vol. 1, EG&G, Washington Analytical Services Inc., Riverdale, Maryland, 1980.

Moritz, H., Linear Solutions of the Geodetic Boundary - Value Problem, Dept. of Geodetic Science and Surveying, The Ohio State University, Columbus, 1966.

Moritz, H., Advanced Physical Geodesy, Abacus Press, Kent, U.K., 1980.

Moritz, H., Local Geoid Determination in Mountain Regions, Report No. 352, Dept. of Geodetic Science and Surveying, The Ohio State University, Columbus, December 1983.

Moritz, H., Geodetic Reference System 1980, in Bulletin Geodesique, Vol. 54, No. 3, 1984.

Paul, M.K., Recurrence Relations for Integrals of Associated Legendre Functions, Bulletin Geodesique, Vol. 52, pp. 177-190, 1978.

Rapp, R.H., The Geopotential to (14,14) from a Combination of Satellite and Gravimetric Data, presented at the XIV General Assembly IUGG/IAG, September 25 - October 7, Lucernce, Switzerland, 1967.

Rapp, R.H., Analytical And Numerical Differences Between Two Methods for the Combination of Gravimetric and Satellite Data, Bollettino di Geofisica Teorica ed Applicata, Vol. XI, No. 41-42, pp. 108-118, 1969.

Rapp, R.H., Determination of Potential Coefficients to Degree 52 from 5° Mean Gravity Anomalies, Bulletin Geodesique, Vol. 51, No. 4, pp. 301-323, 1977.

Rapp, R.H., A Global 1°x1° Anomaly Field Combining Satellite, GEOS-3 Altimeter, and Terrestrial Data, Report No. 278, Dept. of Geodetic Science, The Ohio State University, Columbus, September, 1978.

Rapp, R.H., The Earth's Gravity Field to Degree and Order 180 Using SEASAT Altimeter Data, Terrestrial Gravity Data, and Other Data, Report No. 322, Dept. of Geodetic Science and Surveying, The Ohio State University, Columbus, December 1981.

Rapp, R.H., Fundamental Geodetic Constants, Report of Special Study Group No. 5.39 of IAG, XVIII General Assembly of IUGG, Hamburg, August, 1983a.

Rapp, R.H., Geometric Geodesy Part II, Dept. of Geodetic Science and Surveying, The Ohio State University, Columbus, September 1983b.

Rapp, R.H., The Determination of High Degree Potential Coefficient Expansions from the Combination of Satellite and Terrestiral Gravity Information, Report No. 361, Dept. of Geodetic Science and Surveying, The Ohio State University, Columbus, 1984.

Rapp, R.H., Detailed Gravity Anomalies and Sea Surface Heights Derived from GEOS-3/SEASAT Altimeter Data, Report No. 365, Dept. of Geodetic Science and Surveying, The Ohio State University, Columbus, 1985; AFGL-TR-85-0191.

Rapp, R.H., Global Geopotential Solutions, Mathematical and Numerical Techniques in Physical Geodesy, Springer-Verlag, pp. 365-415, Austria, August 25 - September 5, 1986.

Rapp, R.H. and J.Y. Cruz, The Representation of the Earth's Gravitational Potential in a Spherical Harmonic Expansion to Degree 250, Report No. 372, Dept. of Geodetic Science and Surveying, The Ohio State University, Columbus, September 1986a.

Rapp, R.H. and J.Y. Cruz, Spherical Harmonic Expansions of the Earth's Gravitational Potential to Degree 360 Using 30′ Mean Anomalies, Dept. of Geodetic Science and Surveying, The Ohio State University, Columbus, December 1986b.

Reigber, C., G. Balmino, H. Müller, W. Bosch, and B. Moynot, GRIM Gravity Model Improvement Using LAGEOS (GRIM3-L1), J. Geophys. Res., Vol 90, No. B11, pp. 9285-9299, September, 1985.

Uotila, U.A., Notes on Adjustment Computations - Part I, Dept. of Geodetic Science and Surveying, The Ohio State University, Columbus, 1986.

Weber, G. and H.-G. Wenzel, Estimation of Error Properties, in: Validation of Seasat-1 Altimetry Using Ground Truth in the North Sea Region, Deutsche, Geodaetische Kommission Reihe B: No. 263, Frankfurt, 1982.

Wenzel, H.-G., Hochaufloesende Kugelfunktionsmodelle fuer das Gravitationspotential der Erde. Wiss. Arb. Fachrichtung Vermessungswesen der Universitaet Hannover, 1985.

Wichiencharoen, C., FORTRAN Programs for Computing Geoid Undulations from Potential Coefficients and Gravity Anomalies, Internal Report, Dept. of Geodetic Science and Surveying, The Ohio State University, Columbus, 1982.

Wieser, M., The Global Digital Terrain Model TUG87, Internal Report on Set-up, Origin and Characteristics, Institute of Mathematical Geodesy, Technical University of Graz, Austria, July 1987.

Wilcox, L.E., Prediction of 5°x5° Mean Anomalies in Gravimetrically Deficient Areas, USAF Aeronautical Chart and Information Center, Department of Defense Gravity Library, Gravity Correlations Section, St. Louis, September 1966.

Wilcox, L.E., An Analysis of Gravity Prediction Methods for Continental Areas, Defense Mapping Agency, Aerospace Center, St. Louis, August 1974.

Wilcox, L.E., and W.J. Rothermel, Prediction of Mean Gravity Anomalies in Unsurveyed Areas, presented at the International Gravity Commission Meeting, Paris, 11-15 September 1978.